Transition Graphs of Interacting Hysterons

Proefschrift

ter verkrijging van
de graad van doctor aan de Universiteit Leiden,
op gezag van de rector magnificus prof.dr. S. de Rijcke,
volgens besluit van het college voor promoties
te verdedigen op woensdag 3 juni 2026
klokke 11:30 uur

door

Margot Henriëtte Teunisse
geboren te Bodegraven, Nederland
in 1998

Promotor:	Prof.dr. M.L. van Hecke
Co-promotor:	Dr. M. Serra Garcia
Promotiecommissie:	Prof.dr. M. Mungan (HHU Düsseldorf, DE) Prof.dr. M. Dijkstra (Utrecht University, NL) Prof.dr. D. J. Kraft Prof.dr.ir. W. van Saarloos Prof.dr.ir. S.J. van der Molen

Printing: Ridderprint, www.ridderprint.nl
ISBN 978-94-6537-547-2
An electronic version of this dissertation is available on
openaccess.leidenuniv.nl

The work described in this thesis was supported by the European Research Council (ERC) under the European Union's Horizon 2020 research and innovation program (grant agreement no.01019474)

The butterfly on the cover is a subgraph of a six-hysteron transition graph. In the general model of interacting hysterons, it is realizable, and excluding the feelers, it is also a period-3 multiperiodic loop. I chose the butterfly due to its rich biodiversity, and in reference to the striking images associated with butterfly classification. The background displays a crumpled sheet of paper, a common example of a multistable material.

Contents

1 Introduction **5**
- 1.1 General Introduction . . . 5
- 1.2 Technical Introduction . . . 6
- 1.3 Aim and Approach . . . 9
- 1.4 Overview . . . 10

2 Graph Structure and Design **11**
- 2.1 Model, Transitions and T-Graphs . . . 12
  - 2.1.1 General model for interacting hysterons . . . 13
  - 2.1.2 Response to driving . . . 14
  - 2.1.3 Transition graphs . . . 22
- 2.2 Graph Design . . . 23
  - 2.2.1 Design Inequalities . . . 24
  - 2.2.2 Partial order and matrix representation . . . 28
  - 2.2.3 Realizability of t-graphs . . . 29
  - 2.2.4 Solving the design inequalities . . . 31
- 2.3 Outlook and Conclusions . . . 32

3 The Space of Possible T-graphs **35**
- 3.1 Constructing and Organizing All Graphs . . . 36
  - 3.1.1 Scaffolds . . . 38
  - 3.1.2 Binary trees of transitions . . . 39
  - 3.1.3 Constructing all t-graphs . . . 41
- 3.2 Statistical Weight of T-Graphs . . . 45
  - 3.2.1 Domain in parameter space and counting total orders 45
  - 3.2.2 The space of two-hysteron t-graphs . . . 47
- 3.3 Outlook and Conclusions . . . 48

4 Periodic Driving Responses **51**
4.1 Introduction 51
4.2 Self-Loops 52
4.2.1 Generating all self-loops 52
4.2.2 Design inequalities for self-loops 56
4.3 Multiperiodic Orbits 60
4.3.1 Constructing multiperiodic loops 60
4.3.2 Quad inequalities 64
4.4 Outlook and Conclusions 70

5 Restricted Models **71**
5.1 Introduction 71
5.2 Restrictions on Coupling 74
5.2.1 Same-sign coupling 74
5.2.2 Global coupling 80
5.2.3 Serial coupling 82
5.2.4 Homogeneous coupling 86
5.3 Large and Small Span 90
5.3.1 Large span 91
5.3.2 The zero-span limit 95
5.3.3 Spin pair constructions for a single hysteron. 100
5.4 Outlook and Conclusions 107

Bibliography **110**

Summary **117**

Samenvatting **121**

List of publications **125**

About the author **127**

Acknowledgements **129**

CHAPTER 1

Introduction

1.1 General Introduction

Memory is complex. We constantly encounter memory in our day-to-day lives: in our brains, to start with, and in our computers. Yet more common objects around us can have memory as well. Sometimes this is obvious and intentional, such as in mattresses which use memory foam, but at other times we may not even realize that an object has memory. When we crumple a piece of paper and throw it in the trash, this piece of paper has memory of the actions we performed on it - otherwise it would unfold the moment it leaves our hands.

This thesis deals with the subject of memory in complex materials, where the state of a system depends on its history. We particularly focus on hysteresis. Hysteresis is a form of memory that is widely known in physics. A well-known example of hysteresis is observed in ferromagnets such as iron [1]: when we apply a magnetic field to a piece of iron and then remove this magnetic field, the iron remains magnetized. If we apply the opposite field, we can flip the direction of magnetization. Hence, in zero field, the magnetization depends on the history, and as a function of a slowly cycling external field, can take on different values at the same value of driving.

These hysteretic effects are not limited to magnetism: another common form of hysteresis can be found in the deformations of materials. For example, if we bend a spoon far enough, it will not spring back to its original shape. Instead, we need to exert additional forcing to push it back to its original position [2]. The aforementioned crumpled sheet

similarly has hysteresis. However, this hysteresis is more complex, as the deformation of a crumpled sheet involves many individual folds. [3]

In this thesis, we describe complex hysteretic systems - like crumpled sheets - via elementary building blocks called 'hysterons'. The hysteron model is a minimal model for hysteresis and memory in materials, where the states of the system are discrete and the response to driving is deterministic, without any (thermal) noise. As a result, the analytical tools and terms which we use here (such as linear programming, partial orders, or race conditions) are somewhat atypical for physics, and are at times closer to computer science. Nevertheless, we make the case that this minimal model is effective in capturing a wide variety of complex memory behaviours in real physical systems.

1.2 Technical Introduction

Multistable systems, ranging from metamaterials to crumpled sheets, exhibit complex responses to sequential driving, often encoding memories of past inputs [5]. For example, the sequential response of a crumpled sheet stores intricate memories within its configuration [3]. Moreover, memory effects play a central role in novel physics-based computing approaches [6, 7].

For athermal systems that are driven quasistatically, both the multistability and sequential response can be encoded in a transition graph (t-graph) [4, 8, 9, 10]. These represent all stable states as nodes, connected by directed edges which represent transitions that occur when the driving U exceeds specific critical values. The beauty of these t-graphs is that they encode the response to *any* driving protocol, thus providing a central tool to study the properties and memory effects [11, 12] of a variety of frustrated media including amorphous solids [4, 13, 14, 15], sequential biological evolution [16], crumpled thin sheets [3, 17, 18], corrugated sheets [19] and metamaterials [6, 11, 20, 21, 22, 23, 24, 25, 26, 27].

To link t-graphs to the microscopic properties of physical models, simulations of frustrated media evolving in complex energy landscapes can be used [4, 28, 29]. Such simulations are computationally expensive, as they consider all degrees of freedom of the entire system. In many systems, however, the evolution is dominated by a small amount of irreversible events associated with localized elements (Fig. 1.1). For example, rearrangements in amorphous particle packings are often composed of rearrangements or 'T1' events of localized clusters of particles. These can

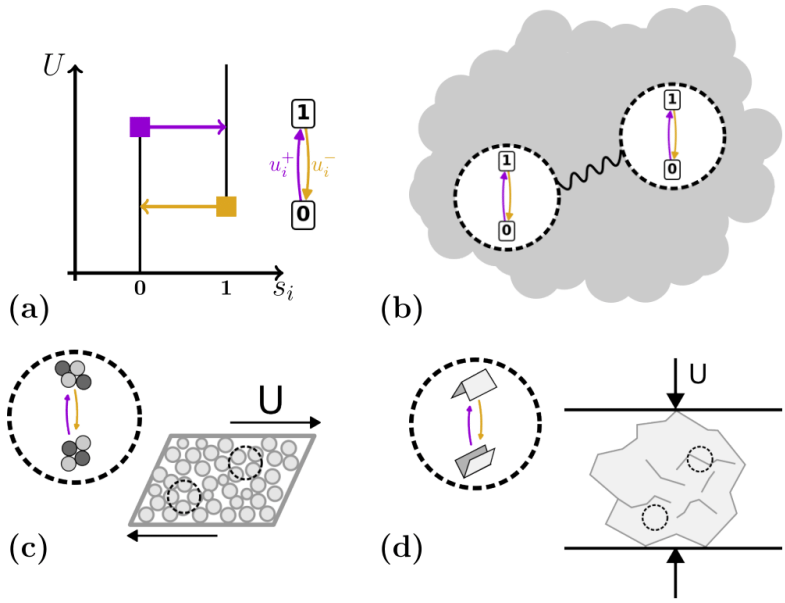


Figure 1.1: Interacting hysterons and the physical systems they inhabit. a) The response to driving with a field U (left) and graph representation (right) of a single hysteron with switching thresholds $u_i^{\pm}$. The phase of the hysteron is expressed in a binary variable s_i. b) Abstract representation of hysterons interacting through their embedding medium. c) Interacting hysterons (local rearrangements) in a sheared amorphous solid [4]. d) Interacting hysterons (mountain/valley folds) in a compressed crumpled sheet [3].

be described as hysteretic, two phase elements, that are refered to as hysterons (Fig. 1.1a). When sheared, the system's evolution is a mix of smooth episodes, interpunctured by sharp and irreversible rearrangements where these localized clusters change configuration [4]. Each of such changes corresponds to one or more hysterons changing their binary phase (Fig. 1.1a). Thus, a computationally efficient method to study memory in such systems is to directly investigate the t-graphs exhibited by collections of hysterons [3, 6, 9, 10, 13, 14, 16, 19, 20, 28, 30, 31, 32].

The modelling of multistable systems through hysterons was introduced by Ferenc Preisach, leading to the so-called Preisach model of hysteresis [33]. The model was originally formulated in the context of magnetic domains that do not experience (significant) interactions, and thus focused on collections of *independent* hysterons. The structure and

multiplicity of the t-graphs of the Preisach model have been characterized in detail [9, 30].

More recently, the hysteron model has been applied to geometrically frustrated media. However, here the hysterons experience interactions (Fig. 1.1b). Going back to our earlier example, the clusters in amorphous packings are embedded in an elastic matrix, so that each rearrangement influences the other rearrangements (Fig. 1.1c). Similarly, in other geometrically frustrated media such as crumpled sheets (Fig. 1.1d), local changes can also be described as interacting hysterons [3, 19, 24, 34, 35].

Interactions between hysterons are thus emerging as a crucial ingredient to understand the response of many frustrated physical systems [3,4,6,10,13,14,19,32]. Such interactions have been directly observed in experiments on macroscopic frustrated materials [3, 19] and metamaterials [6, 21, 22, 23, 24, 35]. In some cases, these interactions can also be calculated from first principles [6, 11, 26]. Moreover, under cyclic driving, these materials exhibit complex responses, including long transients and multi-periodic orbits [12, 13, 14, 19], that can not be understood in the Preisach model, but that can be captured in models of interacting hysterons. These interacting hysteron models are the focus of this thesis.

At the time that this project was started in 2021, Mungan and Terzi [9] had shown in detail that, so long as t-graphs have the property of *loop return point memory* (l-RPM), their structure is subject to a strict hierarchy. However, insights into general interacting hysteron systems, where l-RPM is allowed to be broken, were more scattered. Several concepts which are discussed in this thesis had been mentioned incidentally in literature, such as design inequalities [10, 14], scrambling [10, 19], and the additional inequalities required to realize a multiperiodic response [14]. However, these works did not aim to provide a comprehensive description of the interacting hysteron model; rather, their focus was on the unusual responses shown by interacting hysterons.

1.3 Aim and Approach

The goal of this thesis is to establish a general framework for understanding the response of interacting hysterons. We have translated this aim into three overarching research questions:

1. How can we check whether a single t-graph response is realizable?
2. How can we efficiently construct all realizable t-graphs?
3. How do we navigate the design space of t-graphs?

We answer the first question for the most general model of interacting hysterons, where we do not choose a specific form of the interactions. We have chosen this approach because, when we choose a specific form of the interactions, the systematics of the hysteron model become obscured. From our analysis of the most general model, we have found that it is fruitful to break a t-graph down into two parts: an underlying structure called the 'scaffold', and a number of avalanches which must comply with this scaffold.

In answer to the second question we provide an algorithm which is guaranteed to find all realizable t-graphs. This is based on a systematic construction of all 'candidate' t-graphs by defining a small number of scaffolds that get dressed by avalanches. This allows us to construct all candidate graphs, after which we can check for each if it is realizable. This approach comes with the major caveat that the number of candidate graphs mushrooms with the number of hysterons so that it quickly becomes computationally unfeasible to generate and check for the realizability of all t-graphs; however, when the number of avalanches and their individual lengths are limited, this method is feasible.

The third research question, concerning the navigation of design space, is the most challenging: while it is straightforward to formulate conditions for a single t-graph, it remains difficult to experimentally 'tweak' a design reach a desired (sub)graph. To tackle this question, we take advantage of various experimentally motivated hysteron models, to which we have applied our methodology over the course of this project. For example, we have investigated serially coupled hysterons, symmetrically coupled hysterons, or hysterons which approach a spin system. These physically grounded models serve as a basis for our navigation of the broader design space of interacting hysterons.

1.4 Overview

The core of this thesis is formed by chapters 2 and 3. Chapter 2 focusses on the response of a single system of interacting hysterons. It describes how a t-graph is constructed for a given set of switching thresholds, and defines core concepts such as the scaffold, scrambling, and avalanches. It then addresses the inverse design question of constructing a set of switching thresholds such that a given t-graph is realized.

Chapter 3 addresses the separate, though related, question of constructing all realizable t-graphs for a given number of hysterons. It details a two-part algorithm, where a set of 'candidate' graphs is generated, and each of these candidates is then evaluated for realizability. This algorithm makes use of the concepts of the 'scaffold' and the 'design inequalities' which were introduced in Chapter 2.

Chapter 4 focusses on two specific features of t-graphs: self-loops and multiperiodic responses. These features are of immediate interest because they can be easily probed in experimental systems. In the case of self-loops, we investigate why self-loops are absent from physical dissipative systems, despite the fact that these occur in the hysteron model. Multiperiodicity, meanwhile, is interesting because it exemplifies how interactions in hysterons can lead to new memory behaviours, where the response of the system under cyclic driving depends on the number of driving cycles. We therefore adapt the methodology described in Chapters 2–3, which describes full t-graphs, for these two features.

Finally, chapter 5 describes several restricted, physically motivated models of interacting hysterons. We distinguish two types of constraints: restrictions on the interactions between hysterons, and restrictions on the hysteron 'span' (i.e., the hysteresis present in the individual hysterons). For the restrictions on interactions, we discuss same-sign coupling, global coupling, serial coupling and homogeneous coupling. For the restrictions on span, we discuss two cases: models where the mean span is large, and spins (i.e., zero-span hysterons). Basing ourselves on the core methodology established in Chapters 2 and 3, we show how the design space for each of these models is simplified.

CHAPTER 2

Graph Structure and Design

In this chapter we address the structure and design of a single t-graph in the context of interacting hysteron models. While the link between microscopic parameters and Preisach graphs, as well as their statistics, are simple, this link is much more complex for interacting hysterons, which moreover display statistical weights that vary over many orders of magnitude [10, 30, 31]. These t-graphs are also much more varied than those of the Preisach model, featuring, e.g., *scrambling* and *avalanches*, which together lead to an enormous variety of remarkable phenomena such as transient memories, multiperiodic responses, and even computational capabilities [3, 6, 8, 10, 13, 19]. However, when this work was started, we lacked a systematic approach to understand the multiplicity, statistics and variability of t-graphs of interacting hysterons.

As a first step in understanding the structure of t-graph space, here we establish a framework for the design of a single t-graph in the most general model of interacting hysterons. As microscopic parameters we take the state dependent switching thresholds $U_i^{\pm}(S)$; this approach encompasses recently studied cases with more limited, specific parameterizations of the switching thresholds [6, 13, 14, 28]. We start by considering the forward problem of how a given set of switching thresholds produces a t-graph. We introduce the concept of the *scaffold* which allows us to precisely define scrambling, as well as the systematic construction of transitions and avalanches.(section 2.1). We then consider the inverse problem: given a (part of a) t-graph, what are the corresponding necessary and sufficient conditions on the switching thresholds? We present a systematic method for obtaining the set of design inequalities, and discuss how these corre-

spond to a partial order on the switching thresholds. This partial order straightforwardly allows us to determine if a given target t-graph topology can be realized in the interacting hysteron model, and provides the underlying structure of the design space (section 2.2).

2.1 Model, Transitions and T-Graphs

In this section we present a general model for interacting hysterons, discuss in detail the response to changes of the global driving parameter U, and the resulting transition graphs. All abstract hysteron models describe interactions via a state dependence of the switching thresholds, which are the critical values of the driving that lead to flipping of the hysterons, but different physical assumptions lead to different functional forms of this state dependence. For example, one may assume that interactions are reciprocal (so that the effect of hysteron i on the switching thresholds of hysteron j equals the effect of hysteron j on the switching thresholds of hysteron i), that they are pairwise, or that they do not affect the hysteron span (so that the effects of hysteron j on the up and down switching thresholds of hysteron i are equal) [10,13,14,32]. However, both in experiments and in physical models, reciprocity and span invariance are not respected [6, 14, 19], and multi-hysteron interactions generically occur in networks of geometrically coupled hysterons [26]. We therefore focus on the most general formulation of the state dependency, which naturally encompasses models with restricted forms of interactions (section 2.1.1).

Once the interactions are specified, we consider transitions between states: events where one or more hysterons change phase in response to changes in the driving parameter U (section 2.1.2). We first discuss the critical hysterons that initiate such transitions, and use these to define the *scaffold*, which underpins the structure of all transitions and which allows for a precise definition of the important property of *scrambling* [10, 19] (section 2.1.2). We then discuss transitions, and in particular avalanches and their relation to the scaffold (section 2.1.2). Finally, we remark on two types of transitions which require special attention (section 2.1.2). First, the scenario where multiple hysterons become unstable during an avalanche leads to race conditions that cannot be resolved in the mode. Second, situations can occur where the model predicts an endless cycle of state transitions [10,13,32]. Both problems stem from the hysteron model being a coarse-grained model that lacks an underlying energy landscape and dynamics. While the first situation can be resolved via the introduc-

tion of an additional dynamical rule - for example, by always flipping the hysteron that is furthest from stability [13,14] - in this chapter we explicitly exclude both situations (section 2.1.2). Altogether, our framework presents an unambiguous mapping from a general set of state-dependent switching thresholds to a t-graph.

2.1.1 General model for interacting hysterons

We now detail the general model for a system of n interacting hysterons. First, let us recall the definition of a hysteron. Each hysteron i is a bistable element characterized by its binary phase s_i—we use the term phase for individual elements to avoid confusion with the collective state. The two switching thresholds $u_i^{\pm}$ ($u_i^+ > u_i^-$) determine the hysteron's response under driving with an external field U. A hysteron in phase $s_i = 0$ is stable when $U < u_i^+$, but when $U > u_i^+$ it is unstable and switches from 0 to 1 – the hysteron 'flips up'. Similarly, a hysteron in phase $s_i = 1$ is stable when $U > u_i^-$, but when $U < u_i^-$ it is unstable and switches from 1 to 0 – the hysteron 'flips down'. This response forms an elementary hysteresis loop.

For a collection of n hysterons, we define the collective state S as

$$S = (s_1, s_2, \ldots, s_n) \ . \tag{2.1}$$

We denote the saturated states where all hysterons are either 0 or 1 as $(00\ldots)$ and $(11\ldots)$. The set of hysteron indices for which $s_i = 0$ ($s_i = 1$) is referred to as $I_0(S)$ ($I_1(S)$) [16].

We model interactions between hysterons via state-dependent hysteron switching thresholds $U_i^{\pm}(S)$:

$$U_i^{\pm}(S) = u_i^{\pm} + \Delta_i^{\pm}(S) \ , \tag{2.2}$$

where Δ_i captures the dependence of the switching thresholds of hysteron i on the collective state S. The switching thresholds encode when hysterons become unstable: starting from state S, hysteron i becomes unstable when U is increased (decreased) beyond $U_i^+(S)$ ($U_i^-(S)$).

We assume that the hysteron switching thresholds $U_i^{\pm}(S)$ are non-degenerate and finite – this implies that the saturated states are always reached when $U \to -\infty$ and $U \to \infty$. The interaction term $\Delta_i^{\pm}(S)$ can encode any specific model for hysteron interactions, including the Preisach model ($\Delta_i^{\pm}(S) = 0$ [33]), pairwise interactions ($\Delta_i^{\pm} = -\Sigma_j c_{ij}^{\pm} s_j$), reciprocal interactions [14], or an equal shift of upper and lower switching

thresholds ($\Delta_i^+(S) = \Delta_i^-(S)$). We finally note that switching thresholds $U_i^+(S)$ ($U_i^-(S)$) are only relevant when the corresponding hysteron i is in phase 0 (1). For example, for the state (001), the only relevant switching thresholds are $U_1^+(001), U_2^+(001)$ and $U_3^-(001)$ – in general there are n switching thresholds per state. Hence, while (2.2) defines $2n \cdot 2^n$ switching thresholds, only half of these are relevant: n interacting hysterons are defined by precisely $n \cdot 2^n$ switching thresholds.

2.1.2 Response to driving

We now consider how a collection of n interacting hysterons responds to driving, i.e., changes in U (Fig. 2.1a). While the state dependent switching thresholds $U_i^{\pm}(S)$ define for each state and value of U whether its hysterons are stable, they do not specify what happens when a hysteron becomes unstable. Here we first consider the stability range of states S and identify the critical hysterons that lose stability when S becomes unstable (sec. 2.1.2). We then discuss the ensuing state transitions, which can take on the form of multi-step avalanches (sec. 2.1.2), and finally discuss two scenarios which have been dubbed 'ill-defined', namely self-loops and race conditions (sec. 2.1.2).

Stability, Scaffold and Scrambling

As a first step in defining the response of a collection of hysterons to variations of the global driving field U, we define here the stability range of a state and its critical hysterons. We then introduce the concept of the *scaffold*, and use it to precisely define the concept of scrambling [10,19,32].

Definition 2.1.1 (*Stability range and state switching thresholds)* *Let S be the state of a collection of hysterons with state-dependent switching thresholds $\{U_i^{\pm}(S)\}$. State S is stable if U is smaller than all its up switching thresholds $U_i^+(S)$ and larger than all its down switching thresholds $U_i^-(S)$. Hence, S has a* stability range *$[U^-(S), U^+(S)]$, where $U_i^{\pm}(S)$ are the* state switching thresholds *(Fig. 2.1b): [9]:*

$$\begin{aligned} U^+(S) &= \min_{I_0} U_i^+(S) \ , \\ U^-(S) &= \max_{I_1} U_i^-(S) \ . \end{aligned} \tag{2.3}$$

When S is initially stable and U is swept up (down) to $U^+(S)$ ($U^-(S)$), S loses stability through the instability of a single hysteron. We use the following definition for these hysterons:

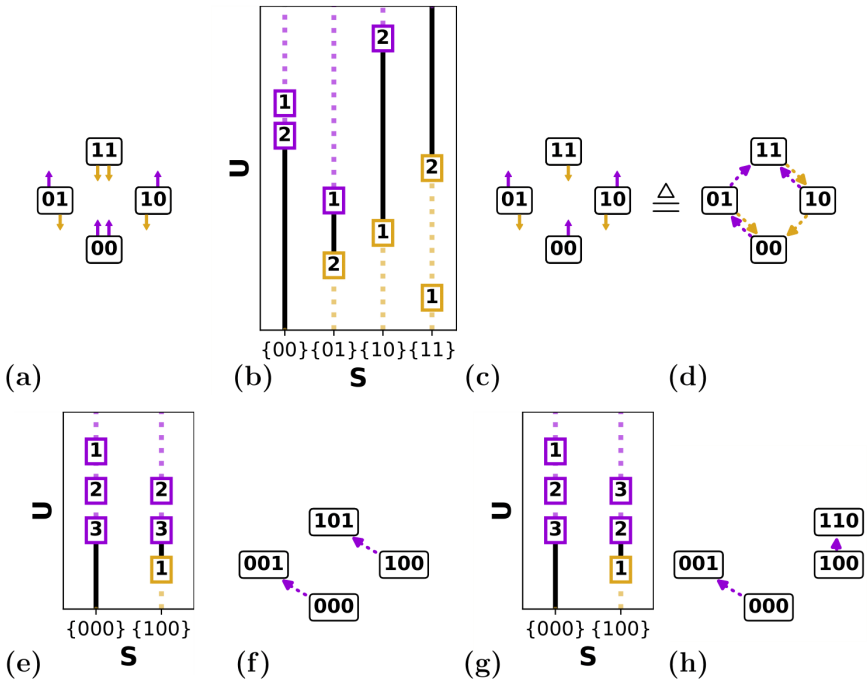


Figure 2.1: Scaffolds and switching thresholds. (a) Graphical representation of the set of $n = 2$ switching thresholds: hysterons in state $s_i = 0$ ($s_i = 1$) have an up (down) switching threshold indicated by purple (gold) arrows. (b) Example of a given set of switching thresholds (boxes) and corresponding stability ranges (black lines) – in the dashed regions, the state is unstable. (c) Corresponding scaffold, with the $2^{n+1} - 2$ critical hysterons $k^{\pm}(S)$ indicated. (d) Alternative yet equivalent graphical representation of the scaffold showing 'passages', i.e., tentative transitions to a landing state $S^{(1)}$ (see text). (e) Example of a subset of $n = 3$ switching thresholds for the Preisach model where $\Delta_i^{\pm}(S) = 0$. Since $U_2^+(000) = U_2^+(001) = u_2^+$, and $U_3^+(000) = U_3^+(001) = u_3^+$, hysterons 2 and 3 flip in the same order for both states, and since $k^+(000) = 3$, $k^+(100) = 3$. (f) Graphical representation of the corresponding scaffold. (g) Example of a subset of $n = 3$ switching thresholds, for the states (000) and (100), for the general model where $\Delta_i^{\pm}(S) \neq 0$. Since the switching thresholds $\{U_i^{\pm}(S)\}$ are independent, the order in which hysterons 2 and 3 flip may be different ('scrambled') between states (000) and (100). (h) Graphical representation of the corresponding scrambled scaffold.

Definition 2.1.2 (*Critical hysterons and scaffold)* *Let S be the state of a collection of hysterons with state-dependent switching thresholds $\{U_i^{\pm}(S)\}$. The* critical hysteron *$k^+(S)$ ($k^-(S)$) is the hysteron which has the lowest up (highest down) switching threshold at state S:*

$$\begin{aligned} k^+(S) &= \arg\min_{I_0} U_i^+(S) \forall S \neq (11\dots) \ , \\ k^-(S) &= \arg\max_{I_1} U_i^-(S) \forall S \neq (00\dots) \ . \end{aligned} \tag{2.4}$$

We refer to the collection of critical hysterons $\{k^{\pm}(S)\}$ at all states for a given set of switching thresholds as the scaffold *of the hysteron system.*

The saturated states have only one critical hysteron, whereas all other states have two critical hysterons. We note that *persistently unstable* states may arise where $U^+(S) < U^-(S)$; such states can play a role as intermediate states in avalanches (section 2.1.2).

The definitions 2.1.1-2.1.2 map the $n \cdot 2^n$ hysteron switching thresholds $\{U_i^{\pm}(S)\}$ to $2^n - 2$ critical hysterons $\{k^{\pm}(S)\}$ and corresponding state switching thresholds $\{U^{\pm}(S)\}$. We note that the scaffold defined in Def. 2.1.2 is an important object: as its name suggests, it provides the underlying structure on which state transitions will be defined (Fig. 2.1c). This key role motivates an alternative yet equivalent graphical representation of the scaffold, where we show tentative transitions associated with flipping the critical hysterons. We term these tentative transitions *passages*. (Fig. 2.1d). We stress here that passages are *not* necessarily equal to state transitions, and we discuss the relation between scaffold and transitions in detail in section 2.1.2.

We now employ the scaffold to clarify the recently introduced *scrambling* property [10, 19, 32]. Loosely speaking, scrambling was introduced for pairs of transitions that evidence hysteron interactions [10], but its definition becomes cumbersome when avalanches are present. As we show below, the scaffold allows for a precise definition that does not suffer from such subtleties.

We will give the formal definition of scrambling first, as this allows us to make a clear argument for why scrambling is not possible in the Preisach model. We then illustrate our argument with specific examples of a scaffold in the Preisach model and of a scrambled scaffold.

Definition 2.1.3 (*Scrambling)* *Let $\{U_i^{\pm}(S)\}$ be the set of switching thresholds of a collection of hysterons. Suppose that, for two states S_A,*

S_B, the critical up hysterons $k^+(S_A)$, $k^+(S_B)$ lie in the intersection of $I_0(S_A)$ and $I_0(S_B)$:

$$k^+(S_A), k^+(S_B) \in I_0(S_A) \cap I_0(S_B) \ . \tag{2.5}$$

This pair of critical up hysterons is scrambled *if*

$$k^+(S_A) \neq k^+(S_B) \ . \tag{2.6}$$

Likewise, the pair of critical down hysterons $k^-(S_A), k^-(S_B)$ is scrambled if:

$$\begin{aligned} k^-(S_A), k^-(S_B) &\in I_1(S_A) \cap I_1(S_B) \ , \\ k^-(S_A) &\neq k^-(S_B) \ . \end{aligned} \tag{2.7}$$

Crucially, we now state the following:

Corollary 2.1.1 *The scaffold $\{k^\pm(S)\}$ for a set of switching thresholds of the form $U_i^\pm(S) = u_i^\pm$ cannot have scrambling.*

To see that Corollary 2.1.1 is true, consider a pair of hysterons i and j. If $k^+(S_A) = i$, and $s_j = 0$, then by Definition 2.1.2, $U_i^+(S) < U_j^+(S)$. Thus, in the Preisach model, $u_i^+ < u_j^+$. Yet, if there is another state S_B where $k^+(S_B)$ and $s_i = 0$, then by the same reasoning, $u_i^+ > u_j^+$. Therefore, this situation cannot occur in the Preisach model.

A practical interpretation of scrambling is that in the Preisach model, the critical hysterons for different states are determined by the fixed ordering of the individual hysteron switching thresholds $u_i^\pm$. For general state-dependent switching thresholds $U_i^\pm(S)$, there is no such constraint. We illustrate this in the example below.

Example 2.1.1 *Suppose that we have a collection of non-interacting hysterons which has $k^+(000) = 2$. In the Preisach model, this implies that $u_2^+ < u_3^+$, and therefore imposes that $k^+(100) = 2$ (Fig. 2.1e-f). In contrast, now suppose that the switching thresholds $U_i^\pm(S)$ can be chosen entirely independently. In this case, the fact that $k^+(000) = 2$ requires that $U_2^+(000) < U_3^+(000)$ does not impose any constraints on $U_2^+(100), U_3^+(100)$, so that it is possible to have $k^+(100) = 3$ in the same scaffold (Fig. 2.1g-h).*

When a scaffold contains at least one pair of scrambled hysterons, we refer to the scaffold as as being scrambled. We emphasize that the

scaffolds which are not possible in the Preisach model, but are possible for interactions, are exactly the scrambled scaffolds.

In summary, scrambling is an effect of hysteron interactions which leads to scaffolds that are not possible in the Preisach model. We note that definition 2.1.3 is only concerned with pairs of critical hysterons which lie in the intersection $I_0(S_A) \cap I_0(S_B)$ or $I_1(S_A) \cap I_1(S_B)$. As a result, scrambling only becomes relevant when $n \geq 3$; for $n = 2$, the only possible scaffolds are the two Preisach scaffolds.

Transitions and Avalanches

When an initially stable state S becomes unstable, due to either an up sweep or a down sweep of U, this triggers a transition to a new stable state S', which we denote as $S \rightsquigarrow S'$. Here we discuss in detail how the system evolves from S to S' and how S' is determined.

Each transition is initiated by the flipping of one of the critical hysterons $k^{\pm}(S)$, leading to a new 'landing' state $S^{(1)}$. In the Preisach model, the landing state is always stable at $U_k^{\pm}(S)$ [9, 30, 36], so that $S' = S^{(1)}$. This produces the transition $S \rightsquigarrow S^{(l)}$ which trivially follows from the passages in the scaffold - in fact, for the Preisach model, transitions are equal to passages, and the scaffold captures all transitions.

In the presence of hysteron interactions, the stability of the landing state $S^{(1)}$ is no longer guaranteed. Interacting hysterons can therefore feature multi-step transitions, i.e. *avalanches*, which proceed via a sequence of intermediate states. We denote such avalanches as $S^{(0)} \rightarrow S^{(1)} \rightarrow \cdots \rightarrow S^{(l)}$, where $S^{(0)}$ is the initial state, $S^{(1)}$ is the landing state, $S^{(1)} - S^{(l-1)}$ are intermediate states and $S^{(l)}$ is the final state. We refer to the l as the *transition length*; for $l > 1$ this is synonymous to avalanche size. Note that, in our notation, straight arrows represent the phase change of a single hysteron, whereas squiggly arrows represent a full transition $S^{(0)} \rightsquigarrow S^{(l)}$.

We now show how a single transition is constructed, given the set of switching thresholds. We remark that each transition starts from an initially stable state $S^{(0)}$; transitions cannot be initiated from persistently unstable states (section 2.1.1). We take this initial stability into account when we construct the design inequalities in section 2.2.1.

A transition is initiated when k flips at $U = U_k^{\pm}(S^{(0)})$, yielding the first step $S^{(0)} \rightarrow S^{(1)}$. There are three possible scenarios (Fig. 2.2a) depending on the stability of the landing state $S^{(1)}$:

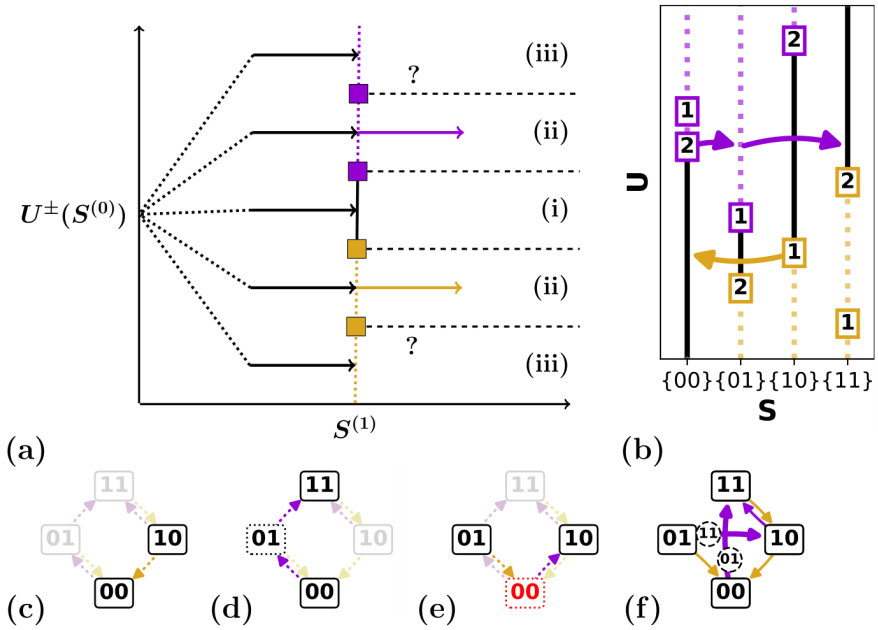


Figure 2.2: Construction of transitions and full transition graph from the set of switching thresholds. (a) Schematic of the three scenarios for the landing state $S^{(1)}$ at driving field $U^{\pm}(S^{(0)})$: (i) $S^{(1)}$ is stable; (ii) a single hysteron in state $S^{(1)}$ is unstable; (iii) $S^{(1)}$ multiple hysterons in $S^{(1)}$ are unstable (see text). (b) Two transitions ($l = 1$ transition (10) $\downarrow$ (00) and $l = 2$ transition (00) $\uparrow$ (01) $\uparrow$ (11)) for the set of switching thresholds shown in Fig. 2.2b. (c) The $l = 1$ transition (10) $\downarrow$ (00) follows the scaffold (faded) (d) The avalanche transition (00) $\uparrow$ (01) $\uparrow$ (11) follows the scaffold. (e) The tentative transition (01) $\downarrow$ (00) $\uparrow$ (10) is incompatible with the scaffold, as the transition requires that $k^{+}(00) = 1$, while the scaffold specifies that $k^{+}(00) = 2$. (f) Full t-graph for the set of switching thresholds shown in panel b.

1. $S^{(1)}$ is stable at $U_k^{\pm}(S^{(0)})$;

2. A single hysteron in state $S^{(1)}$ is unstable at $U_k^{\pm}(S^{(0)})$;

3. Multiple hysterons in state $S^{(1)}$ are unstable at $U_k^{\pm}(S^{((0)})$.

When the landing state $S^{(1)}$ is stable (case (i)), we obtain the $l = 1$ transition $S^{(0)} \rightsquigarrow S^{(1)}$. For example, the switching thresholds shown in Fig. 2.2b produce the $l = 1$ transition (10) $\downarrow$ (00) (Fig.2.2b-c).

We now turn to case (*ii*), where a single hysteron κ in state $S^{(1)}$ is unstable at $U = U_k^{\pm}(S)$. This provokes the next step $S^{(1)} \to S^{(2)}$ - please note that this scenario can occur even for a persistently unstable state (section 2.1.1). For the state $S^{(2)}$, the same three scenarios can occur as for $S^{(1)}$: if $S^{(2)}$ is stable (case (*i*)), the transition terminates. This produces the $l = 2$ avalanche $S^{(0)} \rightsquigarrow S^{(2)}$, which proceeds as $S^{(0)} \to S^{(1)} \to S^{(2)}$. We illustrate an example of an $l = 2$ avalanche (00) $\uparrow$ (01) $\uparrow$ (11) in Fig. (2.2b,d). If one of the hysterons in $S^{(2)}$ is unstable (case (*ii*)), the transition proceeds to the next state $S^{(3)}$. Assuming that case (*iii*) does not occur and that states are not revisited, we see that avalanches are constructed iteratively, i.e., as a sequence of single hysteron flips.

We now show that the scaffold (Definition 2.1.2) plays an important role in determining possible avalanches.

Theorem 2.1.1 (*Relation between scaffold and avalanches*) *Let $S^{(0)} \to S^{(1)} \to \cdots \to S^{(l)}$ be a transition consistent with a set of switching thresholds $\{U_i^{\pm}(S)\}$, which has the corresponding scaffold $\{k^{\pm}(S)\}$. If the transition proceeds via a sequence of single hysteron flips $\kappa_0, \kappa_1, \ldots, \kappa_{l-1}$, each hysteron κ_λ must be one of the critical hysterons $k^{\pm}(S^{(\lambda)})$.*

It is easily shown that Theorem 2.1.1 is true via proof by contradiction. Suppose for definiteness that κ_λ switches up, and $\kappa_\lambda \neq k^+(S^\lambda)$. Then, from Definition 2.1.2, the switching threshold of hysteron κ_λ is higher than that of $k^+(S^{(\lambda)})$. Thus, if κ_λ is unstable, then $k^+(S^{(\lambda)})$ is unstable as well, which contradicts with the prerequisite that only a single hysteron flips at a time.

In essence, Theorem 2.1.1 states that avalanches must follow the passages of the scaffold. Hence, once the scaffold is constructed from the switching thresholds, it immediately restricts the transitions that can occur; for example, for the scaffold shown in Fig. 2.2e, the transition (01) $\downarrow$ (00) $\uparrow$ (10) is forbidden. This relation between scaffold and avalanches can be explored to label an avalanche solely by its starting state and its sequence of up/down flips, letting the scaffold dictate the full transition path. For example, the transition path (00) $\uparrow$ (01) $\uparrow$ (11) shown in Fig. 2.2d is labeled as 00uu. Consequently, all possible (avalanche) transitions can simply be collected in a set of binary trees; we further elaborate on and make use of this scaffold/avalanche relation in sec. 3.1.

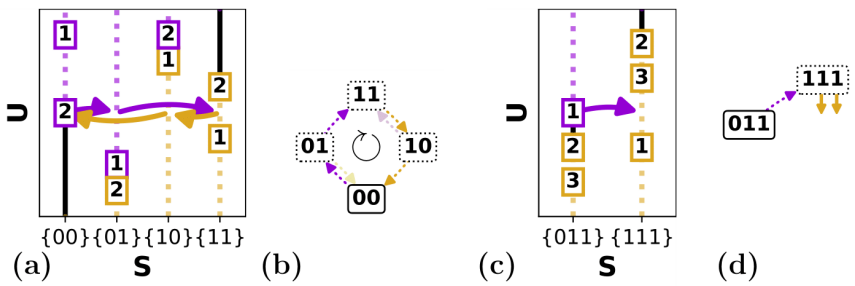


Figure 2.3: The two types of 'ill-defined' transitions. (a) Set of switching thresholds that leads to a self-loop (00) ↑ (01) ↑ (11) ↓ (10) ↓ (00) ↑ .... (b) Graphical representation for this self-loop. (c) Example of a (subset of) switching thresholds that leads to a race condition, due to the instability of multiple hysterons in state (111) at $U^+(011)$. (d) Graphical representation for this race condition: we cannot draw a tentative down transition because the order in which hysterons 2 and 3 flip is not well defined.

Self-loops and race conditions

So far, we have discussed how a given set of switching thresholds produces transitions. In the construction of such transitions, two scenarios require special attention, namely self-loops and race conditions. In previous works, these two types of transitions have been collectively referred to as 'ill-defined' [10]. However, we here avoid using the term 'ill-defined', except where we make an explicit comparison to previous results (see Chapter 3). We do so to avoid confusion with mathematical ill-definedness (i.e., inconsistency), and to emphasize that these are two distinct features, which need to be dealt with separately.

First, certain choices of switching thresholds produce self-loops, where after a number of steps, an avalanche revisits an earlier state [37]. In the simplest case, the switching hysteron is unstable in its landing state: for example, if after the partial transition (00) ↑ (01) hysteron 2 is unstable in (01), this sets up a loop (00) ↑ (01) ↓ (00) ↑ (01) ↓ .... More generally, self-loops can arise from any cyclical path within the scaffold - for an example of a longer loop, see Fig. 2.3a-b. Such an orbit can never reach a stable state, and such loops cannot occur in dissipative systems. We exclude these loops when we construct all t-graphs (Chapter 3), but discuss them separately in the context of periodic responses (Chapter 4).

Second, when a transition reaches an intermediate state $S^{(\lambda)}$ where

more than one hysteron is unstable at the critical field $U^{\pm}(S^{(0)})$ this causes the transition to become ambiguous - for an example of such a scenario, see Fig. 2.3c-d. The problem here is that flipping operations do not commute for interacting hysterons: for example, when the hysterons κ_1 and κ_2 are unstable, and hysteron κ_1 flips first, this may make hysteron κ_2 stable again, whereas when hysteron κ_2 flips first, hysteron k_1 may remain unstable. Hence, different choices for the sequence of hysteron flips may then lead to different transition paths, a situation known as a critical race condition [38]. This ambiguity cannot be resolved in our general framework, and we therefore choose to forbid race conditions entirely in Chapters 2–3.

We note that some authors resolve race conditions by simply demanding that each intermediate step in a transition only flips one hysteron, and picking the most unstable hysteron if there is more than one; for such a model, the scaffold/avalanche relation specified by Theorem 2.1.1 is maintained [13, 14].

While self-loops and race conditions present unique challenges, in essence, both arise because models for interacting hysterons have a very simple update rule. In more physically complete models, based on an energy landscape and physical dynamics, these two scenarios do not present an issue as they can be explicitly resolved. The occurrence of self-loops and race conditions thus highlights the limitations of hysteron models. Nevertheless, studies of more complex models come at a significant computational expense, and despite their (over)simplicity, hysteron models have proven valuable in capturing experimental and numerical data, as well as giving insight in memory effects.

2.1.3 Transition graphs

All ingredients are now in place to construct the transition graph (t-graph) which encodes the full driving response for a set of hysteron switching thresholds $U_i^{\pm}(S)$. To do so, we first construct the scaffold (section 2.1.2), and then iteratively construct the full transition path $S^{(0)} \to S^{(1)} \to \cdots \to S^{(l)}$ for each up and down transition. We collect these transitions in a directed graph, where the states form the nodes, and the transitions $S^{(0)} \rightsquigarrow S^{(l)}$ form the edges. Furthermore, the intermediate states $S^{(1)}, \ldots, S^{(l-1)}$ are saved as edge attributes.

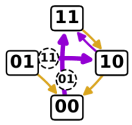
As an example, the set of switching thresholds $\{U_i^{\pm}(S)\}$ shown in Fig. 2.2b produces the t-graph shown in Fig. 2.2f. In summary, the

driving response of a collection of n hysterons, characterized by a set of switching thresholds $\{U_i^{\pm}\}$, is captured by a directed t-graph.

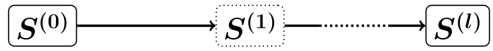
We note that our t-graphs contain more information than what is usually considered. First, for a given set of switching thresholds the intermediate states are fully specified, whereas in, e.g., experimental contexts intermediate states in an avalanche can typically not be observed [19]. Second, our t-graphs may contain so-called Garden-of-Eden (GoE) states that are not reachable from the saturated states (for an example see state (01) in Fig. 2.2f) [10, 20]. Unless otherwise specified, we will deal with t-graphs where GoE states and intermediate states are both included. In our visualization of t-graphs, we thus not only indicate a transition's direction (up/down) and length l [10] but also explicitly indicate the intermediate states.

2.2 Graph Design

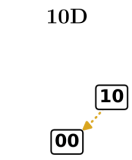
In this section we consider the design question, also referred to as the inverse problem: given a transition graph, or part of a transition graph, what are the necessary and sufficient conditions on the switching thresholds so that they lead to this (sub)graph? Consistent with earlier work on this inverse problem [10, 14], we find that the design conditions take the form of sets of inequalities of the switching thresholds. Here, we establish a systematic approach for constructing and utilizing these design inequalities. We first present their systematic derivation (section 2.2.1), then discuss how the design inequalities specify a partial order on the switching thresholds (section 2.2.2). In particular, we utilize the inequalities to determine if a given t-graph topology is realizable (section 2.2.3), and finally discuss how to construct explicit sets of switching thresholds that realize specific (sub)-graphs (section 2.2.4).



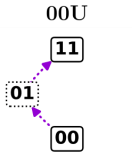
(a)



(b)



(c)



(d)

(e)

	Initial	Intermediate	Final
00U	$U_2^+(00) < U_1^+(00)$	$U_2^+(00) > U_1^+(01)$ $U_2^+(00) > U_2^-(01)$	$U_2^+(00) > U_1^-(11)$ $U_2^+(00) > U_2^-(11)$
01U	$U_1^+(01) > U_2^-(01)$	$U_1^+(01) > U_1^-(11)$ $U_1^+(01) < U_2^-(11)$	$U_1^+(01) > U_1^-(10)$ $U_1^+(01) < U_2^+(10)$
01D	$U_2^-(01) < U_1^+(01)$		$U_1^-(01) < U_1^+(00)$ $U_1^-(01) < U_2^+(00)$
10U	$U_2^+(10) > U_1^-(10)$		$U_2^+(10) > U_1^-(11)$ $U_2^+(10) > U_2^-(11)$
10D	$U_1^-(10) < U_2^+(10)$		$U_1^-(10) < U_1^+(00)$ $U_1^-(10) < U_2^+(00)$
11D	$U_2^-(11) > U_1^-(11)$		$U_2^-(11) > U_1^-(10)$ $U_2^-(11) < U_2^+(10)$

Figure 2.4: Design inequalities. (a) Example of an $n = 2$ target t-graph. (b) The design inequalities are organized in three groups pertaining to the initial state $S^{(0)}$, intermediate states $S^{(1)}, \ldots, S^{(l-1)}$, and final state $S^{(l)}$. (c) Length-1 transition $(10) \downarrow (00)$. (d) Length-2 transition $(00) \uparrow (01) \uparrow (11)$. (e) The design inequalities for the target graph shown in panel (a). We label transitions by their starting state $S^{(0)}$ and their up or down direction: for example, the up transition starting from state (00) is labeled 00U, and the down transition starting from state (10) is denoted 10D (see also panels (c) and (d)). Note that all inequalities are organized by transition, and can be further separated by whether they are given by the initial state (scaffold), intermediate state (if present), or final state inequalities.

2.2.1 Design Inequalities

We define the *design inequalities* as the necessary and sufficient conditions on the switching thresholds $\{U_i^{\pm}(S)\}$ that produce a specific (sub)graph. We will frequently illustrate our approach with specific examples, such as the t-graph and its scaffold shown in Fig. 2.4a. As we show, each transition in a t-graph corresponds to a set of design inequalities that

result from *(i)* conditions on the initial state (its stability and critical hysterons), *(ii)* the stability of the final state, and, if the transition is an avalanche, *(iii)* the (in)stabilities and critical hysterons of the intermediate states. Combining the individual design inequalities for multiple transitions, taking potential redundancies into account, produces the set of inequalities for a specific t-graph or part thereof.

Conditions for single transitions

We now formulate the design inequalities for a single transition. As avalanches for which only the initial state $S^{(0)}$ and final state $S^{(l)}$ are specified may proceed along various paths of intermediate states, each producing a different set of design inequalities, we assume that the full transition path $S^{(0)} \to S^{(1)} \to \cdots \to S^{(l)}$ is known (Fig. 2.4b). We illustrate that these inequalities readily emerge by constructing transitions as in section 2.1.2, and keeping track of the requirements that the switching thresholds must obey at each step.

Initial inequalities.– The first set of design inequalities follows from the required stability of state $S^{(0)}$ for some range of U, and from the critical hysteron k that flips when the driving U is increased or decreased. For hysteron k in phase 0 (1) to be the critical hysteron that initiates an up (down) transition $S^{(0)} \rightsquigarrow S^{(l)}$, the set of switching thresholds $\{U_i^{\pm}(S)\}$ must obey the set of inequalities:

$$\text{up}: \qquad U_k^+(S^{(0)}) < U_i^+(S^{(0)}) \;\forall i \in I_0(S^{(0)})\backslash\{k\}\;, \tag{2.8}$$

$$\text{down}: \qquad U_k^-(S^{(0)}) > U_i^-(S^{(0)}) \;\forall i \in I_1(S^{(0)})\backslash\{k\}\;, \tag{2.9}$$

where $I_{0/1}(S^{(0)})\backslash\{k\}$ is the collection of hysterons in phase 0 (1), unequal to k in state $S^{(0)}$.

Moreover, for $S^{(0)}$ to be initially stable in the case of an up (down) transition, all down (up) switching thresholds must be below (above) the critical switching threshold $U_k^{\pm}(S^{(0)})$:

$$\text{up}: \qquad U_k^+(S^{(0)}) > U_i^-(S^{(0)}) \;\forall i \in I_1(S^{(0)})\;, \tag{2.10}$$

$$\text{down}: \qquad U_k^-(S^{(0)}) < U_i^+(S^{(0)}) \;\forall i \in I_0(S^{(0)})\;. \tag{2.11}$$

Example 2.2.1 *In Fig. 2.4a, the condition for the up transition from state* (00) *to be initiated by critical hysteron* $k^+(00) = 2$ *is* $U_2^+(00) < U_1^+(00)$*, and the stability condition is trivially satisfied. Similarly, the*

down transition from state (11) *produces one critical hysteron condition and no stability conditions. In contrast, the up and down transitions from the states* (01) *and* (10) *specify one stability condition and no conditions for the critical hysterons.*

Final inequalities.– A second set of inequalities arises from the requirement that the final state $S^{(l)}$ is stable. For the final state $S^{(l)}$ of a transition $S^{(0)} \rightsquigarrow S^{(l)}$ to be stable at the critical driving $U_0 := U_k^+(S^{(0)})$ where it is initiated, a set of switching thresholds $\{U_i^\pm(S)\}$ must obey the set of inequalities:

$$U_0 < U_i^+(S^{(l)}) \ \forall i \in I_0(S^{(l)}) \ , \tag{2.12}$$
$$U_0 > U_i^-(S^{(l)}) \ \forall i \in I_1(S^{(l)}) \ , \tag{2.13}$$

For a down avalanche at $U_0 = U_k^-(S^{(0)})$, the equations are identical.

Example 2.2.2 *For the transition* (10) $\downarrow$ (00) *(Fig. 2.4c), the stability of the final state* (00) *at* $U_1^-(10)$ *yields:*

$$U_1^-(10) < U_1^+(00) \ ,$$
$$U_1^-(10) < U_2^+(00) \ .$$

Intermediate inequalities.– While $l = 1$ transitions, like (10) $\downarrow$ (00) in the example of Fig. 2.4, only produce initial state and final state inequalities, each intermediate step in an avalanche of length $l > 1$ produces additional conditions to ensure that each intermediate step is unambiguous and proceeds as described. Consider again an avalanche initiated at $U_0 = U_k^+(S^{(0)})$ (for an up transition) or $U_0 = U_k^+(S^{(0)})$ (for a down transition). We now look at at an intermediate state $S^{(\lambda)}$ where for definiteness hysteron κ switches up, so $\kappa = k^+(S^{(\lambda)})$ For hysteron κ to be unstable at $U_k^\pm(S)$, while all other hysterons are stable, a set of switching thresholds $\{U_i^\pm(S)\}$ must obey the set of inequalities:

$$U_0 < U_i^+(S^{(\lambda)}) \ \forall i \in I_0(S^{(\lambda)}) \backslash \{\kappa\} \ , \tag{2.14}$$
$$U_0 > U_i^-(S^{(\lambda)}) \ \forall i \in I_1(S^{(\lambda)}) \ , \tag{2.15}$$
$$U_0 > U_\kappa^+(S^{(\lambda)}) \ . \tag{2.16}$$

Analogously, when hysteron κ switches down, $\{U_i^{\pm}(S)\}$ must obey the inequalities:

$$U_0 < U_i^{+}(S^{(\lambda)}) \ \forall i \in I_0(S^{(\lambda)}) \ , \tag{2.17}$$
$$U_0 > U_i^{-}(S^{(\lambda)}) \ \forall i \in I_1(S^{(\lambda)}) \backslash \{\kappa\} \ , \tag{2.18}$$
$$U_0 < U_\kappa^{-}(S^{(\lambda)}) \ . \tag{2.19}$$

Example 2.2.3 *Consider the* $l = 2$ *avalanche* $(00) \uparrow (01) \uparrow (11)$ *(Fig. 2.4d). The instability of hysteron 1 at the intermediate state* (01) *gives rise to the equations:*

$$U_2^{+}(00) > U_1^{+}(01) \ ,$$
$$U_2^{+}(00) > U_2^{-}(01) \ .$$

Note that between the cases where κ switches up and down, the inequalities involving the non-critical hysterons stay the same, and the only difference is a sign change in the inequality that involves κ – compare (2.16) and (2.19). The number of inequalities of each type is fixed: in general, there are $n-1$ initial state inequalities, which arise from the comparison of the critical hysteron k against every other hysteron. In addition there are n final inequalities, which specify that each hysteron in the final state $S^{(l)}$ is stable. Similarly, there are n intermediate inequalities for each of the states $S^{(1)}, \ldots, S^{(l-1)}$, which specify the stability of each hysteron in $S^{(\lambda)}$ under $U_k^{\pm}(S)$.

Full Graph

Combining the initial, intermediate and final inequalities, one obtains a set of inequalities that the switching thresholds must obey so that a given transition is realized. We see that, for example, the transition $(00) \uparrow (01) \uparrow (11)$ requires five inequalities: one initial inequality, two intermediate inequalities, and two final inequalities. In general, the number of inequalities per transition is $(l+1)n - 1$.

This approach constructs conditions on the level of individual transitions, and is therefore modular. To construct the necessary and sufficient conditions on the switching thresholds corresponding to a given t-graph or subgraph thereof, we simply combine the conditions of their respective transitions, as these graphs are nothing more than the collection of transitions from different initial states for a given $\{U_i^{\pm}(S)\}$. We note that there are often redundancies between these inequalities: for example, in Figure 2.4e, the inequality $U_2^{+}(10) > U_2^{-}(11)$ appears twice.

2.2.2 Partial order and matrix representation

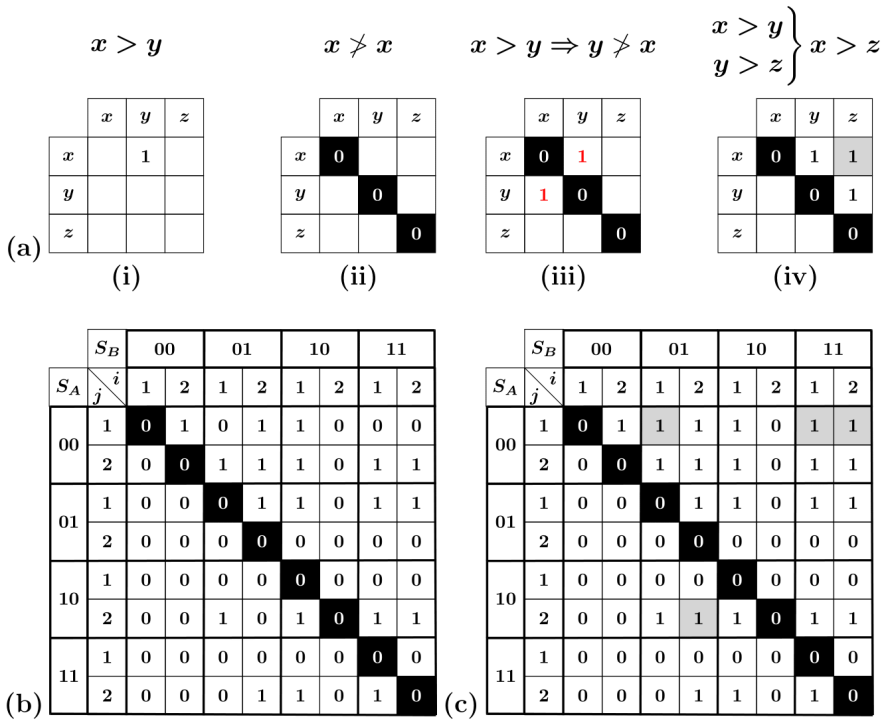


Figure 2.5: Partial order represented by adjacency matrices. (a) Representation of a partial order as an adjacency matrix (i) and three properties of a partial order: (ii) irreflexivity, shown by the diagonal highlighted in white-on-black; (iii) asymmetry, shown by a pair of entries highlighted in red, where $x > y$ rules out that $y > x$; and (iv) transitivity, where the induced inequality $x > z$ is highlighted in gray. (b) Example of the list of design inequalities shown in Fig. 2.4e in adjacency matrix form. For the sake of readability, we index the switching thresholds $U_i^{\pm}(S)$ via the state S and hysteron index i. The matrix thus contains $n \times n$ blocks of inequalities which concern the same states S_A, S_B as shown by thicker lines. (c) Transitive closure of the adjacency matrix shown in (b); note the addition of induced inequalities, highlighted in gray.

Considering the design inequalities from section 2.2.1, we observe that they specify a *partial order* on the switching thresholds $U_i^{\pm}(S_j)$. To see this, note that the design inequalities are a collection of pairwise inequalities of the form $U_i^{\pm}(S_A) > U_j^{\pm}(S_B)$. We briefly discuss how this helps our understanding of the design inequalities; for a more detailed overview

of partial orders, we refer to established literature from discrete mathematics [39, 40].

We choose to represent a partial order as an adjacency matrix, where a 1 at position (x, y) indicates the presence of a design inequality $x > y$, and a 0 indicates no relation (Fig. 2.5a-(i)). It is useful at this point to recall the general properties of partial orders – irreflexivity, asymmetry, and transitivity. First, *irreflexivity* entails that $x \not> x$ (Fig. 2.5a-(ii)). Second, a partial order relation is *asymmetric*, such that if $x > y$, then $y \not> x$ (Fig. 2.5a-(iii)). Finally, a partial order has *transitivity*, meaning that if $x > y$ and $y > z$, then $x > z$ (Fig. 2.5a-(iv)).

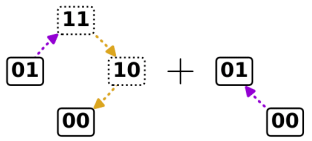
It is straightforward to convert the inequalities tabulated in Fig. 2.4f to a square matrix, where the rows and columns represent the $n \times 2^n$ switching thresholds (Fig. 2.5b). This conversion also immediately gets rid of redundancies - note that Fig. 2.5b contains only seventeen inequalities whereas Fig. 2.4e contained twenty-two. This matrix is not yet sufficient to represent a partial order, however, because the third property – transitivity – is not satisified. To obtain a proper representation, we must construct a matrix that also includes all induced inequalities: the *transitive closure* [40]. This is achieved by using a transitive closure algorithm such as Warshall's algorithm [41].

We emphasize that, while the specific set of design inequalities that correspond to a given t-graph topology may depend on the algorithm used to generate it, the partial order associated with each t-graph is unique. In turn, this partial order corresponds to a finite (and possibly very large) number of *total* orders of the switching thresholds. We further discuss the counting of these total orders in section 3.2.

2.2.3 Realizability of t-graphs

While any target t-graph can be mapped to a set of design inequalities, design inequalities may at times contradict each other, such that they are not consistent with any set of switching thresholds. Hence, the question of existence of a set of switching thresholds that realize a target t-graph is tantamount to checking the satisfiability of the set of design inequalities. To solve the general problem of checking whether a set of inequalities is consistent, one can use the classical method of Fourier-Motzkin elimination [42], or alternatively, more refined linear programming methods such as the simplex algorithm [43].

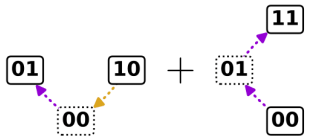
For our sets of pairwise inequalities, this general methodology is not



(a)

(b)

S_A	S_B / j \ i	00		01		10		11	
		1	2	1	2	1	2	1	2
00	1	0	1	1	1	0	0	1	0
	2	0	0	1	1	0	0	1	0
01	1	0	1	0	1	0	0	1	0
	2	0	0	0	0	0	0	0	0
10	1	0	1	1	1	0	0	1	0
	2	0	1	1	1	0	0	1	0
11	1	0	0	0	0	0	0	0	0
	2	0	1	1	1	0	0	1	0



(c)

(d)

S_A	S_B / j \ i	00		01		10		11	
		1	2	1	2	1	2	1	2
00	1	0	1	1	1	1	0	1	1
	2	0	0	1	1	1	0	1	1
01	1	0	1	0	1	1	0	1	1
	2	0	0	0	0	0	0	0	0
10	1	0	1	1	1	0	0	1	1
	2	0	1	1	1	1	0	1	1
11	1	0	0	0	0	0	0	0	0
	2	0	0	0	0	0	0	0	0

Figure 2.6: Illustration of impossible subgraphs and corresponding design inequalities. (a) Tentative combination of transitions $00 \uparrow 01$ and $01 \uparrow 11 \downarrow 10 \downarrow 00$. (b) Corresponding design inequalities shown as an adjacency matrix, with entries induced via transitivity highlighted in gray. The entries (00, 2; 01, 1) and (01, 1; 00, 2) show that asymmetry is broken (highlighted in red). (c) Tentative subgraph containing transitions $00 \uparrow 01 \uparrow 11$ and $10 \downarrow 00 \uparrow 01$. (d) Corresponding design inequalities. The three pairs of entries highlighted in red show that the asymmetry condition is broken; note that this breaking of asymmetry only becomes visible via the transitive closure (highlighted in gray).

needed, because inconsistencies show up as violations of asymmetry, i.e., pairs of inconsistent inequalities of the form $x > y$ and $x < y$ occurring simultaneously. Such inconsistencies can be directly inferred from the adjacency matrix. We illustrate our approach by discussing two examples

of non-realizable t-graphs.

First we consider a target t-graph that contains a subgraph consisting of the $l = 1$ up transition $(00) \uparrow (01)$, and the $l = 3$ up transition $(01) \uparrow (11) \downarrow (10) \downarrow (00)$ (Fig. 2.6a). For this example, there is a direct contradiction between two of the design inequalities: the stability of the final state (01) of the transition $(00) \uparrow (01)$ requires $U_2^+(00) < U_1^+(01)$, while the stability of the final state 00 of the transition $(01) \uparrow (11) \downarrow (10) \downarrow (00)$ requires $U_2^+(00) > U_1^+(01)$ (Fig. 2.6b).

Second, we consider Fig. 2.6c. For this example the contradiction in the design inequalities is not directly visible from the original design inequalities, but becomes manifest once the transitive closure is constructed. To see this, note that the up transition $(00) \uparrow (01) \uparrow (11)$ requires that $U_2^+(00) > U_1^+(01)$, while the down transition $(01) \downarrow (00) \uparrow (10)$ requires $U_1^+(01) > U_2^-(10)$ and $U_1^-(10) > U_2^+(00)$. Together, this leads to the inconsistent chain of inequalities $U_2^+(00) > U_1^+(01) > U_2^-(10) > U_2^+(00)$ (Fig. 2.6d). Hence, this target graph can not be realized.

We emphasize that we focus here on realizability in a mathematical sense, i.e., asking if there is a partial order of the switching thresholds that realizes a certain t-graph. The question of physical realizability is a separate issue. We note that for specific physical models, the switching thresholds can not be chosen arbitrarily. For example, when the switching thresholds arise from pairwise interactions [10, 26] this imposes constraints on the switching thresholds, which further limit the set of realizable t-graphs, beyond mere considerations of partial order. Other physical constraints that have been considered include interactions being symmetric [8, 37] and global coupling, which arises when e.g. hysterons are serially coupled [6]. These physical considerations complicate the design inequalities beyond a mere partial order, such that one needs to fall back on generic linear programming techniques. However, the space of t-graphs as a whole can often be simplified for physical models, as we discuss in section 3.1. These models, while of great interest, deserve individual consideration, which goes beyond the general framework established here.

2.2.4 Solving the design inequalities

To conclude, we discuss how explicit solutions for the switching thresholds $\{U_i^{\pm}(S)\}$ can be constructed for a given set of (consistent) design

inequalities. For our sets of pairwise inequalities, an explicit solution can be constructed by finding a total order (or 'linear extension' [32]) that satisfies the partial order specified by the design inequalities. We use a topological sorting algorithm such as Kahn's algorithm [44,45] to produce a random linear extension, without regard for the range and distributions of gaps between switching thresholds.

To convert such a random linear extension to an explicit solution, we set the switching thresholds to be equidistant with a spacing of $\epsilon = \left(n \cdot 2^n\right)^{-1}$, and set the lowest switching threshold to $\epsilon/2$. This is a convenient choice because it guarantees that the switching thresholds lie within the range $[0, 1]$, and the system is in the saturated states (00...), (11...) at driving values of 0 and 1 respectively.

Although we have emphasized that the design inequalities for a given t-graph topology only impose a partial order relation, additional constraints - for example, those imposed by the use of a specific model for $\Delta_i^{\pm}(S)$ - can lead to more complex sets of inequalities. In these cases, one can fall back on general linear programming methods such as the simplex algorithm [43] to solve the full set of inequalities. We note that, to make use of linear programming, one must first transform the set of strict design inequalities to a set of non-strict design inequalities $U_i^{\pm}(S_A) - U_j^{\pm}(S_B) \geq b$, with b a small positive number. Like ϵ in the method described above, b here sets an explicit spacing between switching thresholds, which is necessary because the problem is scale-invariant otherwise.

Altogether we have outlined how for any t-graph or subgraph, we can construct corresponding design inequalities. These design inequalities allow us to check if a t-graph is realizable and, if so, to generate a random set of switching thresholds that realizes the graph. We make use of this in section 3.1 to generate all valid t-graphs for $n = 2$. Moreover, the process of checking solvability and finding a solution is facilitated by the observation that the design inequalities only specify a partial order on the switching thresholds (section 2.2.2). This observation has further implications for the statistical weight of t-graphs, as we will discuss in section 3.2.

2.3 Outlook and Conclusions

In this chapter we have discussed the relation between design parameters and t-graphs for the most general model for interacting hysterons. We

introduced *scaffolds* which allow us to precisely define scrambling and facilitate the systematic construction of transitions including avalanches. We presented a systematic method for obtaining the set of design inequalities for a given t-graph (or subgraph), discussed the corresponding partial order of the switching thresholds, and used the partial order to straightforwardly determine the realizability of t-graphs.

We close this chapter with two observations regarding the critical and noncritical switching thresholds and the significance of the scaffold for the design inequalities, and the relation between the ordering of the state switching thresholds and responses to specific driving protocols.

Critical and noncritical switching thresholds.— In the preceding text, we have described the design inequalities in terms of the *individual* switching thresholds $U_i^{\pm}(S)$. We note, however, that once a scaffold has been enforced and thus a distinction made between critical and noncritical switching thresholds, the noncritical switching thresholds are largely irrelevant for the transition graph topology.

An important corollary is related to race conditions, and the rules which are used to resolve these (section 2.1.2). We can distinguish between two types of race conditions: those where only a single critical hysteron (up or down) is unstable, and those where both critical hysterons are unstable. This latter type of race conditions can occur when an intermediate state is persistently unstable, i.e., $U^-(S) > U^+(S)$.

In general, race conditions of the first type are more easily resolved than those of the second type, because we can simply prescribe that the hysteron which flips is the critical hysteron. For example, in some contexts, a rule has been used where the most unstable hysteron is flipped [14, 37]. Under this rule, the scaffold is respected, and the noncritical switching thresholds can be ignored entirely. By contrast, for race conditions of the second type, the 'most unstable flips' rule requires that the exact values of the two critical switching thresholds are known. This can be troublesome, as it means that the design inequalities can no longer be described purely by a partial order of the switching thresholds (section 2.2.2).

All in all, the role of the noncitical switching thresholds can be easily trivialized by using a rule to resolve race conditions. However, such a rule should also consider how race conditions are resolved when both critical hysterons are unstable. Moreover, it can be physically relevant to investigate rules where other hysterons than the critical hysteron are

allowed to flip – for example, where a critical and a noncritical hysteron flip at the same time [46]. For these reasons, we have not applied such a rule in this general framework.

Total order and finite state machines.— The same t-graph *topology* can correspond to many total orders of the switching thresholds (section 3.2.1). However, these total orders can lead to different responses when the system is subjected to specific driving protocols, as can be seen by considering subharmonic loops under cyclical driving [10, 14], and breaking of return point memory under asymmetric driving [31]. In other words, while t-graphs describe the response to arbitrary driving, extracting qualitative information, such as whether there is a cyclical driving protocol that produces a subharmonic orbit is not easy, and cannot be decided based on the graph topology alone [6]. One strategy to effectively describe the response of systems characterized by t-graphs to specific driving inputs, such as cyclic driving or sequences of driving pulses, is to use finite state machines (FSMs) [6]. In brief, the idea is that any finite t-graph has only a finite number of relevant switching thresholds, such that the number of, e.g., pulses in U that result in a different response is also finite. Defining a finite set of symbols $\{a_i\}$ then allows us to determine a transition table $S' = a_i(S_j)$ that maps an initial state S_j and driving a_i to a final state S', and therefore defines a FSM. This framework is effective in identifying specific types of responses, such as transients, for arbitrary t-graphs [6]. Moreover, this approach facilitates engineering applications, such as counting [47] and smart actuation for soft robots under a single input [6, 24, 48, 49].

The FSM framework is deeply linked with the total order of the state switching thresholds, with preliminary explorations indicating that any permutation in the critical switching thresholds produces a different transition table, and hence a different FSM. Hence, in addition to the design inequalities required for the t-graph topology, a more restricted partial order is required to ensure that the driving protocol leads the specific desired behavior, or to a specific FSM. Open questions for the future include how specific classes of hysteron interactions lead to, or limit, the associated FSMs and their computational power, and how to effectively design a (minimal) set of hysterons (and signals) that realize a target FSM [6, 50].

CHAPTER 3

The Space of Possible T-graphs

In this chapter, we consider the construction and organization of all t-graphs for a given number of hysterons n. In the Preisach model, the number of scaffolds grows with the number of hysterons n as $n!$, and each of these $n!$ scaffolds is associated with a single *Preisach graph*. Here a Preisach graph only includes transitions between reachable states; we do not include Garden-of-Eden states in this definition, because these can be persistently unstable depending on the ordering of $u_i^{\pm}$ [36].

Numerical explorations of models of interacting hysterons have shown that even weak interactions lead to a dramatic increase in the number and complexity of t-graphs for a given number of hysterons [10, 13, 14]. For example while the Preisach model yields two Preisach graphs for $n = 2$ and six for $n = 3$, numerical sampling reveals a much larger number of t-graphs for interacting hysterons (13 t-graphs for $n = 2$, excluding GoE states, and more than 1.5×10^4 t-graphs for $n = 3$) [10].

We consider two questions:

1. How can we understand the combinatorial explosion of the number of t-graphs and how are they organized?

2. How can we understand the wide variation in statistical weight of t-graphs in design space?

To address the first question, we start by considering how all scaffolds can be generated, and derive a simple expression for their number. We further show that all possible transitions for a given scaffold can be organized in finite binary *trees*, one for each state and initial transition

direction (up or down). Combining scaffolds and trees, we obtain all *candidate graphs*, that need to be checked for realizability using their design inequalities. This method allows us to systematically label all candidate t-graphs - the complexity lies in checking their realizability. As specific examples, we count and construct all possible t-graphs for $n = 2$, all scaffolds for $n = 3$ and all t-graphs for $n = 3$ that contain one or two short avalanche(s) (section 3.1).

We then address the second question by computing the statistical weight of t-graphs in design space. In particular, the number of total orders consistent with a given partial order is a proxy for the volume in design space, thus giving insight in the widely varying statistical weight of distinct t-graphs, as well as the percentage of parameter space that produces self-loops and/or race conditions) [10, 13, 32] (section 3.2). Together, the combination of the systematic construction of design inequalities and the focus on the scaffold (see Chapter 2) may facilitate the practical design of (meta)materials that realize targeted pathways, memory effects and embodied computations.

3.1 Constructing and Organizing All Graphs

In this section we consider the space of all t-graphs. While the profusion of t-graphs with $n \geq 3$ makes brute force explorations unfeasible [10], we build here on the observation that any t-graph is created by combining transitions which proceed on a scaffold (sections 2.1.2, 2.1.3). Thus, to systematically explore the space of all t-graphs, we proceed in three steps. First, for given n, we create and count all scaffolds (section 3.1.1). Second, for any state in a scaffold, all possible (avalanche) transitions can be organized by finite binary trees (section 3.1.2). Third, by combining scaffolds and selecting transitions from the binary trees, all *candidate* t-graphs can be systematically generated. Only a fraction of these are consistent with the corresponding design inequalities, and these are the sought-after valid t-graphs. We use this approach to determine all valid t-graphs for $n = 2$, all scaffolds (and all avalanche-free t-graphs) for $n = 3$, and a loose upper bound on the number of t-graphs for $n = 3$ (section 3.1.3). Our approach uncovers the root cause of the multiplicity and complexity of the space of all t-graphs: as each state allows for a number of potential transitions, the multiplication of these numbers very quickly leads to astronomical numbers, while at the same time, the combination of longer and longer avalanches eventually leads to many t-graphs of

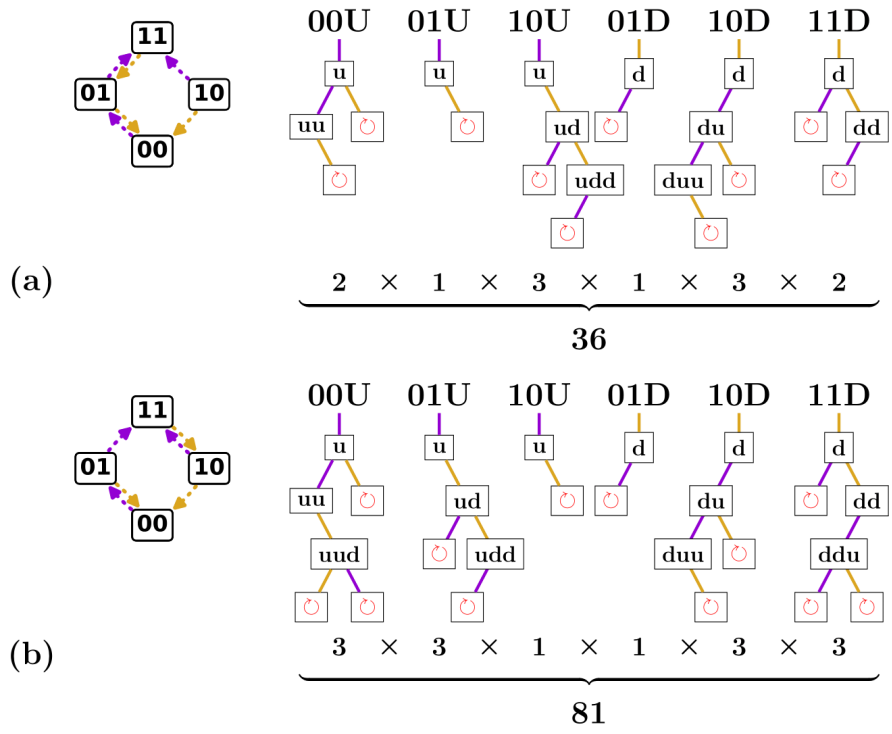


Figure 3.1: Binary trees of possible avalanches for $n = 2$. a) First of two possible scaffolds for $n = 2$, and associated binary trees of avalanches per transition. We label transitions by their starting state $S^{(0)}$ and their up or down direction marked respectively as U or D (see also Fig.2.4). Each tree node represents a transition $S^{(0)} \to \cdots \to S^{(l)}$, characterized by a starting state and up/down sequence - please note the difference between uppercase and lowercase labels, as U and D signify the initial direction of a transition, whereas u and d signify intermediate steps. A length-l transition can be extended to a transition of length $l + 1$ by an up flip if $S^{(l)} = (00...)$, by a down flip if $S^{(l)} = (11...)$, and by either an up or down flip otherwise. Branches of the tree terminate where there is a self-loop, indicated in red. The number of avalanches in each tree is indicated below each transition; the product of these counts gives the number of avalanches for the given scaffold. b) Second of two possible scaffolds for $n = 2$, and associated binary trees of avalanches per transition. Note that the structure of each tree is as in (a), but the nodes at which self-loops are encountered are different.

which the design inequalities are inconsistent. Thus, while the number of

valid t-graphs for general n is presumably much smaller than the number of candidate graphs, the complexity of the underlying design inequalities makes it challenging to systematically construct - or even enumerate - these graphs.

3.1.1 Scaffolds

We now consider the multiplicity and organization of the scaffolds. To aid us in counting the scaffolds, we first define several useful attributes of the scaffold:

Definition 3.1.1 (*Magnetisation*) *Let $S = (s_1, \ldots, s_n)$ be a state of collection of n hysterons. We define the* magnetization $m := \Sigma_i s_i$.

Definition 3.1.2 (*Up/down boundary and main loop*) *For a given scaffold $k^{\pm}(S)$, the* up (down) boundary *is the monotone sequence of up (down) passages that connect the saturated states* $(00\ldots)$ *and* $(11\ldots)$.

The up and down boundary together form the main loop *of the scaffold [30, 36].*

We break the relabeling symmetry of the hysterons by requiring that the up boundary of the main loop is fixed, so that the hysterons flip in the order $n, n-1, \ldots, 1$ [30]. With this convention, there are $n!$ possible down boundaries and hence $n!$ main loops, which can be labeled by the sequence of down transitions. For example, the main loop of the scaffold in Fig. 3.1a, $(00) \uparrow (01) \uparrow (11) \downarrow (01) \downarrow (00)$, can be denoted as $(1, 2)$ [30, 36].

The number $N_S(n)$ of scaffolds for n hysterons can now be obtained from a simple combinatorial argument. For each up (down) transition, the number of possible critical hysterons $n^{\pm}(S)$ equals the number of hysterons in phase 0 (1), so that $n^+(S) = n - m$ and $n^-(S) = m$, where m follows from S straightforwardly. As the number of states with magnetisation m equals $\binom{n}{m}$, we immediately find that

$$N_S = \frac{\prod_S (n^+(S)\ n^-(S))}{n!} = \frac{\left(\prod_{m=1}^{n} m^{\binom{n}{m}}\right)^2}{n!}\ , \tag{3.1}$$

where the division by $n!$ takes care of the relabeling symmetry.

The scaffolds can simply be labeled by the values of the critical hysterons, and can be organized by their main loop and by the minimal

number of scrambled passages. First, each main loop allows for the same number of scaffolds ($N_S/n!$) – to see this, note that, irrespective of the main loop, the same number of choices of up and down transitions is available at each value of m. Second, for each main loop we can define one unscrambled or Preisach scaffold, where all critical transitions follow the order of the up and down transitions along the main loop; all other scaffolds are obtained by scrambling, i.e. changing one or more critical hysterons. This suggests that we can characterize the complexity of the scaffold by the minimal number of such changes.

The scaffolds are far less numerous than the t-graphs. For example, for $n = 3$, there are only 96 scaffolds in total, and sixteen scaffolds per main loop. For $n = 2$ we see that $N_S = 2$, and so there is only a single scaffold per main loop; this reaffirms that scrambling can only occur for $n > 2$. Because they are less numerous, scaffolds facilitate exploration of t-graphs.

3.1.2 Binary trees of transitions

We now discuss how, for a given scaffold, all (avalanche) transitions starting at a given state $S^{(0)}$ and initial direction can be generated. We note that, because an avalanche may visit states only once due to the no-loop condition, and the magnetization spans a finite range, the number of transitions starting at a given state and initial direction is finite. We formulate the following algorithm for constructing all such possible transitions:

Algorithm 3.1.1 *Let $\{k^{\pm}(S)\}$ be a given scaffold. For each initial state $S^{(0)}$ and each direction (up/down):*

1. *Initialize the queue as consisting only of the transition $S^{(0)} \to S^{(1)}$, where $S^{(1)}$ is the landing state reached by flipping $k^{\pm}(S^{(0)})$.*
2. *Let $S^{(0)} \to \cdots \to S^{(l)}$ be the next transition in the queue.*
   (a) *If $S^{(l)} \neq (11\ldots)$, attempt to extend it in the up direction by flipping $k^{+}(S^{(l)})$. If the resulting transition $S^{(0)} \to \cdots \to S^{(l+1)}$ is not a self-loop ($S^{(l+1)} \notin \{S^{(0)}, \ldots, S^{(l)}\}$), add it to the end of the queue.*
   (b) *Similarly, if $S^{(l)} \neq (00\ldots)$, attempt to extend it in the down direction by flipping $k^{-}(S^{(l)})$. If the resulting transition is not a self-loop, add it to the end of the queue.*

(c) Save the current transition $S^{(0)} \to \cdots \to S^{(l)}$ as a possible transition for the chosen state and direction, and remove it from the queue.

3. Repeat step (2) until the queue is empty.

Algorithm 3.1.1 generates $2(2^n - 1)$ sets of transitions. We note that these possible transitions for each state and initial direction can be organized in a finite binary tree (Fig. 3.1).

Example 3.1.1 *We consider the $n = 2$ scaffold with down boundary (1, 2), and focus on the up transitions starting from* (00) *(Fig. 3.1a). First, we construct the $l = 1$ transition 00u - note the scaffold stipulates that $k^+(S) = 2$, so that 00u corresponds to the transition* (00) ↑ (01)*. We now check if the $l = 2$ extensions of this transition, 00uu and 00ud, are allowed. Using the scaffold, we find that 00uu corresponds to the valid transition* (00) ↑ (01) ↑ (11)*, whereas 00ud leads to a self-loop and is forbidden; we terminate this branch (Fig. 3.1a). Extending 00uu, we find that 00uuu (not drawn) does not exist as there are no hysterons to flip up, and 00uud leads to a self-loop. All branches have now terminated, so we find that the only valid up sequences for transition 00U are 00u and 00uu. Repeating this procedure for all states and initial directions, we can construct six binary trees for this example scaffold containing twelve potential transitions in total(Fig. 3.1a). For $n = 2$ there are only two scaffolds, and for the second scaffold we can construct fourteen potential transitions (Fig. 3.1b).*

3.1.3 Constructing all t-graphs

Given the $2(2^n - 1)$ sets of possible transitions, one can construct a 'candidate' graph by selecting one of the transitions for each initial state and direction; if the corresponding design inequalities are consistent, such a candidate graph is a valid t-graph (section 2.2.3). By iterating over all scaffolds and selecting (avalanche) transitions from the corresponding binary trees, one can thus systematically generate all valid t-graphs. Formally, our algorithm is as follows:

Algorithm 3.1.2 *Let n be a given number of hysterons.*

1. *Generate all scaffolds for n hysterons (section 3.1.1).*
2. *For each scaffold generated in (1):*
   (a) *Construct all $2(2^n - 1)$ sets of possible transitions (Algorithm 3.1.1).*
   (b) *Generate all candidate graphs by constructing all possible combinations of transitions from the $2(2^n - 1)$ sets.*
   (c) *Check for each candidate graph whether the design inequalities are valid (section 2.2.3); if so, add it to the list of valid t-graphs.*

For the $n = 2$ case, by multiplying the sizes of all binary trees of transitions, we find that the first scaffold yields $2 \times 1 \times 3 \times 1 \times 3 \times 2 = 36$ candidate graphs (Fig. 3.1a), while the second scaffold yields 81 candidate graphs (Fig. 3.1b), yielding a total of 117 $n = 2$ candidate graphs. We observe that the list of candidate graphs is often dominated by a single or small set of scaffold(s), due to the combinatorial explosion associated with large trees.

To determine all valid t-graphs, we simply check for each candidate graph whether it is realizable (section 2.2.3). For $n = 2$, we find that 35 of the 117 candidate graphs are realizable. When we exclude Garden-of-Eden states from the graph topology (section 2.1.3) this number reduces to only thirteen. When we ignore the intermediate states of the avalanches, the number reduces further to eleven. All of these graphs were found previously using sampling [10]; we can now state conclusively that these are the only possible graphs for $n = 2$ interacting hysterons.

The number of candidate graphs to be checked increases very rapidly with the number of hysterons. For just $n = 3$ hysterons, we can systematically construct all trees for each of the 96 possible scaffolds, obtain

all candidate graphs by multiplying the sizes of these trees for each scaffold, and then sum over the scaffolds; doing so, we obtain 4725217377852 candidate graphs. All of these candidate graphs need to be individually checked for realizability; thus, it is not feasible to use this method to find all realizable t-graphs for more than two interacting hysterons.

However, the enumeration of scaffolds and trees allows us to gain insight into the space of possible t-graphs. For example, the 96 scaffolds for $n = 3$ produce exactly 96 avalanche-free t-graphs. When GoE states are excluded, this number even reduces further to 35. We note in passing that a total order of the state switching thresholds can easily be constructed such that an avalanche-free t-graph is obtained, for any choice of the scaffold. For example, one can use a 'staircase' construction, where one first orders the state switching thresholds according to magnetization as $U^-(m = 1) < U^+(m = 0) < U^-(m = 2) < U^+(m = 1) < U^-(m = 3) \ldots$, and then arbitrarily choose an order of the state switching thresholds at each magnetization to obtain a well defined total order. By substituting these state switching thresholds $U^{\pm}(S)$ for the appropriate hysteron switching thresholds $U_i^{\pm}(S)$, one can obtain a total order that produces an avalanche-free t-graph for any scaffold. Thus, all 96 avalanche-free candidate graphs for $n = 3$ (or 35 when excluding GoE states) are valid t-graphs.

We now illustrate how one can use the binary tree structure to include avalanches step by step. Considering again the $n = 2$ transitions in Fig. 3.1, we first focus on only the $l = 2$ avalanches. We see that there are four of these $l = 2$ avalanches per scaffold. For the scaffold with main loop (1, 2), the corresponding sequences are 00uu, 10ud, 10du and 11dd - the sequences 00ud, 01du are forbidden because of self-loops. Similarly, the scaffold with main loop (2, 1) allows for four $l = 2$ transitions 00uu, 01ud, 10du and 11dd. Thus, in total, we can construct eight candidate graphs with only a single $l = 2$ avalanche. We find that all these candidate graphs are realizable.

We can apply the same approach for $n = 3$. Considering the binary trees of transitions for each of the 96 scaffolds, we find that each of the scaffolds allows for either fourteen, sixteen or eighteen possible $l = 2$ transitions - as we saw for $n = 2$, this number depends on the number of $l = 2$ transitions that lead to self-loops, and because these transitions must come in pairs, the total number of $l = 2$ transitions is even. Summing over all scaffolds, we find that there are 1440 candidate graphs with a single $l = 2$ transition. Again checking for each of these candidate

graphs whether the design inequalities are consistent, we find that all these graphs are realizable. We believe that this phenomenon - where *all* candidate graphs with a single $l = 2$ avalanche are realizable - extends to general n. To see that all such graphs are realizable, we need to construct a consistent order for the switching thresholds. To do so, one starts from a 'staircase' construction to create a total order for the t-graph without avalanches, and then only modifies the switching thresholds responsible for the avalanche, leading to a minor change in the ordering.

For the next step in complexity, we have two options: we can either consider t-graphs with a single $l = 3$ avalanche, or t-graphs which have two $l = 2$ avalanches. We note that whereas candidate graphs with a single $l = 2$ avalanche appear to always be realizable, neither candidate graphs with a single $l = 3$ avalanche nor those with two $l = 2$ avalanches are necessarily realizable, as can be seen from the example subgraphs in Figure 2.6.

We first consider the case of a single $l = 3$ avalanche, once again starting with the simple $n = 2$ case shown in Fig. 3.1. Like in the $l = 2$ case, we can simply count the number of $l = 3$ transitions in Fig. 3.1 to find that the scaffold with main loop (1, 2) has two possible $l = 3$ transitions (10udd and 10duu) and the scaffold with main loop (2, 1) has four (00uud, 01udd, 10duu and 11ddu). Thus, one can construct six candidate graphs with a single $l = 3$ avalanche. Checking the design inequalities, we find that two of these are realizable. Similarly, for $n = 3$ there are 1488 possible $l = 3$ avalanches and thus 1488 candidate graphs with a single $l = 3$ avalanche. We find that 672 of these candidate graphs are realizable.

Constructing and counting all graphs with two $l = 2$ avalanches is slightly more demanding: in Fig. 3.1, we must now find all possible pairs of $l = 2$ transitions. Let us first consider the scaffold with main loop (1, 2). We note that there are four combinations of state and initial direction that allow for a $l = 2$ transition (00U, 10U, 01D and 11D), out of which we must choose two: the number of ways in which this can be done is $\binom{4}{2} = 6$. Furthermore, each of the initial states and directions 00U, 10U, 01D and 11D has only a single possible $l = 2$ avalanche, namely 00uu, 10ud, 01du and 11dd respectively. Thus, for the $n = 2$ scaffold with main loop (1, 2), there are six possible pairs of $l = 2$ avalanches. The scaffold with main loop (2, 1) gives another six pairs, so that there are a total of twelve candidate graphs that have two $l = 2$ avalanches. Once again checking whether the design inequalities are consistent, we find that

eight of these are realizable. For $n = 3$, using the same methodology, we find 9864 candidate graphs with two $l = 2$ avalanches, and checking whether the design inequalities are consistent, we find that 9000 of these are realizable.

Generally speaking we see that, when even a few avalanches are included, the number of realizable t-graphs mushrooms, eventually becoming intractable. However, as each step of an avalanche includes additional design inequalities, we expect that more avalanche steps lead to less total orders consistent with the design inequalities, and hence a smaller volume in design space (see section 3.2) – such t-graphs, though numerous, are thus statistically rare [10]. Moreover, many of the interesting features of t-graphs rely on scrambling and the scaffold structure, rather than avalanches, and our method of separating these thus gives practical tools to explore the space of t-graphs.

We note that when the switching thresholds are restricted by specific physical considerations, like pairwise interactions, avalanches or combinations thereof might be forbidden from the outset, thus greatly reducing the number of candidate graphs. A striking example is provided by serially coupled hysterons [6], where the only possible scaffolds are Preisach scaffolds, and the only possible avalanches are $l = 2$ antiferromagnetic avalanches (an up flip followed by a down flip, or vice versa). Furthermore, avalanches involving the same pair of hysterons i, j are grouped together. As a result of these constraints, for three serially coupled hysterons there are only 45 candidate graphs, out of which 44 are realizable [6]. We further discuss restricted models, including the serially coupled case, in Chapter 5.

3.2 Statistical Weight of T-Graphs

In this section, we apply our framework to gain insight into the t-graph probabilities that were found using sampling [10]. We first use the design inequalities to quantify the statistical weight of a single t-graph (section 3.2.1). We then apply this method to all $n = 2$ t-graphs found in section 3.1, then find the percentage of parameter space that produces 'ill-defined' responses – i.e., self-loops and/or race conditions (section 3.2.2).

3.2.1 Domain in parameter space and counting total orders

Previously, the parameter space of switching thresholds has been explored through random sampling [10]. We now show how the statistical weight of a target t-graph can be quantified via the design inequalities, and corresponding partial order.

To start with, for each partial order there are one or more total orders which satisfy that partial order (or 'linear extensions', see section 2.2.2) [51,52]. The problem of generating all linear extensions for a given partial order is conceptually similar to that of generating a random linear extension, and several algorithms have been proposed based on topological sorting [53, 54, 55]. Yet, the computational time required blows up rapidly for more complex partial orders, and the general problem of generating all linear extensions - or even counting these - is in fact known to be #P-complete [52,56]. For $n = 2$, however, the number of inequalities is small, and so the problem of finding all linear extensions is manageable. Using a method based on successive counting of the number of downsets [57], we find that for example the graph in Fig. 2.4a is associated with eighteen total orders of the switching thresholds.

As observed by Brightwell and Winkler [56], the problem of counting the number of linear extensions is closely related to that of computing the volume of a polyhedron. Namely, since there are $(n \cdot 2^n)!$ possible permutations of the switching threshold order, and by symmetry each total order takes up the same volume in parameter space, the fractional volume of a t-graph is obtained by dividing its corresponding number of total orders by $(n \cdot 2^n)!$. Applying this to the example t-graph in Fig. 2.4a, one obtains a fractional volume of $18/8! \approx 4.5 \times 10^{-4}$.

We check this result by directly computing the volume bounded by the design inequalities. As each design inequality forms a codimension-1

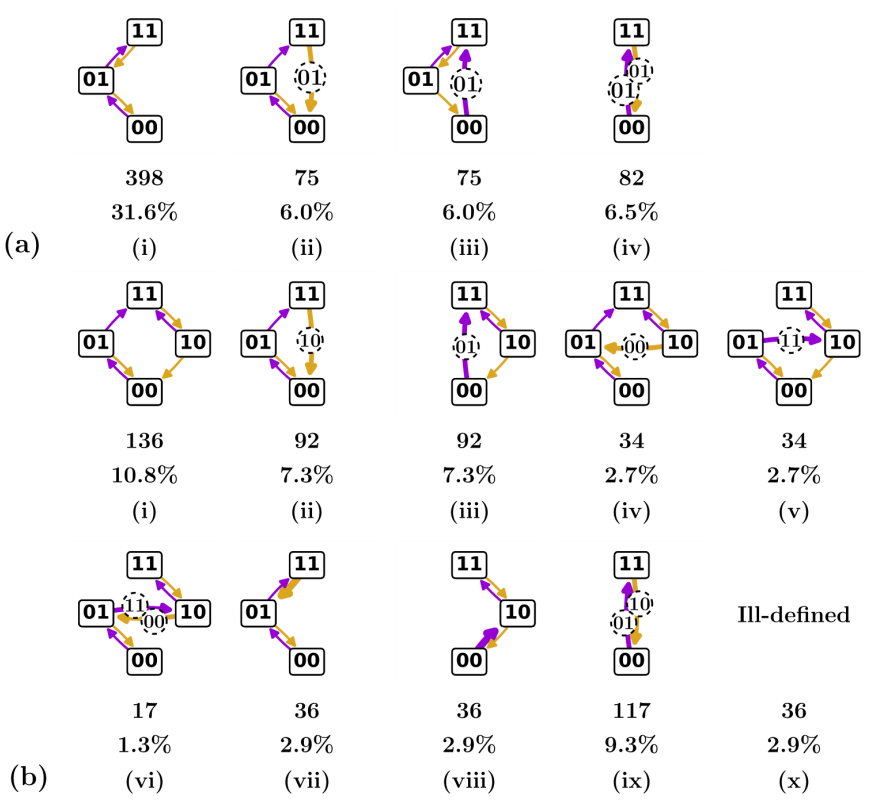


Figure 3.2: The thirteen $n = 2$ t-graphs found via Algorithm 3.1.2; here we ignore GoE states. Note that, when intermediate states are ignored, graphs (a)-(ii) and (b)-(ii), and graphs (a)-(iv) and (b)-(ix) are equal, leading to the same eleven t-graphs as found previously via numerical sampling [10]. The corresponding number of total orders and associated percentages of parameter space, when eliminating simple self-loops, are shown below each graph. The sum of total order counts (1224) is higher than that obtained when GoE states are included (850). This is because GoE states are now allowed to be persistently unstable, and transitions from GoE states can feature race conditions and self-loops (see 2.1.2). (a) T-graphs, total order counts and percentages for the $n = 2$ scaffold with main loop (1, 2) (see also Fig. 3.1). (b) T-graphs, total order counts and percentages for the $n = 2$ scaffold with main loop (2, 1). In panels (vii) and (viii), thicker arrows indicate $l = 3$ avalanches; the full transition paths are (11) ↓ (10) ↓ (00) ↑ (01) and (00) ↑ (01) ↑ (11) ↓ (10) respectively.

hyperplane in the design space, each t-graph corresponds to an intersection of half-spaces, which is a convex polyhedron[1] [58]. This polyhedron is unbounded: we can arbitrarily increase the switching thresholds for a given graph as long as their order remains the same. Following the example of Keim and Paulsen [14], we generate the vertices of this polyhedron to generate a convex hull, and compute its volume using appropriate Python packages. To ensure the volume is finite, we set $U_i^{\pm}(S) \in [0, 1]$ for all switching thresholds. Using this approach, we indeed find a fractional volume of 4.5×10^{-4} for our example t-graph, in agreement with our exact result.

3.2.2 The space of two-hysteron t-graphs

Our method for generating candidate graphs via scaffolds and trees (section 3.1) allows us to gain insight in the (relative) volume in design space occupied by different t-graphs. Here we focus in particular on the fraction of design space that produces self-loops and/or race-conditions; following [10], we collectively call these responses 'ill-defined'. To determine the probability under random sampling of an 'ill-defined' response, we first determine the total volume of design space, which is quantified by a finite number of total orders. We then determine the the volume in design space which is 'well-defined' by first constructing all t-graphs, as in section 3.1.3, and then counting the number of total orders associated with each t-graph (section 3.2.1). By comparing the sum of these volumes to the total volume of design space, we determine what fraction is ill-defined.

First off, since we are dealing with eight switching thresholds, the number of possible total orders equals $8!/2! = 20160$, where we divide by 2! to take care of the relabeling symmetry. Each scaffold takes up an equal partition in this parameter space, as can be seen from a symmetry argument: for given state S, no hysteron is more likely than another to be critical. Thus, for $n = 2$ each scaffold corresponds to 50 percent of parameter space, or 10080 total orders, where we note that these total orders may produce both race conditions and self-loops.

If we include GoE states, following section 3.1.3, we find that there are 35 well-defined t-graphs. From the design inequalities, we find that these correspond to 850 total orders of the switching thresholds. Similarly, excluding GoE states, the 13 well-defined $n = 2$ t-graphs correspond to

[1] Credit to M. Mungan, personal communication, 2022.

1977 total orders. This suggests that only a small part of parameter space yields well-defined t-graphs.

We have found that the vast majority of ill-defined t-graphs can be attributed to simple self-loops of length two – as discussed in section 2.1.2, in such a case a hysteron becomes unstable in both phases, as in $(00) \uparrow (01) \downarrow (00) \uparrow (01) \downarrow \ldots$. We note in passing that this situation cannot occur in the pairwise additive model (see Chapter 5), but can easily occur when all switching thresholds are chosen independently.
We can straightforwardly prohibit such simple self-loops by enforcing additional pairwise inequalities: there are four of such inequalities for $n = 2$, namely $U_1^+(00) > U_1^-(10)$, $U_2^+(00) > U_2^-(01)$, $U_1^+(01) > U_1^-(11)$ and $U_2^+(10) > U_2^-(11)$. We note that these inequalities are independent of each other and of the symmetry requirement $U_1^+(00) > U_2^+(00)$, and therefore, enforcing these inequalities reduces the number of possible total orders simply to $20160/2^4 = 1260$. Accordingly, the number of total orders per scaffold reduces to 630.

In the case where we include GoE states, the well-defined graphs still correspond to 850 total orders, as the mentioned four inequalities already emerge from each t-graph's design inequalities. Thus, by elimination of the trivial self-loops from the set of total orders, the fraction of parameter space taken up by well-defined $n = 2$ t-graphs becomes $850/1260 = 67.4\%$. When we exclude the GoE states, prohibiting simple self-loops via the same four inequalities yields 1224 total orders. We show the individual total order counts for each of the thirteen graphs, as well as the corresponding percentages of parameter space, in Fig. 3.2. The fraction of parameter space taken up by these well-defined $n = 2$ t-graphs becomes $1224/1260 = 97.1\%$, which is qualitatively consistent with earlier estimates, although those concerned a specific parametrization of the switching thresholds [10].

3.3 Outlook and Conclusions

In this chapter, we showed that the construction and organization of t-graphs can be seen as a three-step process: first, all scaffolds can easily be counted and generated; second, each transition in a scaffold can be selected from easily constructible finite binary trees that encode avalanches; third, the realizability of candidate graphs formed by combining scaffolds and trees can be checked using their design inequalities. As specific examples, we count all possible t-graphs for $n = 2$, and when we exclude

Garden-of-Eden states, we find thirteen distinct t-graphs; when we furthermore ignore differences between intermediate states, we find eleven t-graphs, consistent with an earlier estimate based on sampling the design space [10]. For $n = 3$, the number of scaffolds is 96, producing exactly 96 avalanche-free t-graphs, and when GoE states are excluded, there are 35 $n = 3$ t-graphs without avalanches; including avalanches, we find more than 4.5×10^{12} candidate t-graphs, of which around 1.5×10^4 have been found as actual t-graphs by random sampling [10]. To enter the complex design space, we show how we can count and determine the candidate graphs and realizable t-graphs for $n = 2$ and $n = 3$ that contain one or two $l = 2$ avalanches, or one $l = 3$ avalanche. We finally discussed the statistical weight of t-graphs in design space by relating it to the number of total orders consistent with a given partial order.

We stress that the rich structure of the t-graphs and design space can be seen as generalizing that of the Preisach model of non-interacting hysterons [9, 30, 33]. First, the $2n$ hysteron-dependent switching thresholds of the Preisach model are generalized to $n \cdot 2^n$ state-dependent switching thresholds. Second, while in the Preisach model the main loop determines all other transitions, here the scaffold can be seen as the generalization of the main loop. Third, while the ordering of the hysteron-dependent switching thresholds determines the different Preisach t-graph topologies, here we need to consider the orderings of the more numerous state-dependent switching thresholds. However, the occurrence of avalanches (including ambiguous avalanches and self-loops) has no obvious pendant in the Preisach model, and it is these avalanches that drive the combinatorial explosion and complexity of design space.

In closing, we note that avalanches play a mixed role. On the one hand, avalanches are not required for a variety of interesting phenomena, or even can obscure their essence: scrambling, transients and multiperiodic responses under cyclic driving do not require avalanches to occur [6, 14, 19, 32, 59]. Moreover, a scaffold-centered approach can simplify the design of experimental systems that exhibit transients [6, 19] or subharmonic loops. On the other hand, avalanches can have a significant effect, for example allowing for transients and breaking of loop-RPM on scaffolds that are consistent with the Preisach model [6]. This suggests that an approach that focusses on the much smaller number of scaffolds, gradually adding a few avalanches of short length, may give already a good starting point to understand the statistics and typical response of systems of interacting hysterons: while adding many avalanches of

longer lengths leads to a combinatorial explosion, and an even more severe growth of the corresponding number of total orders of the switching thresholds (these grow as $(n \cdot 2^n)!/n!$ which already exceeds 3×10^{23} for $n = 3$), the corresponding growth of the number of design inequalities suggest that such avalanche-heavy t-graphs may only cover a small part of design space or even not be realizable. Whether such an approach truly captures the broad variety and statistics of transition graphs and memory effects remains an open question.

CHAPTER 4

Periodic Driving Responses

4.1 Introduction

Two of the most striking features of interacting hysteron models are *self-loops*, avalanches that get trapped in a repeating sequence of states which never settles [10, 13, 14, 37], and multiperiodic responses, where, under cyclic driving, the system returns to a previous state after multiple driving cycles [5,11,13,14]. We investigate both, using tools developed in chapter 2 and 3, and find that self-loops and multiperiodic responses are deeply connected.

First, we detail the systematic construction and required conditions for self-loops, where the system exhibits a cyclic orbit for a fixed value of U (section 4.2). We then consider periodic driving where U cycles between U_m and U_M, and investigate multiperiodic orbits where the system returns to a given state after more than one driving period (section 4.3). For both, the conditions take the form of inequalities on the switching thresholds and driving U, using a similar methodology to that which we have outlined in Chapters 2-3.

We argue that self-loops and multiperiodic orbits are connected. First, their orbits are linked via the 'scaffold' framework as established in Chapter 2. Second, one could think of self-loops as multiperiodic orbits for $U_M - U_m \to 0$. We show that, given a particular cycle in the scaffold, groups of multiperiodic loops can be derived, one of which is the self-loop.

Based on the analysis presented here, we stress that self-loops are in integral part of interacting hysteron models. This conception of self-loops is supported by findings which show that self-loops are linked to physically

active elements in real systems [37]. Having established a framework for multiperiodic orbits in interacting hysteron systems, including self-loops, we discuss how this framework can serve as a basis for the further design and study of multiperiodic responses.

4.2 Self-Loops

Here we describe methods to generate self-loops and construct their design inequalities, similarly to the framework introduced in Chapter 2; this method also forms a basis for exploring multiperiodic responses, which we will discuss in Section 4.3[1]. We are interested in self-loops because these can be considered nonphysical for dissipative systems, where energy is dissipated during state changes (e.g., when a beam snaps in a mechanical system). Since the driving is kept constant for a self-loop, there is no energy being injected into the system. Hence, the construction of self-loops and the determination of the conditions for which they occur in the hysteron model opens a route towards statistical sampling of hysteron models that purport to describe physical systems in which self-loops are forbidden.

4.2.1 Generating all self-loops

Here we discuss how to count the number of self-loop structures of length l and involving n elements, irrespective of whether they are realizable in a certain interaction ensemble. We specify each self-loop by its starting state $S^{(0)}$ and the sequence of element flips $(\kappa^{(0)}, \ldots, \kappa^{(l-1)})$ (Fig. 4.1).

We can determine all potential self-loops using a naive procedure based on the combinatorics of flip sequences, which generates cycles of length l on a n-hypercube. However, many of these are related under two trivial symmetries. We refer to the complete set of (n, l)-loops that cannot be mapped onto one another via trivial symmetries as the *fundamental* self-loops. We here describe a procedure to construct the fundamental self-loops, and by extension, determine the number of fundamental self-loops $M(n, l)$. To illustrate this procedure, we focus on $M(3, 6)$.

A naive count works as follows. First, we count the number of self-loops possible from a single starting state, e.g., $S = (000)$. By generically counting cycles of length l from a vertex of a n-hypercube (here a 3D

[1] This work was previously published as supplementary information [37].

cube), we find that there are 24 such self-loops. Second, there are 2^3 possible starting states. Together, this yields a total of $2^3 \times 24 = 192$ potential self-loops, but clearly there are redundancies here. To find the fundamental self-loops, we must account for two symmetries—relabelling and cyclic permutations—of their corresponding sequence of states.

First, we consider self-loops equivalent if they can be mapped onto each other by relabelling of the hysterons. Consider the example of the sequence of element flips of an $n = 3, l = 6$ self-loop as shown in Fig. 4.1. The relabelling symmetry implies that the sequence of flips $(2, 1, 3, 2, 3, 1)$ from state $S^{(0)} = (001)$ gives rise to the same self-loop as the sequence $(3, 2, 1, 3, 1, 2)$ from state $S^{(0)} = (100)$. We break this relabelling symmetry by only keeping loops where the first flips of the hysterons occur in descending order, such as $(3, 2, 1, \dots)$ and $(3, 2, 3, 1, \dots)$. Using this convention, we discard $(2, 1, 3, 2, 3, 1)$ and only keep the sequence $(3, 2, 1, 3, 1, 2)$. Overall this convention reduces the number of generated self-loops by a factor $n!$ – e.g., from 192 to 32 for $n = 3, l = 6$.

Second, since any state in a self-loop can be taken as the starting state, we consider self-loops equivalent if they can be mapped on each other by a cyclic permutation (Fig. 4.2-4.3). For example, the sequence $(3, 2, 1, 3, 1, 2)$ from state (100) can also be 'shifted' by one, such that we obtain the sequence $(2, 1, 3, 1, 2, 3)$ starting from state (101); with the relabelling convention described above, this self-loop maps to $(3, 2, 1, 2, 1, 3)$ starting from state (110) (Fig. 4.2). We note that all loops related by cyclic permutations lead to the same partial order of the switching thresholds, and that although the initial state is reflected in the design inequalities, it is not essential – see next section.

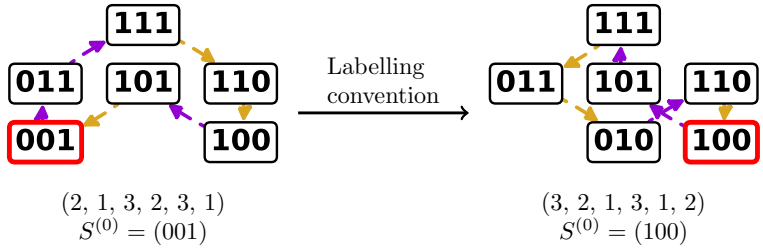


Figure 4.1: **Permutation symmetry.** A self-loop is defined by the sequence of flips $(\kappa^{(0)}, \ldots, \kappa^{(l-1)})$ and the starting state $S^{(0)}$. Here shown are two self-loops that are related by permutation symmetry, i.e., can be mapped on each other by relabelling the hysterons. Note that these are single transitions rather than graph topologies, with arrows denoting individual flipped hysterons.

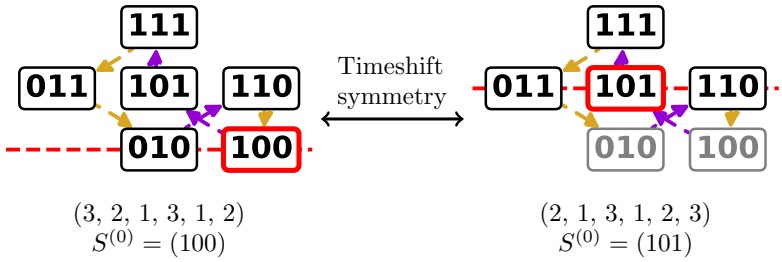


Figure 4.2: **Cyclic permutation symmetry.** Two self-loops that are related by cyclic permutation of the starting state. Our algorithm excludes the self-loop on the right, because it contains states with magnetisations lower than the initial magnetisation $m = 2$.

For computational efficiency, we break up the check for timeshift symmetry in two parts. First, when generating self-loops, we order these by their minimum magnetization $m := \sum_i s_i$:

$$M(n, l) = \sum_{m=0}^{n} M_m(n, l) \tag{4.1}$$

where $M_m(n, l)$ is the number of self-loops which starts and ends at the same magnetisation m, and does not go below m. Hence, we first generate all loops starting at state $(00\ldots)$ with magnetization $m = 0$; next, we start at states with magnetization $m = 1$, but whenever such potential

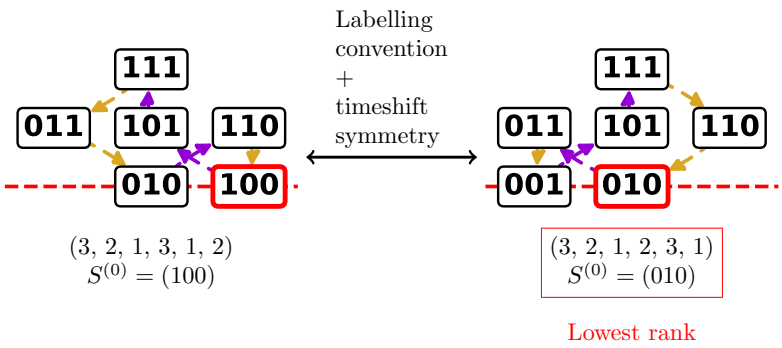


Figure 4.3: **Combining cyclic permutation symmetry and relabelling symmetry.** To systematically map all loops to representative loops, we compare the ranking of self-loops (see text), and pick the loop with the smallest ranking. Note that any of the loops in Figs. 4.1– 4.3 can be designated as the fundamental self-loop, so long as the conventions used to take care of cyclic permutation and relabelling symmetry are consistent.

loop reaches a lower magnetization, we dismiss it. This approach filters out loops such as $(3, 2, 1, 3, 1, 2)$ starting from state (110) (see Fig. 4.2). Iterating over all magnetizations is computationally effective, e.g., for $n = 3, l = 6$, this procedure reduces the number of potential self-loops from 32 to 7.

Second, the labeling and magnetization conventions limit the number of self-loop structures, but do not fully eliminate all duplicates. For our example, both loops $(3, 2, 1, 3, 1, 2)$ from state (100) and $(3, 2, 1, 2, 3, 1)$ from state (010) would be included, even though they are related by shifting and relabelling (Fig. 4.3). To select which of these to keep, we assign to each of these loops a ranking composed of the initial state and the sequence of flipped hysterons: in the above example these rankings would be 100321213 and 010321231. For equivalent loops, we only include the loop with the lowest ranking. This allows us to identify one more pair of duplicates for $n = 3, l = 6$.

In summary, for the example of $n = 3, l = 6$, the relabelling symmetry reduces the 192 potential self-loops to 32, and cyclic permutation symmetry lowers it further to six distinct fundamental self-loops (Fig. 4.4).

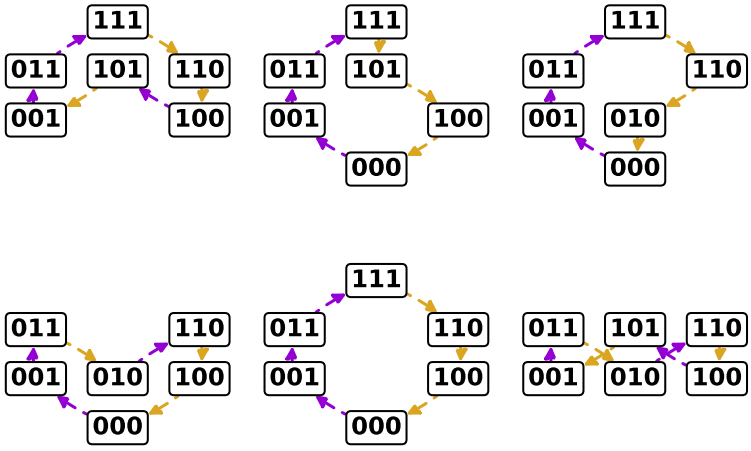


Figure 4.4: Fundamental self-loops for $n = 3, l = 6$. These self-loops have been converted such that they obey the symmetry breaking convention we have used in Chapter 2. This uses an equivalent convention to that described in the text, though slightly more complex; note that such conversions can freely be made once the set of fundamental self-loops has been constructed.

4.2.2 Design inequalities for self-loops

Now that we have established the structure of the fundamental self-loops as a function of (n, L), we determine their realizability in the interacting hysteron model. For every fundamental self-loop we can construct a set of linear inequalities of the switching thresholds, using a variation on the method introduced in Chapter 2. We focus on the relation between the state switching thresholds $U^{\pm}(S)$ because, once a scaffold has been established, the role of the noncritical switching thresholds is largely trivial – see also the concluding section of Chapter 2.

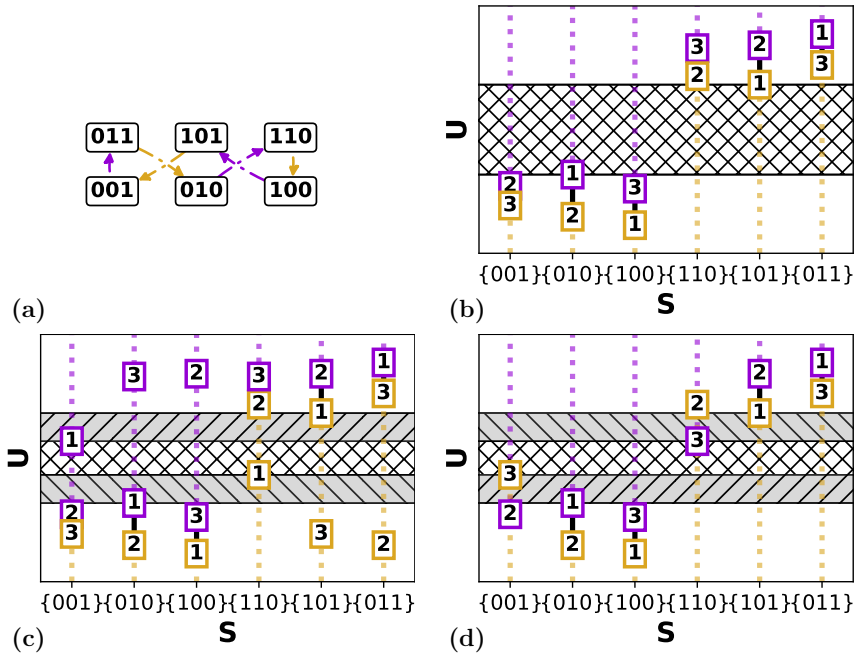


Figure 4.5: Inequalities for self-loops. a) Example self-loop where arrows denote individual hysteron flips. b) Set of switching thresholds that realize the self-loop in panel (a) without race conditions; the cross-hatched region indicates the range of U for which a self-loop occurs. c) Switching thresholds with race conditions induced by the specific ordering of the noncritical switching thresholds. For example, both hysterons 1 and 2 are unstable to flipping from 0 to 1 in state (001) when $U > U_1^+(001)$ (upper grey band); and similarly, both hysterons 1 and 2 are unstable to flipping from 1 to 0 in state (110) when $U < U_1^-(110)$ (lower grey band). The '/' and '\' hatchings indicate the regions where, respectively, $U > \max_{S\in B^+} U^+(S)$ and $U < \min_{S\in B^-} U^-(S)$. The (non-grey) overlap between these regions produces an unambiguous self-loop. Resolving the race conditions in the grey regions, by allowing the most unstable hysteron to flip (see Chapter 2), also leads to self-loops. d) Race conditions induced by persistently unstable states; for example hysteron 2 is unstable to flipping from 0 to 1 and hysteron 3 is unstable to flipping from 1 to 0 in state (001) for U in the lower grey band. Such extreme choices lead to ambiguities that are not easily lifted.

The framework in Chapter 2 did not explicitly discuss parameter conditions to realize self-loops, but instead focused on non-loop transitions, for which separate design inequalities for the initial, intermediate and final state of an avalanche were derived. As self-loops have no final state, it suffices to construct the initial and intermediate inequalities. Moreover, we do not focus on the state from which a self-loop is initiated, and rather investigate whether a self-loop is realizable for *any* driving. We account for this by eliminating the driving from the set of linear inequalities. For example, if we have the set of design inequalities:

$$\begin{aligned} U &> U^+(001), \\ U &< U^-(011), \\ U &> U^+(010), \\ U &< U^-(110), \\ U &> U^+(100), \\ U &< U^-(101), \end{aligned} \tag{4.2}$$

which realizes the self-loop in Fig. 4.5a, we can eliminate the driving U to obtain inequalities that enforce that there is a range of the driving U where a self-loop occurs (Fig. 4.5b):

$$\begin{aligned} U^-(011) &> U^+(001), \\ U^-(011) &> U^+(010), \\ U^-(011) &> U^+(100), \\ U^-(110) &> U^+(001), \\ U^-(110) &> U^+(010), \\ U^-(110) &> U^+(100), \\ U^-(101) &> U^+(001), \\ U^-(101) &> U^+(010), \\ U^-(101) &> U^+(100). \end{aligned} \tag{4.3}$$

Note that, for the solution in (Fig. 4.5b), the self-loop is triggered from the states (010) and (101).

We can generalize these equations to:

$$\min_{S \in B^-} U^-(S^-) > \max_{S \in B^+} U^+(S) \tag{4.4}$$

where we define B^+ (B^-) as the set of states from which there is an up (down) flip in the target self-loop. Formally, we can write this group of

states as:

$$B^{\pm} = \{S^{(\lambda)}\}_{\kappa^{(\lambda)}=k^{\pm}(S^{(\lambda)})} \tag{4.5}$$

This expression denotes that each of the states $S^{(0)}, \dots S^{(l-1)}$ is assigned to B^+ resp. B^- depending on whether the associated critical hysterons $\kappa^{(0)}, \dots, \kappa^{(l-1)}$ flip up or down. For our example, where the sequence of states is (001, 011, 010, 110, 100, 101) and the associated sequence of flips is (2, 3, 1, 2, 3, 1), we retrieve that $B^+ = \{001, 010, 100\}$ and $B^- = \{011, 110, 101\}$.

Race conditions—. Just like other avalanches, self-loops can run into race conditions where more than one hysteron becomes unstable at once, such that the transition becomes ambigous (see Chapter 2). Such race conditions are of little consequence when the aim is to *prevent* self-loops; for this purpose, ambiguous self-loops can simply be counted as self-loops, and the conditions formulated in Eq. (4.4) suffice. Yet, if the aim is to *realize* a self-loop, then race conditions must be accounted for. While self-loops are unphysical for purely dissipative systems, recent numerical work has shown that self-loops hold physical meaning for active elements [37]. Thus, the impact of race conditions on the conditions for self-loops is worth considering.

As discussed in Chapter 2, race conditions arising from the noncritical switching thresholds can be dealt with straightforwardly (Fig. 4.5c). Yet, special attention needs to be given to the case where the critical up *and* down hysteron are unstable, as can occur for a persistently unstable state. (Fig. 4.5d). To prevent cases where both the up and down critical hysteron are unstable, we need to enforce:

$$\min_{S\in B^-} U^+(S), \min_{S\in B^-} U^-(S) > \max_{S\in B^+} U^+(S), \max_{S\in B^+} U^-(S)\ . \tag{4.6}$$

Note that the conditions in Eq. (4.6) assume that race conditions must be prevented entirely. If a dynamical rule is used to resolve race conditions, then the conditions for an ambiguous self-loop can be looser than those in Eq. (4.6): e.g., if the rule is employed where the most unstable hysteron always flips [14, 37].

In summary, we have formulated conditions for the occurrence of self-loops for a given set of switching thresholds. We do not focus on a fixed value of the driving U, but rather formulate conditions for the occurrence of 'gaps' between thresholds where there is a self-loop. We find that such a gap is captured by the expression $\min_{S\in B^-} U^-(S^-) > \max_{S\in B^+} U^+(S)$,

where B^+ (B^-) are the sets of states from which there is an up (down) flip within the self-loop. When the aim is to unambiguously realize a certain self-loop, rather than merely prevent self-loops, then the 'gap' may become narrower due to the need to account for race conditions.

4.3 Multiperiodic Orbits

Here we discuss the design of systems that show multiperiodic orbits. Multiperiodic responses (i.e., responses where a system returns to its initial state only after multiple driving cycles) are an emergent behaviour in interacting hysteron systems [5, 13, 14]. Such multiperiodic orbits are notable because they evidence the presence of memory and interactions in disordered systems; in particular, for the hysteron model, interactions are required [14]. The study of multiperiodic responses is therefore a first step in investigating the complex memory responses possible in disordered systems.

In this section, we extend the techniques that we have developed in Chapters 2- 3 to investigate multiperiodic orbits. In section 4.3.1, we construct all possible loop topologies, where we build on the framework that we have established in Chapter 3. In section 4.3.2, we discuss additional conditions – called the 'quad' inequalities – which are needed to obtain a multiperiodic *orbit* under purely periodic driving, from a given multiperiodic *loop topology*. In both subsections, we also make explicit the connection between multiperiodic orbits and self-loops (see 4.2), by showing that both types of responses can be traced back to cyclical structures within the scaffold. Together, these techniques provide a basis for the study and design of multiperiodic orbits in disordered systems.

4.3.1 Constructing multiperiodic loops

In the hysteron model, multiperiodic orbits require multiperiodic *loop topologies*. Thus, the study of possible (multiperiodic) loop topologies is a necessary first step towards designing and understanding multiperiodic behaviour in hysteron systems. In this section, we systematically construct all possible loop topologies and then categorize these by loop period. We construct the loops in two steps: we first construct all possible 'cycles' in the scaffold, then count all possible loops for each cycle.

For the first step of our algorithm for constructing all loops, we recall the algorithm for constructing all fundamental self-loops (Section 4.2).

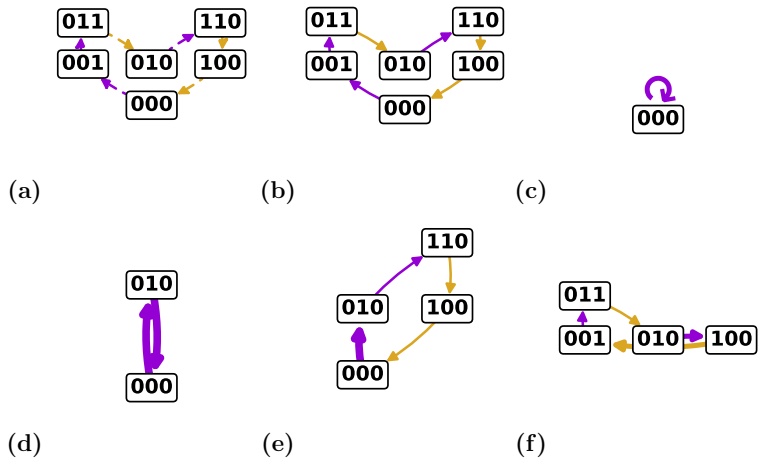


Figure 4.6: Various loops that share a given cycle. a) Example of a $n = 3, l = 6$ cycle. b) Avalanche-free loop for the example cycle; this loop has period $T = 2$. c) Marginal self-loop for the example cycle, starting from state (000). d) Forbidden $T = 0$ loop construction (this is a self-loop in disguise). e) Potential $T = 1$ loop for the example cycle. f) Potential $T = 2$ loop for the example cycle. Note the extrema here are (001, 011, 010, 100), in contrast to the $T = 2$ loop in panel (b) which has extrema (000, 011, 010, 110).

We observe that this methodology applies more broadly than to self-loops alone. For example, if we have the sequence (3, 2, 3, 1, 2, 1) from state (000) (Fig. 4.6a), then by letting the system be stable after each flip, we obtain the avalanche-free subgraph shown in Fig. 4.6b. We refer to such a sequence of transitions, which starts end ends at the same state, as a loop.

We define the extremal states of the loop $(S_{m,1}, S_{M,1}, \ldots, S_{m,T}, S_{M,T})$ as the states where the driving changes from increasing to decreasing (for $S_{M,i}$) or vice versa (for $S_{m,i}$). We refer to $S_{m,i}$ and $S_{M,i}$ as the minimal resp. maximal states. For example, the loop in Fig. 4.6b has extremal states $(000, 011, 010, 110)$. The *period* of a loop, T, is equal to half the number of extremal states: for the avalanche-free loop, we obtain $T = 2$. In contrast, the *self-loop* with the same sequence (3, 2, 3, 1, 2, 1) starting from (000) (Fig. 4.6c) has no stable states, and we therefore say that it has period $T = 0$.

In addition to self-loops and avalanche-free loops, we can also use avalanches to create other loops based on this scaffold, and such a construction may impact the period, as shown in Fig. 4.6e ($T = 1$) and Fig. 4.6f ($T = 2$). Hence, the self-loops, which correspond one-to-one to 'cycles' in the scaffold, are each associated with various (multiperiodic) loop topologies.

As the second step in our algorithm for constructing multiperiodic loops, we now calculate the number of loops per cycle. Suppose that we have a sequence of hysteron flips $\kappa^{(0)}, \ldots, \kappa^{(l-1)}$, corresponding to a cycle of states $S^{(0)} \to \cdots \to S^{(l-1)} \to S^{(0)} \to \ldots$ – note that the number of flips l defines a length for the cycle, similarly to how we have defined l for individual transitions. Naively, we can mark each of the states $S^{(0)}, \ldots S^{(l-1)}$ as either a stable state or an intermediate state, giving 2^l possibilities. For our example cycle in Fig. 4.6a, which has length $l = 6$, we find that there are $2^6 = 64$ combinations.

However, we must apply corrections to this naive loop count for two reasons, both related to $T = 0$ loops. The first of these corrections concerns $T = 0$ loops which are evidently unrealizable, and the second considers marginal self-loops. First, if we obtain a $T = 0$ loop where more than one state is stable, this loop is nonsensical, because it implies that the driving perpetually increases or decreases as the loop is traversed (Fig. 4.6d, see also section 2.2 for further discussion of impossible graph topologies).

Second, if all but one of the states are intermediate, then this gives

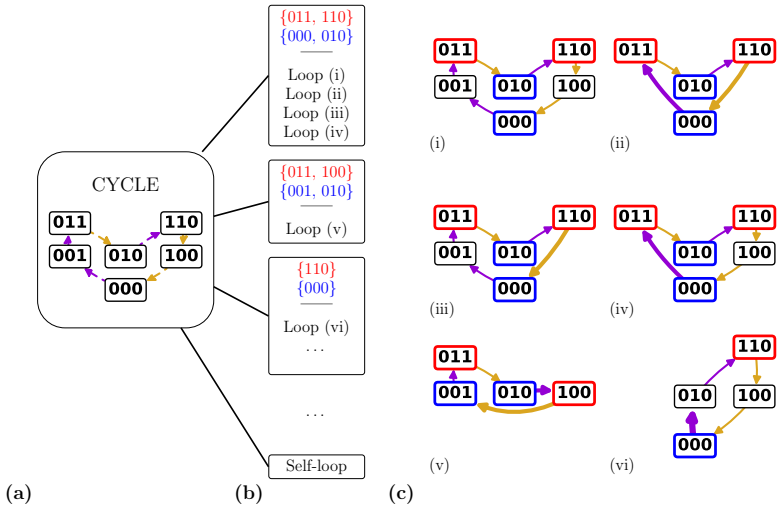


Figure 4.7: Loops and categorization by extremal states for a given cycle. a) Example $n = 3, l = 6$ cycle with natural period $T_0 = 2$. b) Possible loops ($2^l - 2^{l/2+1} + 2 = 50$) and grouping by extremal states for the example cycle; not all loops are shown. For the natural extrema (top) there are $2^{l-2T_0} = 4$ possible loops. c) Loops corresponding to the labels (i)-(vi). Minimal and maximal states are indicated in blue and red, respectively. Loops (i)-(iv) have the natural extrema and period $T = T_0 = 2$, loop (v) has period $T = 2$, and loop (vi) has period $T = 1$.

a marginal self-loop from a given initial state (i.e., a self-loop where the initial state is marginally stable). For example, in Fig. 4.6c we show a marginal self-loop from state (000). Since we do not consider these marginal self-loops to be distinct from the case where all states are intermediate (see section 4.2), we remove these from the count.

We must thus remove all but one of the $T = 0$ cases from the count. Given that a cycle must feature an equal number of up and down flips, the number of up flips and the number of down flips are both exactly $l/2$. Taking care not to double-count the case where all states are intermediate – i.e., the self-loop case – we find that the number of $T = 0$ loops is $2 \times 2^{l/2} - 1$. Subtracting this number from the total count, and adding the self-loop back in, we obtain that the number of loops per cycle is $2^l - 2^{l/2+1} + 2$. For our example cycle, there are $2 \times 2^3 - 1 = 15$ loops which have $T = 0$, of which we only count one – namely, the self-loop shown in Fig. 4.6a. Thus, there are $64 - 15 + 1 = 50$ loops. One of these is

the self-loop as mentioned (Fig. 4.6a), and another is the avalanche-free loop, which has period $T = 2$ (Fig. 4.6b). The remaining 49 loops either have period $T = 1$ (Fig. 4.6e) or $T = 2$ (Fig. 4.6f).

In general, for a cycle of length l we have $2^l - 2^{l/2+1} + 2$ loops, out of which one is a self-loop, and one is the loop without any avalanches. We conclude this section by commenting on the distribution of the possible periods T over the remaining $2^l - 2^{l/2+1}$ loops.

First, we note that the avalanche-free loop always has the maximal period possible for the given cycle - in this case, $T = 2$. We refer to the period of the avalanche-free loop as the natural period T_0 for a given cycle, and to its extremal states – in this case, the minimal states (000), (010) and the maximal states (011), (110) – as the cycle's natural extrema. In general, we can then state that there are are $2^l - 2^{l/2+1} + 2$ loops with periods $0 \leq T \leq T_0$ corresponding to this cycle.

The natural extrema deserve particular mention, because the number of loops which feature these extremal states is predictable. Namely, when the extremal states are the natural extrema of the cycle, only these states are required to be stable; for the remaining states, the stability can be freely chosen without altering the extrema of the loop. Since there are $2T_0$ extremal states, the number of loop topologies is 2^{l-2T_0}. For our example with $l = 6, T_0 = 2$, we retrieve that there are four possible loops (denoted (i)-(iv) in Fig. 4.7).

By contrast, the number of loops for extrema that are not the natural extrema is difficult to count, even for the loops that have $T = T_0$. For example, in Fig. 4.7b the choice of extrema (001, 011, 010, 100) yields only a single loop (denoted (v)), despite also having period $T = 2$.

In summary, we can systematically generate (multiperiodic) loop topologies in two steps: first by generating fundamental cycles, using the same algorithm that we used to generate self-loops (see section 4.2), and then by constructing the $2^l - 2^{l/2+1} + 2$ possible loop topologies for each cycle. One of these is a self-loop, and 2^{l-2T_0} are the loops whose extremal states are the natural extrema, one of which is the loop without avalanches. The other loops have periods $1 \leq T \leq T_0$ and have a complex combinatorial structure.

4.3.2 Quad inequalities

The existence of a multiperiodic loop topology, as discussed above, guarantees that the loop can be traversed via T alternating up and down

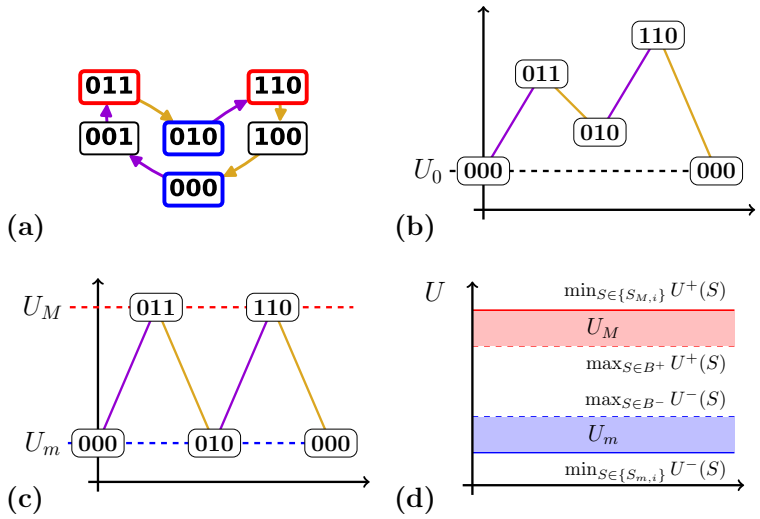


Figure 4.8: Traversal of a multiperiodic loop topology under periodic driving. a) Example of a $T = 2$ multiperiodic loop topology; see also loop (i) in Fig. 4.7c. b) Traversal of the example multiperiodic loop under a specific sequences of up and down sweeps; selecting such a sequence is always possible if the topology is realized. Without loss of generality, we can impose that such a driving protocol begins and ends at the same value U_0. c) Traversal of the example multiperiodic loop under *periodic* driving, where U is cycled between a maximum driving U_M and minimum driving U_m. d) Upper and lower bounds for U_M and U_m, as prescribed by the quad inequalities; see also Eq. (4.21).

sweeps – for example, the loop in Fig. 4.8a can be traversed via two up and down sweeps as in Fig. 4.8b. However, the existence of a loop does not guarantee that the loop is traversed for a *periodic* driving protocol, here defined as a driving protocol that alternates a monotonic increase from U_m to U_M with a monotonic decrease from U_M back to U_m (Fig. 4.8c).

For a multiperiodic loop to be traversable under periodic driving, we require that we can choose U_m and U_M such that all the states of the loop are traversed. This leads to upper and lower bounds for both U_m and U_M, which are expressed via sets of additional inequalities which we refer to as the *quad* inequalities. We will show that for each group of loops with the same extremal states, we can formulate a single set of quad inequalities (Fig. 4.8d).

Quad inequalities for example loops.— Here we formulate the quad inequalities. In general, U_M must be high enough that the maximal states are reached, but low enough that these states are stable, and similar for U_m; the driving should not 'overshoot' the extremal states.

To illustrate how these conditions arise—and that they are identical for loops sharing the same extremal states—we examine the example cycle in Fig. 4.6a and derive the conditions for U_M for three specific loops. The first loop is the avalanche-free loop, denoted in Fig. 4.7c as (i). The second loop has the same extrema as the avalanche-free loop but features ferromagnetic avalanches (Fig. 4.7c-(ii)). The third loop has different extrema than the first two examples (Fig. 4.7-(v)). Based on these three examples, we then formulate general conditions on U_M and U_m.

For loop (i), enforcing for each of the up sweeps that U_M is high enough to reach the maxima (011) and (110) but does not surpass these, we obtain:

$$\begin{aligned} U^+(001) <& U_M < U^+(011) \ , \\ U^+(010) <& U_M < U^+(110) \ . \end{aligned} \tag{4.7}$$

These inequalities essentially define an upper and lower bound for U_M Similarly, by enforcing that the minimal states (010) and (000) are reached but not surpassed at U_m, we obtain:

$$\begin{aligned} &U^-(011) > U_m > U^-(010) \ , \\ &U^-(100) > U_m \ , \end{aligned} \tag{4.8}$$

where we note that the second inequality has a different form because (000) does not have a down switching threshold. If U_M and U_m satisfy the quad inequalities Eq. (4.7)-(4.8), then loop (i) is traversed.

For loop (ii) from Fig. 4.7c, following the same logic, the quad inequalities are:

$$U^+(000) < U_M < U^+(011) \ , \tag{4.9}$$
$$U^+(010) < U_M < U^+(110) \ , \tag{4.10}$$
$$U^-(011) > U_m > U^-(010) \ , \tag{4.11}$$
$$U^-(110) > U_m \ , \tag{4.12}$$

We note that the quad inequalities for loops (i) and (ii) are distinct. However, we can define a single set of inequalities for the *group* of loops, making use of the design inequalities. For example, the quad inequalities

for the group of loop (i) and loop (ii) are

$$\begin{aligned}
&U^+(000) < U_M < U^+(011) \ , \\
&U^+(001) < U_M \ , \\
&U^+(010) < U_M < U^+(110) \ , \\
&U^-(011) > U_m > U^-(010) \ , \\
&U^-(100) > U_m \ , \\
&U^-(110) > U_m \ .
\end{aligned}$$

Note that these inequalities can be expressed as upper and lower bounds for U_M and U_m:

$$\max_{S\in\{000,001,010\}} U^+(S) < U_M < \min_{S\in\{011,110\}} U^+(S) \ , \tag{4.13}$$

$$\max_{S\in\{010\}} U^-(S) < U_m < \min_{S\in\{011,110,100\}} U^-(S) \ . \tag{4.14}$$

The combination of these bounds with the design inequalities for loop (i), which contain $U^+(000) < U^+(001)$ and $U^-(110) > U^-(100)$, is equivalent to the design and quad inequalities for loop (i); likewise, the combination with the design inequalities for loop (ii), which contain $U^+(000) > U^+(001)$ and $U^-(110) < U^-(100)$, is equivalent to the design and quad inequalities for loop (ii). Hence, taking onto account the design inequalities, we can capture the quad inequalities for a group of loops – and thus, the region in parameter space bounded by the quad inequalities – in a single expression.

We now illustrate that it is only possible to group the quad inequalities of multiple loops when these loops share extrema. We consider the example loop (v) from Fig. 4.7, which has the same cycle as the first two examples, but has the minimal states (001), (010) and maximal states (011), (100). Constructing the quad inequalities for this loop yields:

$$\begin{aligned}
&U^+(001) < U_M < U^+(011) \ , \\
&U^+(010) < U_M < U^+(100) \ , \\
&U^-(011) > U_m > U^-(010) \ , \\
&U^-(100) > U_m > U^-(100) \ .
\end{aligned}$$

While the quad inequalities of the first two loops can be grouped, those of loop (v) cannot be combined with either. Namely, if we compare the quad inequalities for loop (v) with, for example, those of loop (i), then

either contains inequalities that are not necessary for the other loop: the inequalities $U_M < U^+(100)$ and $U_m > U^-(100)$ are not necessary for loop 1, and the inequality $U_M < U^+(110)$ is not necessary for loop (v). Thus, when combining the inequalities of loops (i) and (v) with either loop's respective design inequalities, the resulting set of inequalities is overly strict. Hence, due to the loops' differing extremal states, there is no set of quad inequalities that is necessary and sufficient for both loops simultaneously.

In summary, for each individual loop, there is a set of quad inequalities that expresses upper and lower bounds for U_M, U_m such that the loop is traversed under periodic driving. The quad inequalities for two loops can be combined into a single expression if and only if the loops' extremal states are the same.

Connection with self-loops and generalization.— We now discuss how to obtain the quad inequalities for any cycle and any set of extremal states. To do so, we first identify the four groups of states and switching thresholds involved in the quad inequalities. We then elucidate the connection between these inequalities and the conditions that we have formulated in section 4.2.2 for a self-loop. We finally present a general expression that captures the quad inequalities for any given cycle and choice of extremal states.

First, we determine the conditions for reaching the extremal states — we deal with overshooting later. Suppose that we have an example cycle, e.g., the cycle shown in Fig. 4.7a. We observe that, in order to traverse any loop corresponding to this cycle, it is necessary to have $U^+(S) < U_M$ for any up flip from any state S in the cycle. In section 4.2, we have defined the group of states from which there is an up flip in a given cycle as B^+. Hence, without loss of generality:

$$\max_{S \in B^+} U^+(S) < U_M \ . \tag{4.15}$$

For our example cycle, $B^+ = \{000, 001, 010\}$.

Similarly, for U_m, we consider the group B^- of states from which there is a down flip in the cycle:

$$\min_{S \in B^-} U^-(S) > U_m \ . \tag{4.16}$$

For our example cycle, $B^- = \{010\}$.

We observe that Eqs. (4.15)–(4.16) apply to *all* of the loops corresponding to a given cycle – including the self-loop case. In fact, we retrieve the self-loop inequalities in Eq. (4.4) from Eqs. (4.15)-(4.16) by requiring that $U_m = U_M$. Thus, the quad inequalities directly relate to the conditions for a self-loop which were established in section 4.2.

As the second step in the construction of the quad inequalities, we require that the maximal states are not surpassed at U_M, and likewise for the minimal states at U_m. Given that we know the maximal states $\{S_{M,i}\}$ and minimal states $\{S_{m,i}\}$, we can straightforwardly impose the stability of the extremal states through the inequalities:

$$\min_{\{S_{M,i}\}} U^+(S) > U_M \ , \tag{4.17}$$

$$\max_{\{S_{m,i}\}} U^-(S) < U_m \ . \tag{4.18}$$

Note that, whereas Eqs. (4.15)–(4.16) apply to all loops corresponding to a given cycle, Eqs. (4.17)–(4.18) are specific to a choice of extremal states.

By combining Eqs. (4.15)–(4.18), we obtain the full generalized set of quad inequalities. We can express the ranges for U_M and U_m as:

$$\max_{S\in B^+} U^+(S) < U_M < \min_{\{S_{M,i}\}} U^+(S) \ , \tag{4.19}$$

$$\max_{\{S_{m,i}\}} U^-(S) < U_m < \min_{S\in B^-} U^-(S) \ . \tag{4.20}$$

Furthermore, observing that $\max_{S\in B^+} U^+(S) > \min_{S\in B^-} U^-(S)$ for any loop that is not a self-loop, we can capture these four bounds in a single expression:

$$\max_{S\in\{S_{m,i}\}^-} U^-(S) < U_m < \min_{S\in B^-} U^-(S) < \max_{S\in B^+} U^+(S) < U_M < \min_{S\in\{S_{M,i}\}} U^+(S) \ . \tag{4.21}$$

We show the upper and lower bounds specified by the quad inequalities in Fig. 4.8d.

We recall that the quad inequalities are necessary, but not sufficient, to ensure a multiperiodic loop is traversed under periodic driving. In particular, we observe that Eqs. (4.17)–(4.18) are both necessary and sufficient in preventing 'overshoots', yet Eqs. (4.15)–(4.16) are merely necessary for reaching the specified extremal states. By combining the quad inequalities with the design inequalities of a specific loop, for the desired cycle and extremal states $\{S_{m,i}\}$ and $\{S_{M,i}\}$, we obtain sufficient conditions for a multiperiodic loop that is traversed under periodic driving.

4.4 Outlook and Conclusions

In this chapter we have studied the construction and required conditions of two related features of hysteron systems: self-loops and multiperiodic orbits. First, we showed that we can systematically construct cycles in the scaffold which correspond one-to-one to self-loops, and have formulated conditions for 'gaps' where self-loops occur. We then showed that each cycle is linked to a number of loops with periods $1 \leq T \leq T_0$, where T_0 is the natural period of the cycle. Finally, we formulated conditions called the quad inequalities, which give a lower and upper bound for U_M, U_m such that a multiperiodic loop topology is traversed under periodic driving. In addition, we illustrated that these quad inequalities can be grouped by the extremal states of the loop topologies, and that the quad inequalities reduce to the conditions for a self-loop when setting $U_m = U_M$.

We conclude this chapter by considering the implications of the discussed techniques for the study and design of multiperiodic responses. We have seen that the period T of a multiperiodic orbit is difficult to select for, because these arise from a number of cycles on the scaffold level, which in turn correspond to a number of loops with periods $0 \leq T \leq T_0$. This difficulty of selecting for loop periods also extends to self-loops, which are closely linked with multiperiodic responses, and cannot be easily excluded from hysteron models.

The design and interpretation of multiperiodic responses are most straightforward when, for a given cycle, the only allowed loops are those that have the natural extrema. These are exactly those loops *without antiferromagnetic avalanches*. We thus suggest that systems without antiferromagnetic avalanches provide a useful direction for the study of multiperiodic orbits, given that the complexity of multiperiodic loops is restrained in such systems.

Note, however, that this restriction does not forbid antiferromagnetic *interactions*; in fact, to satisfy both the initial inequalities (which specify the scaffold) and the quad inequalities, antiferromagnetic interactions are a necessity, as it is known that purely ferromagnetic interactions preserve the no-passing property and RPM, and thus forbid complex scaffolds and multiperiodic cycles. Therefore, the most promising avenue for multiperiodic orbits seems to be systems that feature a mix of ferromagnetic and antiferromagnetic interactions, but do not feature antiferromagnetic avalanches.

CHAPTER 5

Restricted Models

5.1 Introduction

In the preceding chapters, we have discussed the response of interacting hysterons in the most general model, where the switching thresholds $U_i^{\pm}(S)$ are completely independent. In this chapter we focus on specific parametrizations of the switching thresholds, where we assume pairwise interactions, quantified by interaction coefficients c_{ij}, such that the switching thresholds can be expressed as:

$$U_i^{\pm}(S) = u_i^{\pm} - \sum_{j \neq i} c_{ij} s_j \ . \tag{5.1}$$

We refer to $u_i^{\pm}$ as the bare switching thresholds, and define the *span* σ_i of a hysteron as the difference between the bare up and down thresholds: $\sigma_i \equiv u_i^{+} - u_i^{-}$. We remark that there are $2n$ bare switching thresholds $u_i^{\pm}$, and $n^2 - n$ coupling coefficients c_{ij} – we assume that there is no self-coupling of the form c_{ii} [10]. Thus, in the model expressed by Eq. (5.1), a hysteron system is specified by $n^2 + n$ parameters. We refer to this model as the pairwise additive model[1] of hysteron interactions.

Tackling the complexity of graph space. In the previous chapters we have developed methods to explore the space of candidate t-graphs, which in the general model is very large: for only three hysterons, we

[1] Also referred to as a linear or first-order approximation; we choose to use 'pairwise additive' to emphasize the abstract and discrete nature of our model.

need to construct and evaluate 4×10^{12} candidate graphs. More restricted models lead to a smaller space, which for some restricted cases can be mapped out completely, as we will show below.

However, in some aspects the pairwise additive model is more challenging to analyze than the general model that we have described in Chapter 2. In the general model, where all switching thresholds $U_i^{\pm}(S)$ are independent, a t-graph is realizable if and only if the design inequalities are a valid partial order on the switching thresholds. When we convert the design inequalities to the pairwise additive model - or indeed any specific parametrization - additional constraints are imposed, and we must numerically check whether the design inequalities are consistent via linear programming. An example of this added complexity can be seen when we construct all scaffolds for $n = 3$: in the general model, we can determine analytically that there are 96 scaffolds for $n = 3$, and all of these are realizable (see Chapter 3). In the pairwise additive model, we find via linear programming that only 76 out of these 96 scaffolds are realizable. It is difficult to extend these results to larger systems, though. For our purposes linear programming is a black box: we can determine numerically whether or not the design inequalities are consistent, but we cannot easily retrace the origin of such inconsistencies. By comparison, in the general model it is relatively easy to identify where inconsistencies arise, as these show up as cycles (of the form $a > b > \cdots > a > \dots$) in the design inequalities.

The pairwise additive model is thus challenging to grasp as a whole. However, it has been found to be a good description for some experimental systems [6,11,13,14,23,46], and it has proven fruitful to analyze restricted regimes of the pairwise additive model, where the constraints placed on the potential t-graphs are straightforward [6, 37, 46, 60].

We distinguish two separate, though related, issues in understanding the space of possible t-graphs. First, the number of t-graphs increases combinatorically as a function of the number of hysterons. Second, the probability of a given candidate graph corresponding to a realizable t-graph strongly decreases with the number of hysterons. Based on these issues, we formulate two research questions:

- How can we minimize the number of candidate graphs which needs to be generated in order to construct all realizable t-graphs?

- How can we meaningfully navigate the space of realizable t-graphs?

By considering restricted models, we address both these questions, focussing on the first.

The regimes which we discuss here are divided into two groups: regimes specified by the coupling c_{ij}, and regimes specified by the span σ_i. In section 5.2 we discuss restrictions on the coupling coefficients c_{ij}, focussing in particular on same-sign coupling (section 5.2.1) and global coupling where $c_{ij} = c_j$ (section 5.2.2). In section 5.3, we discuss the role of the span σ_i, and compare the response of finite-span hysterons to that of interacting zero-span hysterons (referred to as spins). While we describe these cases separately, sections 5.2 and 5.3 together form a picture of the role played by the parameters $u_i^{\pm}$ and c_{ij} in t-graph design.

Center and scale invariance—. For all of the systems discussed in this chapter, it is relevant to keep in mind that the response of a hysteron system is center and scale invariant: when all switching thresholds undergo a transformation $U_i^{\pm}(S) \mapsto aU_i^{\pm}(S) + b$, where $a > 0$, the driving response does not change. It is necessary here to specify that $a > 0$, because a negative a would invert the ordering of the switching thresholds, while for $a = 0$, the switching thresholds become degenerate. Note that we have made use of center and scale invariance in Chapter 3 when calculating the probability of each $n = 2$ graph under random sampling. Namely, without loss of generality, we can set the range from which the switching thresholds $U_i^{\pm}(S)$ are pulled to $[0, 1]$.

In the pairwise additive model, center invariance implies that the mean of the bare switching thresholds, $u := \langle u_i^{\pm} \rangle$ does not matter: rather than the $n^2 + n$ parameters

$$(\{u_i^+\}, \{u_i^-\}, \{c_{ij}\}) \tag{5.2}$$

we only need to consider $n^2 + n - 1$ parameters in order to fully specify the response of a hysteron system. An example of such a parametrization is

$$(\sigma, \{u_i^+ - u_j^+\}, \{u_i^- - u_j^-\}, \{c_{ij}\}) \ , \tag{5.3}$$

where $\sigma := \langle u_i^+ - u_i^- \rangle$ is the mean span.

The role played by scale invariance is more subtle than that of center invariance. While all parameters Eq. (5.3) can be scaled by a factor $a > 0$, there is no obvious normalization that works for the pairwise additive model in its entirety. For example, while it can be useful in some instances to set the mean span σ to 1, this normalization becomes problematic when we discuss zero-span hysterons as in section 5.3.2. Therefore, when we

discuss specific regimes of the pairwise additive model, it is important to explicitly take scale invariance into account.

In this chapter, scale invariance is most relevant for section 5.3.1, where we discuss the limit of a large mean span σ. There, we narrowly define a large mean span σ as being much larger than all other parameters $u_i^+ - u_j^+$, $u_i^- - u_j^-$ and c_{ij}. By contrast, for zero-span hysterons (section 5.3.2) scale invariance poses no issue, because the constraint that $\sigma_i = 0$ remains in place when all switching thresholds are multiplied by a factor $a > 0$. The same is true for the constraints on coupling which we discuss in section 5.2.

5.2 Restrictions on Coupling

In this section we discuss several restrictions on the coupling coefficients c_{ij}. First, we discuss systems where all coupling coefficients c_{ij} have the same sign. Next, we discuss global coupling, meaning that $c_{ij} = c_j$. Finally, we discuss serial coupling, which is global coupling where $c_j < 0$. For all three classes of systems, we show that possible t-graphs can be constructed more systematically than in the general model (see Chapter 3). For serial coupling, we explicitly construct all realizable t-graphs for three hysterons [6].

5.2.1 Same-sign coupling

One of the simplest restraints on the coupling coefficients c_{ij} is same-sign coupling, where the coefficients c_{ij} are either all positive ($c_{ij} \geq 0$) or all negative ($c_{ij} \leq 0$). We here argue that, when all coupling coefficients have the same sign, many avalanches are prevented from occurring. As a result, it is more feasible to generate all t-graphs for same-sign coupling than for mixed-sign coupling.

We first note that same-sign coupling does not affect the number of potential scaffolds. We can see this from the design inequalities imposed by the the scaffold, which are of the form $U_i^+(S) > U_j^+(S)$ or $U_i^-(S) > U_j^-(S)$ (see Chapter 2). When these inequalities are converted to the

pairwise additive model, we obtain:

$$(u_i^+ - u_j^+) - \sum_{k\neq i,j}(c_{ik} - c_{jk}) > 0 \ , \tag{5.4}$$

$$(u_i^- - u_j^-) - (c_{ij} - c_{ji}) - \sum_{k\neq i,j}(c_{ik} - c_{jk}) > 0 \ . \tag{5.5}$$

From Eq. (5.4)–(5.5), we see that the scaffold does not depend on the mean coupling $\langle c_{ij}\rangle$, but only on the differences between couplings $c_{ik}-c_{jk}$ and $c_{ij} - c_{ji}$. Hence, if a scaffold is generally realizable in the pairwise additive model for interactions of arbitrary sign, a simple overall shift of their values allows us to realize the same scaffold for strictly positive or negative same-sign coupling.

The same-sign coupling constraint greatly limits the number of possible avalanches. When all coupling coefficients are positive ($c_{ij} \geq 0$), the only possible avalanches are purely ferromagnetic avalanches: avalanches which either consist of only up flips, or only down flips. For example, to have a $l = 2$ ferromagnetic avalanche where first hysteron j, then hysteron i flips up, we must have $c_{ij} > 0$. Similarly, when all coupling coefficients are negative ($c_{ij} \leq 0$), the only possible avalanches consist of alternating up and down flips; for example, to have a length-2 avalanche where j flipping up triggers an down flip of hysteron i, one must have $c_{ij} < 0$. We refer to avalanches which consist of alternating up and down flips as purely antiferromagnetic avalanches. Below, we formally show that purely ferromagnetic and purely antiferromagnetic avalanches are the only unambiguous avalanches that are possible for same-sign positive and negative coupling, respectively. We then discuss the structure of t-graph space when the only allowed avalanches are either purely ferromagnetic or purely antiferromagnetic.

Proof for restrictions on avalanches—. To see that it is not possible for subsequent flips in an avalanche to be of opposing sign (up/down) if all coupling coefficients c_{ij} are positive or zero, we recall the design inequalities which we have formulated in Chapter 2. We show that avalanches must be purely ferromagnetic via proof by contradiction: for same-sign positive coupling, an avalanche cannot have a down flip follow an up flip or vice versa.

Consider a tentative avalanche that has a number of up flips, and then a down flip: $S^{(0)} \uparrow \ldots S^{(\lambda)} \uparrow S^{(\lambda+1)} \downarrow \ldots S^{(l)}$. From the intermediate

inequalities, derived in Chapter 2, we directly obtain for state $S^{(\lambda)}$:

$$U^+(S^{(0)}) < U_i^+(S^{(\lambda)}) \; \forall i \in I_0(S^{(\lambda)}) \backslash \{k\} \; , \tag{5.6}$$

$$U^+(S^{(0)}) > U_i^-(S^{(\lambda)}) \; \forall i \in I_1(S^{(\lambda)}) \; , \tag{5.7}$$

$$U^+(S^{(0)}) > U_k^+(S^{(\lambda)}) \; , \tag{5.8}$$

where $I_0(S)$ ($I_1(S)$) is the collection of hysterons that is in phase 0 (1) in state S, and k is the critical up hysteron at state $S^{(\lambda)}$ (denoted as $k^+(S^{(\lambda)})$).

For state $S^{(\lambda+1)}$, we similarly have the intermediate inequalities

$$U^+(S^{(0)}) < U_i^+(S^{(\lambda+1)}) \; \forall i \in I_0(S^{(\lambda+1)}) \; , \tag{5.9}$$

$$U^+(S^{(0)}) > U_i^-(S^{(\lambda+1)}) \; \forall i \in I_1(S^{(\lambda+1)}) \backslash \{\kappa\} \; , \tag{5.10}$$

$$U^+(S^{(0)}) < U_\kappa^-(S^{(\lambda+1)}) \; , \tag{5.11}$$

where $\kappa = k^-(S^{(\lambda+1)}$. We now highlight Eqs. (5.7) and (5.11). First, we note that $\kappa \in I_1(S^{(\lambda)})$, so from Eq. (5.7) we have

$$U^+(S^{(0)}) > U_\kappa^-(S^{(\lambda)}) \; . \tag{5.12}$$

Furthermore, in the pairwise additive model, we obtain from Eq. (5.11):

$$U^+(S^{(0)}) < U_\kappa^-(S^{(\lambda)}) - c_{\kappa k} \; . \tag{5.13}$$

Combining Eqs. (5.12) and (5.13), we retrieve the requirement that $c_{k\kappa} < 0$; thus, for same-sign positive coupling, an up avalanche initiated from an initially stable state $S^{(0)}$ cannot contain *any* down flips. Analagously, if we consider the down avalanche $S^{(0)} \downarrow S^{(\lambda)} \downarrow S^{(\lambda+1)} \downarrow \dots S^{(l)}$, the intermediate inequalities contain a pair of inequalities

$$U^-(S^{(0)}) < U_\kappa^+(S^{(\lambda)}) \; , \tag{5.14}$$

$$U^-(S^{(0)}) > U_\kappa^+(S^{(\lambda)}) + c_{\kappa k} \; , \tag{5.15}$$

such that for same-sign positive coupling, a down avalanche initiated from an initially stable state $S^{(0)}$ cannot contain any up flips. Hence, via proof by contradiction, this shows that the only unambiguous avalanches that can occur for same-sign positive coupling are purely ferromagnetic avalanches.

To prove that avalanches must be purely antiferromagnetic (strictly alternating between up and down flips) if all coupling coefficients are

negative or zero, we similarly consult the intermediate inequalities from Chapter 2. Again, we use proof by contradiction. In principle, we could start from an avalanche that initially is alternating, and then has a sequence of multiple up flips, but it is is sufficient to consider a succession of up flips (the earlier steps do not matter). Hence, we consider a tentative avalanche $S^{(0)} \uparrow \ldots S^{\lambda} \uparrow S^{(\lambda+1)} \uparrow \ldots S^{(l)}$, which features two successive up flips starting at some state $S^{(\lambda)}$. For state $S^{(\lambda+1)}$, the inequalities are exactly Eqs. (5.6)–(5.8). For state $S^{(\lambda)}$, the intermediate inequalities are:

$$U^{+}(S^{(0)}) < U_i^{+}(S^{(\lambda+1)}) \; \forall i \in I_0(S^{(\lambda+1)}) \; , \tag{5.16}$$

$$U^{+}(S^{(0)}) > U_i^{-}(S^{(\lambda+1)}) \; \forall i \in I_1(S^{(\lambda+1)}) \backslash \{\kappa\} \; , \tag{5.17}$$

$$U^{+}(S^{(0)}) > U_\kappa^{-}(S^{(\lambda+1)}) \; , \tag{5.18}$$

where $\kappa = k^{+}(S^{(\lambda+1)})$. We now consider Eqs. (5.6) and (5.18). We observe that $\kappa \in I_0(S^{(\lambda)})/k$, so from Eq. (5.6) we obtain

$$U^{+}(S^{(0)}) < U_\kappa^{+}(S^{(\lambda)}) \; . \tag{5.19}$$

Furthermore, converting Eq. (5.18) to the pairwise additive model, we have

$$U^{+}(S^{(0)}) > U_\kappa^{+}(S^{(\lambda)}) - c_{\kappa k} \; . \tag{5.20}$$

Combining Eqs. (5.19) and (5.20), we retrieve that $c_{\kappa k} > 0$. We remark that this conclusion remains the same if the avalanche is initiated by a down flip rather than an up flip; hence, if all coupling coefficients are negative or zero, it is not possible to have two up flips in succession in an avalanche. Analogously, if the avalanche contains two down flips in succession rather than two up flips, the intermediate inequalities contain the pair of inequalities

$$U^{+}(S^{(0)}) > U_\kappa^{-}(S^{(\lambda)}) \; , \tag{5.21}$$

$$U^{+}(S^{(0)}) < U_\kappa^{-}(S^{(\lambda)}) + c_{k\kappa} \; , \tag{5.22}$$

which imply that $c_{k\kappa} > 0$. In conclusion, for same-sign negative coupling, it is not possible to have flips of the same sign (up/down) in succession within an avlanche initiated from an initially stable state $S^{(0)}$. Thus, the only possible unambiguous avalanches are purely antiferromagnetic avalanches.

For completeness, it should be noted that the design inequalities in Chapter 2 strictly enforce that avalanches are unambiguous, meaning that race conditions are not allowed. This distinction is important for

purely antiferromagnetic avalanches because, while is not possible for an hysteron to trigger another flip of the same sign, it is possible that a single up (down) flip triggers multiple down (up) flips *at the same time*. For example, for an up avalanche from the state (011), it is possible that both hysteron 2 and 3 both flip down in response to hysteron 1 flipping up; in fact, such cases have been observed in physical systems [46]. This behaviour highlights the significance of race conditions within the hysteron model.

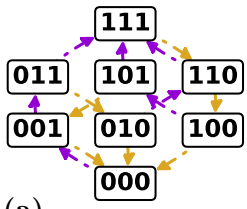
Purely ferromagnetic avalanches—. We now consider the space of t-graphs that only have purely ferromagnetic avalanches – here simply referred to as purely ferromagnetic t-graphs. In contrast to the avalanches that are possible for general interactions (Chapter 3), the number of purely ferromagnetic avalanches for a given scaffold can be systematically counted, and does not depend on the scaffold. Namely, from each state S with magnetisation m, it takes $n-m$ up flips to reach the maximal state $(11\ldots)$; hence, there are $n-m$ up avalanches possible from state S which are purely ferromagnetic. Likewise, there are m possible avalanches in the down direction which are purely ferromagnetic. By combining these avalanches, we obtain the number of purely ferromagnetic candidate graphs per scaffold:

$$N_F/N_S = \left(\prod_{m=1}^{n} m^{\binom{n}{m}}\right)^2 , \tag{5.23}$$

where N_F is the number of purely ferromagnetic candidate graphs for a given n that has purely ferromagnetic avalanches, and N_S is the number of scaffolds fo the same n. For example, for $n=2$, we find that there are four purely ferromagnetic candidate graphs per scaffold: the first has no avalanches, the second has an avalanche from state (00) up to (11), the third has an avalanche from state (11) down to state (00), and the fourth has both avalanches. For $n=3$, we find that $N_F/N_S = 576$.

We note that we have previously calculated the number of scaffolds for a given number of hysterons, N_S, in Chapter 3. Thus, we can analytically calculate the total number of candidate graphs N_F for ferromagnetic interactions:

$$N_F = N_S \times \frac{N_F}{N_S} = \frac{\left(\prod_{m=1}^{n} m^{\binom{n}{m}-1}\right)^2}{n!} \left(\prod_{m=1}^{n} m^{\binom{n}{m}}\right)^2 = \frac{\left(\prod_{m=1}^{n} m^{2\binom{n}{m}-1}\right)^2}{n!} . \tag{5.24}$$



(a)

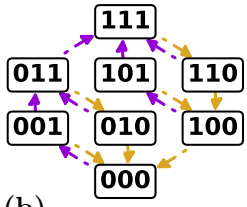
Number of up transitions

000	001	010	100	011	101	110
1	5	5	5	2	1	1

Number of down transitions

111	110	101	011	100	010	001
1	5	5	5	2	1	1

$2^2 \times 5^6 = 62500$



(b)

Number of up transitions

000	001	010	100	011	101	110
1	2	1	1	2	1	1

Number of down transitions

111	110	101	011	100	010	001
1	2	1	1	2	1	1

$2^6 = 64$

Figure 5.1: Number of purely antiferromagnetic avalanches which are possible for two example $n = 3$ scaffolds. a) Example scrambled scaffold for $n = 3$, and the number of possible purely antiferromagnetic transitions for each state and direction. b) Example Preisach scaffold for $n = 3$, and the number of possible purely antiferromagnetic transitions for each state and direction.

For two hysterons we find that $N_F = 2 \times 4 = 8$, while for three hysterons, $N_F = 96 \times 576 = 55296$. We recall that for general interactions, the number of candidate graphs for $n = 3$ is 4×10^{12} (Chapter 3). We emphasize that Eq. (5.24) quantifies a number of *candidate* graphs which are purely ferromagnetic; the number of *realizable* t-graphs can be lower.

Purely antiferromagnetic avalanches—. We now discuss the space of potential t-graphs which only have purely antiferromagnetic avalanches – we simply refer to these as purely antiferromagnetic t-graphs. First, we note that purely antiferromagnetic avalanches can be self-loops, where the avalanche revisits a previous state. The simplest such self-loop is the $l = 2$ self-loop where a single hysteron flips up, then down, or vice versa; however, we typically exclude these cases by requiring hysterons to have negative span ($u_i^+ > u_i^-$). Excluding these trivial cases, the simplest purely antiferromagnetic self-loops occur for $n = 3$: for example, the self-loop $(001) \uparrow (011) \downarrow (010) \uparrow (110) \downarrow (100) \uparrow (101) \downarrow \ldots$ (Fig. 5.1a).

As a consequence of the fact that purely antiferromagnetic avalanches can be self-loops, the number of purely antiferromagnetic avalanches

varies strongly with the scaffold. For the scaffold in Fig. 5.1a, there are four purely antiferromagnetic up avalanches possible from state (001) (or five if the $l = 6$ self-loop is included as a valid transition). By contrast, for the $n = 3$ Preisach scaffold shown in Fig. 5.1a, the only purely antiferromagnetic up avalanche that is realizable from state (001) is (001) $\uparrow$ (011) $\downarrow$ (010). In fact, all potential purely antiferromagnetic avalanches for this scaffold are of length $l = 2$ – this is a general feature of Preisach scaffolds, which we delve further into when discussing serial coupling in section 5.2.3. As a result, while for the scaffold in Fig. 5.1a there are $2^2 \times 5^6 = 62500$ purely antiferromagnetic candidate graphs, for the scaffold in Fig. 5.1b there are only $2^6 = 64$ purely antiferromagnetic candidate graphs.

We conclude this section by comparing the number of purely ferromagnetic and purely antiferromagnetic candidate graphs. From Eq. (5.24), we find that the number of purely ferromagnetic candidate graphs per scaffold for $n = 3$ is 528. For the scaffold in Fig. 5.1b, the number of purely antiferromagnetic candidate graphs is lower than this; however, for the scaffold in Fig. 5.1a, it is much higher. This contrast highlights the potential complexity of purely antiferromagnetic t-graphs, in particular for t-graphs with scrambled scaffolds.

5.2.2 Global coupling

A commonly encountered type of interactions is *global* coupling, where a single hysteron flipping causes an equal shift in the switching thresholds of all other hysterons [6]. In the pairwise additive model the interactions take the form $c_{ij} = c_j$, such that

$$U_i^{\pm}(S) = u_i^{\pm} - \sum_{j \neq i} c_j s_j \ . \tag{5.25}$$

We note that for a two-hysteron system, general pairwise interactions and global interactions take the same form; hence, the global coupling restriction only becomes meaningful for three or more hysterons.

The most notable feature of global coupling is that it forbids scrambled scaffolds; only Preisach scaffolds where the state dependent switching thresholds follow the ordering of the individual switching thresholds $u_i^{\pm}$ are allowed (see Chapter 2). We can derive this feature of global coupling from the design inequalities. Namely, we write the differences

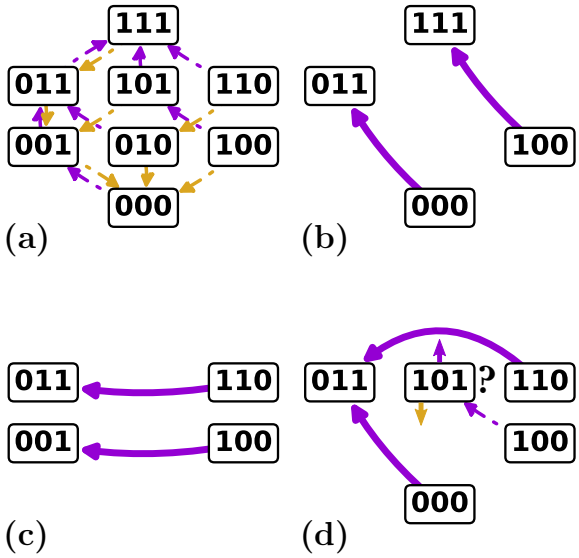


Figure 5.2: Grouping of avalanches for global coupling. a) An example Preisach scaffold which is realizable for global coupling. This scaffold is consistent with a Preisach system with ordering $u_1^+ > u_2^+ > u_3^+$, $u_1^- > u_2^- > u_3^-$; we note in passing that the states (100), (010), (101) and (110) are Garden-of-Eden states (i.e., cannot be reached from the saturated states). b) Grouping of two ferromagnetic avalanches for the scaffold in panel (a). c) Grouping of two antiferromagnetic avalanches for the scaffold in panel (a). d) Race conditions arising from a mix of ferro- and antiferromagnetic avalanches under global coupling: the state (101) is persistently unstable. An example set of parameters for which these race conditions occur is $u_1^+ = 10$, $u_2^+ = 2$, $u_1^+ = 1$, $u_1^- = 0$, $u_2^- = -7$, $u_3^- = -11$, $c_1 = 6$, $c_2 = 0$, $c_3 = 3$.

between up switching thresholds at the same state S as

$$U_i^+(S) - U_j^+(S) = (u_i^+ - u_j^+) \ , \tag{5.26}$$

and the differences between down switching thresholds as

$$U_i^-(S) - U_j^-(S) = (u_i^- - u_j^-) + (c_i - c_j) \ . \tag{5.27}$$

We see from these expressions that the ordering of the switching thresholds of two hysterons i, j only depends on the phases of the two hysterons, and is otherwise independent of the state S. Consequently, the only possible scaffolds for global coupling are those possible in the Preisach model; scrambled scaffolds are forbidden. For example, if we have $u_1^+ > u_2^+ > u_3^+$ and $u_1^- + c_1 > u_2^- + c_2 > u_3^- + c_3$, we obtain the scaffold shown in Fig. 5.2a.

A second, more subtle consequence of global coupling is that the design inequalities of an avalanche only feature those hysterons involved in the avalanche. For example, if a t-graph contains the ferromagnetic avalanche $(000) \uparrow (001) \downarrow (011)$, this implies that the $(100) \uparrow (101) \downarrow (111)$ also exist, because both transitions follow the pattern $(X00) \uparrow (X01) \uparrow (X11)$ (Fig. 5.2b). Similarly, the avalanche $(100) \uparrow (101) \downarrow (001)$ implies the existence of the avalanche $(110) \uparrow (111) \downarrow (011)$: both avalanches follow the pattern $(1X0) \uparrow (1X1) \downarrow (0X1)$ (Fig. 5.2). The grouping of avalanches for global coupling is an important feature of global coupling, as it can be employed to efficiently construct all t-graphs. This is because grouping of avalanches reduces the number of *candidate* graphs that needs to be constructed (see Chapter 3). In the next section, we describe this procedure for the case of a system where all coupling coefficients c_{ij} are negative (i.e., coupling 'in series') [6].

For completeness we note that, for mixed-sign global interactions, race conditions can arise where the up and down critical hysterons are both unstable. For example, suppose that the avalanche $(011) \uparrow (111) \downarrow (110)$ and the avalanche $(000) \uparrow (100) \uparrow (101)$ both occur in the same t-graph. The avalanche $(010) \uparrow (110) \downarrow (100)$ is then enforced, but so is the avalanche $(010) \uparrow (110) \uparrow (111)$: the state (101) is persistently unstable (Fig. 5.2d).

5.2.3 Serial coupling

We now consider a model of globally coupled hysterons which have $c_j \leq 0$ for all j; physically, this model is associated with bistable elements coupled in series [6]. We illustrate that for such serially coupled hysterons,

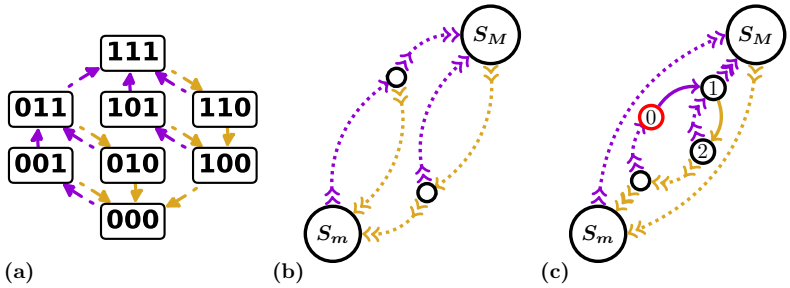


Figure 5.3: Loop return point memory for a Preisach scaffold. a) An example Preisach scaffold. b) Definition of loop return point memory: for a given loop (S_m, S_M), state S_M (S_m) is up-reachable (down-reachable) from any state on the down (up) boundary of the loop. Here purple and gold arrows of the form $>> \cdots >>$ indicate up- and down reachability. c) A sequence of transitions $S^{(0)} \uparrow S^{(1)} \downarrow S^{(2)}$ within a loop (S_m, S_M). Here the states $S^{(0)}, S^{(1)}, S^{(2)}$ are simply indicated as 0, 1, 2 respectively. State $S^{(0)}$ (highlighted) lies within the loop (S_m, S_M).

avalanches of lengths greater than two are forbidden. We show how this length-two restriction, together with the grouping of avalanches described in section 5.2.2, can be employed to efficiently construct all possible t-graphs for n serially coupled hysterons.

When all coupling coefficients c_{ij} are negative, the only possible avalanches are purely antiferromagnetic avalanches, where up and down flips alternate (see section 5.2.1). We now argue that for *serially* coupled hysterons, it is not possible to have purely antiferromagnetic avalanches of lengths longer than $l = 2$. The reason for this is that, as we have discussed above, the only possible scaffolds for global coupling are Preisach scaffolds. As an illustration of the length-2 restriction, we consider the avalanche $(001) \uparrow (011) \downarrow (010)$ in the scaffold shown in Fig. 5.3a. If we attempt to extend this avalanche via an up flip, the avalanche revisits state (011), thus forming a self-loop. The same is true for all other purely antiferromagnetic avalanches that are possible for this scaffold. Note that we only focus on avalanches here ($l > 1$), as $l = 1$ transitions for a given Preisach scaffold can be trivially realized by setting $c_j = 0$ and choosing appropriate values for $u_i^{\pm}$.

The phenomenon where purely antiferromagnetic avalanches are restricted to length $l = 2$ for Preisach scaffolds results from the fact that Preisach graphs have *loop return point memory*, which restrains the possible transitions from states S that lie within a loop [9]. Here a loop is

defined by a pair of states (S_m, S_M), where S_M can be reached from state S_m via a sequence of up transitions, and S_m can be reached from S_M via a sequence of up transitions – we say that S_M is 'up-reachable' from S_m, and S_m is 'down-reachable' from S_M. We refer to the sequences of up and down transitions between S_m and S_M as the up and down boundaries of the loop, respectively. If a system has l-RPM, then for any loop (S_m, S_M), the end point S_M (S_m) is up-reachable (down-reachable) from any state S^* that lies on the down (up) boundary of the loop (Fig. 5.3b). The resultant subloops must in turn comply with l-RPM, so that l-RPM implies a strict hierarchy of loops-within-loops [9].

Because Preisach graphs have l-RPM, the possible avalanches for a t-graph with a Preisach *scaffold* are restricted. Suppose that we have a sequence of transitions $S^{(0)} \uparrow S^{(1)}$, $S^{(1)} \downarrow S^{(2)}$, $S^{(2)} \uparrow S^3$ within a Preisach graph. Under the hierarchy imposed by l-RPM, if $S^{(0)}$ lies within a loop (S_m, S_M), then the turning point $S^{(1)}$ forms the endpoint of a subloop where the states $S^{(0)}$ and $S^{(2)}$ lie on the up and down boundary respectively (Fig. 5.3c). Thus, $S^{(1)}$ must be up-reachable from $S^{(2)}$. Furthermore, for a Preisach graph, each up (down) transition causes the magnetisation $m(S) := \sum_i s_i$ to increase (decrease) by one. We therefore have $m(S^{(3)}) = m(S^{(1)})$. If $S^{(1)} \neq S^{(3)}$, then l-RPM is broken; hence, $S^{(3)} = S^{(1)}$.

Note that we here assumed that $S^{(0)}$ lies within a loop (S_m, S_M). This entails that the state $S^{(0)}$ is reachable from the end points S_m and S_M without 'escaping' the loop, i.e., without making an up transition from S_M or a down transition from S_m. This is always the case in a t-graph if $S^{(0)}$ is reachable from the saturated states $(00\ldots)$, $(11\ldots)$. However, transitions from Garden-of-Eden states – i.e., states which cannot be reached from the main loop – are not necessarily restricted by l-RPM. Therefore, we exclude Garden-of-Eden states from our description.

In conclusion, in a Preisach graph, we cannot have a sequence of transitions $S^{(0)} \uparrow S^{(1)}$, $S^{(1)} \downarrow S^{(2)}$, $S^{(2)} \downarrow S^{(3)}$ where $S^{(3)} \neq S^{(1)}$. Consequently, if a t-graph has a Preisach scaffold, it cannot have purely antiferromagnetic avalanches of lengths longer than $l = 2$. Hence, the maximal length of avalanches in t-graphs of serially coupled hysterons is two.

Constructing all graphs—. To construct all realizable t-graphs for a given number of hysterons n, we must first construct all scaffolds, then generate all candidate graphs per scaffold, and finally check for each candidate graph whether it is realizable via the design inequalities (see

Chapter 3). We now adapt this methodology to a system of serially coupled hysterons. Constructing all candidate t-graphs is simpler than for the general case, as serially coupled hysterons feature Preisach scaffolds and only $l = 2$, 'horizontal' avalanches (magnetization is preserved) [6].

We formulate the following algorithm to generate all t-graphs:

Algorithm 5.2.1 *Let n be a given number of hysterons coupled in series.*

1. *Generate all Preisach scaffolds for n hysterons.*
2. *For each scaffold generated in (1):*
   (a) *Construct all possible length-2 antiferromagnetic avalanches (an up flip followed by a down flip or vice versa).*
   (b) *Group all transitions by their initial direction (up/down) and the hysterons flipped.*
   (c) *Generate all candidate graphs by turning each group of transitions on or off.*
   (d) *Check for each candidate graph whether the design inequalities can be satisfied for $c_{ij} = c_j$, $c_j \leq 0$; if so, add it to the list of valid t-graphs.*

We illustrate Algorithm 5.2.1 for $n = 3$. First, there are six Preisach scaffolds, which each correspond to a number of candidate graphs. For the example Preisach scaffold in Fig. 5.4a, there are six possible $l = 2$ antiferromagnetic avalanches:

- $(001) \uparrow (011) \downarrow (010)$
- $(101) \uparrow (111) \downarrow (110)$
- $(011) \uparrow (111) \downarrow (110)$
- $(110) \downarrow (100) \uparrow (101)$
- $(010) \downarrow (000) \uparrow (001)$
- $(100) \downarrow (000) \uparrow (001)$

We can divide these six avalanches into four groups:

- hysteron 2 flips up, then hysteron 3 flips down. (2 avalanches)
- hysteron 1 flips up, then hysteron 3 flips down. (1 avalanche)
- hysteron 2 flips down, then hysteron 3 flips up. (2 avalanches)
- hysteron 1 flips down, then hysteron 3 flips up. (1 avalanche)

Thus, we must construct $2^4 = 16$ candidate graphs for this scaffold. By checking the design inequalities, we find that all of these candidate graphs correspond to realizable t-graphs for coupling in series.

For all six Preisach scaffolds for $n = 3$ together, the total number of candidate graphs generated by Algorithm 5.2.1 is $16+16+4+4+4+1 = 45$. By checking the design inequalities, we find that only a single one of these candidate graphs does not correspond to a realizable t-graph; thus, there are 44 possible t-graphs for three hysterons coupled in series.

We emphasize that the number of candidate graphs that is generated by Algorithm 5.2.1 for three hysterons is drastically reduced compared to the general algorithm described in Chapter 3; in the general case, we have stated that the number of candidate graphs for three hysterons is 4×10^{12}. This reduction in the number of candidate graphs is possible because we can categorically exclude many transitions and combinations thereof. At the same time, it remains necessary to explicitly check whether each graph is realizable, as is highlighted by the occurence of a single non-realizable candidate graph.

5.2.4 Homogeneous coupling

To conclude this section, we discuss homogeneously coupled systems. We have discussed global interactions, where $c_{ij} = c_j$, in sections 5.2.2–5.2.3. Homogeneous interactions are further restricted, as $c_{ij} = C$. Notably, the state dependence of the switching thresholds $U_i^{\pm}(S)$ is only through the magnetisation, $m := \sum_i s_i$, and takes the simple form

$$U_i^+ = u_i^+ - mC \ , \tag{5.28}$$

$$U_i^- = u_i^- - (m-1)C \ . \tag{5.29}$$

Note that due to the absence of self-coupling ($c_{ii} = 0$), the up switching thresholds feature the term mC while the down switching thresholds feature the term $(m-1)C$.

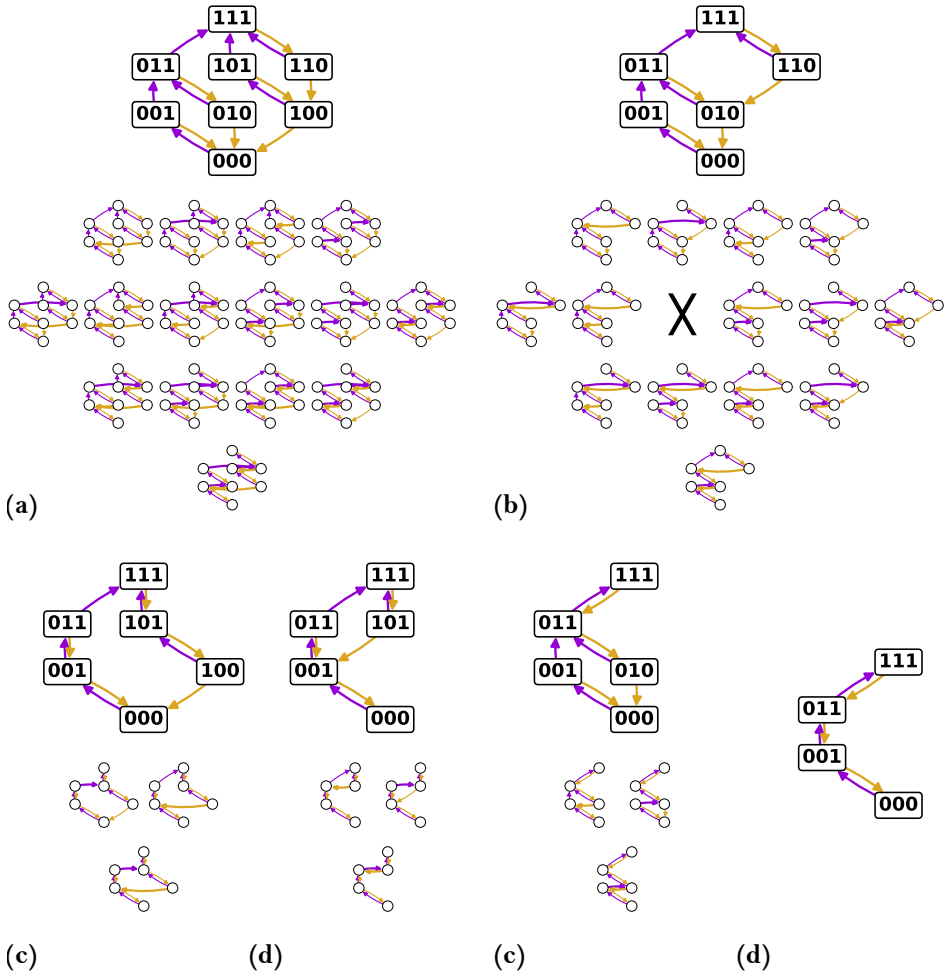


Figure 5.4: Hierarchy of candidate graphs for serially coupled hysterons. For scaffold (a) there are four groups of avalanches, thus $2^4 = 16$ candidates, which all correspond to realizable t-graphs. For scaffold (b) there are also 16 candidates, out of which 15 are realizable. For scaffolds (c)-(e) there are $2^2 = 4$ candidates per scaffold, all of which are realizable. For scaffold (f), no purely antiferromagnetic avalanches are possible, so the only candidate graph is the graph without avalanches.

Scaffold and stability—. We first consider the potential t-graphs under homogeneous coupling. Since homogeneous coupling is a restricted version of global coupling, the only allowed scaffolds are the Preisach scaffolds, with the specific scaffold following directly from the ordering of the bare switching thresholds $u_i^{\pm}$. We can see this from the design inequalities for the scaffold that are of the form $U_i^+(S) > U_j^+(S)$ and $U_i^-(S) > U_j^-(S)$; when these inequalities are written out for homogeneous coupling using Eqs. (5.28)-(5.29), we obtain

$$u_i^+ - mC > u_j^+ - mC \ , \tag{5.30}$$

$$u_i^- - (m-1)C > u_j^- - (m-1)C \ , \tag{5.31}$$

so that the magnetization drops out and the design inequalities reduce to $u_i^+ > u_j^+$ and $u_i^- > u_j^-$, which are exactly the form of the inequalities which determine a Preisach graph.

While homogeneous coupling does not affect the scaffold, it can affect the stability ranges of states. We recall that, in order for a state S to be stable, we require

$$U_i^+(S) > U_j^-(S) \ , \tag{5.32}$$

for all pairs of hysterons (i, j) where $s_i = 0$ and $s_j = 1$. Converting this inequality to homogeneous coupling, we obtain:

$$u_i^+ - mC > u_j^- - (m-1)C \ , \tag{5.33}$$

which we can rewrite as

$$C < u_i^+ - u_j^- \ . \tag{5.34}$$

Hence, if $C < u_i^+ - u_j^-$ for all i, j, all states have a valid stability range. Conversely, if $C > u_i^+ - u_j^-$ for all i, j, all states are persistently unstable except for the saturated states $(00\ldots)$ and $(11\ldots)$. Hence, varying C allows to progressively stabilize or destabilize the states.

Purely antiferromagnetic avalanches—. We now ask which avalanches can be realized when, starting from a collection of independent hysterons with bare switching thresholds $u_i^{\pm}$, we gradually introduce a homogeneous coupling C. We first note that, because all coupling coefficients have the same sign, the possible avalanches for homogeneous coupling are either purely ferromagnetic (if $C > 0$) or purely antiferromagnetic (if $C < 0$) – see section 5.2.1. We focus on the case where $C < 0$, which is a special case of serial coupling (section 5.2.3). For $C > 0$, we refer back

to our conclusions for global coupling (section 5.2.2): purely ferromagnetic avalanches must occur in groups, based on the hysterons which are flipped in the avalanche.

We have shown in section 5.2.3 that for serial coupling, the purely antiferromagnetic avalanches from a state S must have lengths $l = 2$, so long as the state S is reachable from the saturated states $(00\ldots)$ and $(11\ldots)$. We now show that, for homogeneous serial coupling, it is not possible to realize *any* purely antiferromagnetic avalanches from a reachable state S. To see this, we show that the following two statements are true:

(i) The conditions for a purely antiferromagnetic avalanche starting from state S for $C < 0$ conflict with the conditions for stability of state S for $C = 0$

(ii) A state must have a finite stability range for $C = 0$ in order to be reachable for $C = 0$.

To show (i), we consider a tentative avalanche from an initially stable state S, where hysteron i flipping up triggers hysteron j to flip down. According to the design inequalities, this requires

$$U_i^+(S) < U_j^-(S^{+i}) \ . \tag{5.35}$$

where S^{+i} is the state which is obtained by flipping up hysteron i in state S. For a homogeneously coupled system, this inequality becomes

$$u_i^+ - mC < u_j^- - mC \ , \tag{5.36}$$

where m is the magnetisation of the initial state S. Since Eq. (5.36) reduces to $u_i^+ < u_j^-$. Similarly, an avalanche where hysteron j flipping down is followed by hysteron i flipping up would yield the requirement

$$U_i^+(S^{-j}) < U_j^-(S) \ , \tag{5.37}$$

which for homogeneous coupling becomes

$$u_i^+ - (m-1)C < u_j^- - (m-1)C \ . \tag{5.38}$$

Again, this inequality reduces to $u_i^+ < u_j^-$. However, the condition $u_i^+ < u_j^-$ implies that the initial state S is persistently unstable for $C = 0$, which shows that (i) is correct.

Note that the condition $u_i^+ < u_j^-$ does *not* necessarily imply persistent instability of the initial state S for $C < 0$. As we have described in Eq. (5.34), stability of state S for homogeneous coupling merely implies that $C < u_i^+ - u_j^-$; for a sufficiently large $C < 0$, no states are persistently unstable. Thus, the mere requirement that state S is initially stable for $C < 0$ does not prevent purely antiferromagnetic avalanches from this state.

We now show (ii), namely that a state must be stable for $C = 0$ in order to be reachable for $C < 0$. This argument consists of three steps. First, following Eqs. (5.30) and (5.31), note that the t-graphs for $C = 0$ and for $C < 0$ have the same scaffold. Second, any state which is reachable for $C < 0$ must also be reachable for $C = 0$. This is because, if states are not reachable in a Preisach *graph*, then the corresponding Preisach *scaffold* does not provide a path for any avalanches to reach these states. Third, we note that, if a state S is reachable for $C = 0$, this implies that the state has a finite stability range (i.e., is not persistently unstable) for $C = 0$. These three steps together show that (ii) is correct: any states that are reachable for $C < 0$ must have a finite stability range for $C = 0$. Thus, combining (i) and (ii), we find that avalanches from a reachable state S are forbidden for $C < 0$.

In conclusion, for homogeneous serial coupling ($C < 0$) it is not possible to realize avalanches from any states that are reachable from the saturated states $(00\ldots)$ and $(11\ldots)$. We stress, however, that homogeneous coupling does not forbid purely antiferromagnetic avalanches entirely (in contrast to large-span systems, which we discuss in section 5.3.1). To see this, consider a Garden-of-Eden state that is persistently unstable in a Preisach system. By introducing a homogeneous coupling $C < 0$, one can stabilize this state, and under the right conditions, a purely antiferromagnetic avalanches from this GoE state are possible.

5.3 Large and Small Span

The interacting hysteron model captures a wide variety of behaviours. One reason for its dazzling complexity is that it features a wide range of choices for the hysteron spans. For example, we can consider the limit of large span, where the average span is much larger than the other relevant parameters (section 5.3.1). On the other end of the spectrum, in the limit where the hysteron span σ_i approaches 0, a hysteron reduces to a binary spin - here simply called a spin (section. 5.3.2). In turn,

interactions between at least two spins can give rise to emergent hysterons (section. 5.3.3). In this section we investigate the hysteron model in the limits of large and vanishing span.

5.3.1 Large span

In this section, we discuss how the t-graph response of an interacting hysteron system is affected by the hysteron span $\sigma_i := u_i^+ - u_i^-$. We show that the scaffold and ferromagnetic avalanches are invariant under changes in the mean span. However, the mean span does affect antiferromagnetic avalanches and the stability of states: if the mean span is sufficiently large, then all states S have a finite stability range, and no antiferromagnetic avalanches (including self-loops) can occur. We argue that the span thus plays a stabilizing role in the response of an interacting hysteron system.

First, we consider how the hysteron span σ_i features into the design inequalities. We recall from Chapter 2 that all design inequalities are of the form $U_i^{\pm}(S_A) > U_j^{\pm}(S_B)$. We can separate these inequalities into three groups, based on the sign (up/down) of the two switching thresholds: inequalities where two up thresholds are compared, inequalities where two down thresholds are compared, and inequalities where an up threshold is compared against a down threshold. Specifically, these differences between switching thresholds $U_i^+(S_A) - U_j^+(S_B)$, $U_i^-(S_A) - U_j^-(S_B)$ and $U_i^+(S_A) - U_j^-(S_B)$ can be written as:

$$U_i^+(S_A) - U_j^+(S_B) = (u_i^+ - u_j^+) - f(S_A, S_B, c_{ij}) \ , \tag{5.39}$$
$$U_i^-(S_A) - U_j^-(S_B) = (u_i^- - u_j^-) - f(S_A, S_B, c_{ij}) \ , \tag{5.40}$$
$$U_i^+(S_A) - U_j^-(S_B) = (u_i^+ - u_j^-) - f(S_A, S_B, c_{ij}) \ . \tag{5.41}$$

Here $f(S_A, S_B, c_{ij})$ is a linear combination of the coupling coefficients:

$$f(S_A, S_B, c_{ij}) = \sum_{k \neq i} c_{ik} s_{k,A} - \sum_{k \neq j} c_{jk} s_{k,B} \ , \tag{5.42}$$

where $s_{k,A}, s_{k,B}$ are the phases of hysteron k in state S_A and S_B, respectively.

We note that Eqs. (5.39) and (5.40) do not feature the mean span $\sigma = \langle u_i^+ - u_i^- \rangle$, but only feature the differences between individual switching threshold $u_i^+ - u_j^+$, $u_i^- - u_j^-$; thus, Eqs. (5.39) and (5.40) are invariant to changes in the mean span. This leads to the following theorem:

Theorem 5.3.1 (Mean span invariance) *Features of a t-graph are invariant to changes in the mean hysteron span $\sigma := \langle u_i^+ - u_j^+ \rangle$ if the associated design inequalities are of the form $U_i^+(S_A) > U_j^+(S_B)$ or $U_i^-(S_A) > U_j^-(S_B)$, so long as the differences between individual switching thresholds $u_i^+ - u_j^+$ and $u_i^- - u_j^-$ remain constant.*

We now focus on the response to changes in the mean span for features with design inequalities of the form $U_i^+(S_A) > U_j^-(S_B)$. We observe that we can write the term $u_i^+ - u_j^-$ in Eq. (5.41) in terms of the mean span σ and the differences between individual switching thresholds $u_i^+ - u_j^+$, $u_i^- - u_j^-$:

$$u_i^+ - u_j^- = \sigma + (u_i^- - u_j^-) + \frac{1}{n}\sum_{k\neq i}\{(u_i^+ - u_k^+) - (u_i^- - u_k^-)\} \ . \quad (5.43)$$

We can use Eq. (5.43) to rewrite Eq. (5.41) as:

$$U_i^+(S_A) - U_j^+(S_B) = \sigma + f(S_A, S_B, \{c_{ij}\}) + g_{ij}(\{u_k^+ - u_k^+\}, \{u_k^- - u_k^-\}) \quad (5.44)$$

where we define g_{ij} as the linear combination:

$$g_{ij}(\{u_k^+ - u_k^+\}, \{u_k^- - u_k^-\}) = (u_i^- - u_j^-) + \frac{1}{n}\sum_{k\neq i}\{(u_i^+ - u_k^+) - (u_i^- - u_k^-)\} \ . \quad (5.45)$$

Hence, the mean span implicitly features into design inequalities of the form $U_i^+(S_A) > U_j^-(S_B)$. Based on Eq. (5.44), we can formulate the following theorem:

Theorem 5.3.2 (Stabilization) *If the mean span σ is sufficiently large compared to $|u_i^+ - u_j^+|$, $|u_i^- - u_j^-|$ and $|c_{ij}|$ for all i, j, then design inequalities of the form $U_i^+(S_A) > U_j^-(S_B)$ are always true.*

Note that Theorem 5.3.2 is a statement of sufficiency, not necessity; design inequalities of the form $U_i^+(S_A) > U_j^-(S_A)$ can still be true if the mean span σ is small. The precise value that the mean span needs to exceed depends on the states S_A, S_B, as well as the hysteron indices i, j. We refer to Theorem 5.3.2 as the 'stabilization' theorem because, as we show below, t-graph features which require a down threshold to be higher than an up threshold are typically those where hysterons are unstable.

While Theorems 5.3.1 and 5.3.2 are simple, these theorems have profound implications for t-graph design, because they suggest that the mean

span can be used to tune select features of a t-graph without affecting others. Moreover, these rules apply regardless of the number of hysterons n. We now detail how Theorems 5.3.1 and 5.3.2 apply to the scaffold, to the stability of individual states, and to avalanches.

Scaffold and state stability—. First, we consider how the scaffold and stability of states depend on the mean span. For the scaffold, the design inequalities are of the form $U_i^+(S) > U_j^+(S)$ and $U_i^-(S) > U_j^-(S)$; these inequalities specify that the critical up and down hysterons are those hysterons with the highest up and lowest down switching thresholds, respectively (see Chapter 2). From Theorem 5.3.1, we find that the scaffold is invariant to changes in the mean span σ.

Next, we consider the stability range of each state S. In order for a state S to be stable at some value of the driving field U, we require that $U^+(S) > U^-(S)$, where $U^\pm(S)$ are the state switching thresholds. If this inequality is not satisfied, we refer to the state S as being persistently unstable. Since these design inequalities compare an up switching threshold against a down switching threshold, this individual state stability is dependent on the mean span σ. Following Theorem 5.3.2, we find that all states have a valid stability range if the mean span is sufficiently large. Note that this does not imply that all states are reachable, starting from one of the saturated states, but only that if the system is placed into a given state (e.g. via physically forcing the system), it is able to stably remain in this state. In conclusion, changes in the mean span do not affect the scaffold, but a sufficiently large mean span does prevent persistently unstable states.

Avalanches—. We now consider the effect of changes in the mean span on the avalanches. To do so, we refer back to the final and intermediate inequalities formulated in Chapter 2.

First, we consider the final inequalities associated with the terminal state $S^{(l)}$ of any (avalanche) transition; for definiteness we consider an up transition $S^{(0)} \uparrow \dots S^{(l)}$. Following Chapter 2, we obtain the inequalities

$$U^+(S^{(0)}) < U_i^+(S^{(l)}) \ \forall i \in I_0(S^{(\lambda)}) \ , \tag{5.46}$$

$$U^+(S^{(0)}) > U_i^-(S^{(l)}) \ \forall i \in I_1(S^{(\lambda)}) \ , \tag{5.47}$$

where $I_0(S)$ ($I_1(S)$) is the collection of hysterons in phase 0 (1) in state S.

We observe that the role of the mean span σ for (avalanche) transitions is more complex than for the inequalities that we have discussed for the scaffold and for state stability, since Eq. (5.46) compares pairs of up switching thresholds, while Eq. (5.47) compares up and down switching thresholds. It is therefore useful to individually consider the features associated with Eq. (5.46) and Eq. (5.47).

To start with, Eq. (5.46) prescribes the conditions that must be satisfied in order for the hysterons in $I_0(S^{(\lambda)})$ to be stable: informally, the hysterons that can switch up. Since these inequalities compare pairs of up switching thresholds, following Theorem 5.46, the (in)stability of these hysterons is invariant under changes to the mean span. By contrast, Eq. (5.47) prescribes that the up threshold $U^+(S^{(0)})$ should be greater than the down thresholds $U_i^-(S^{(l)})$ in order for the hysterons in $I_1(S^{(l)})$ (the hysterons that can switch down) to be stable. Following Theorem 5.3.2, these inequalities are always satisfied if the mean span σ is sufficiently large. Thus, if a t-graph contains a complex up avalanche which consists of both up and down flips, then for sufficiently large span, this avalanche will be cut off at the first state where all up hysterons are stable. Analogously, a down avalanche is terminated at the first state where all down hysterons are stable. If an up (down) avalanche is unambiguous – i.e., there are no race conditions – then a sufficiently large span simply cuts off the avalanche at the first down (up) flip. For example, the $l = 5$ avalanche $(0001) \uparrow (0011) \uparrow (0111) \downarrow (0110) \uparrow (1110) \downarrow (1010)$ would reduce to the $l = 2$ avalanche $(0001) \uparrow (0011) \uparrow (0111)$ for sufficiently large span.

In short, if a hysteron system has an unambiguous t-graph response, then a sufficiently large mean span σ truncates the avalanches in the t-graph, such that all up (down) avalanches consist of only up (down) flips. We have previously encountered such avalanches, called purely ferromagnetic avalanches, in section 5.2.1, when discussing same-sign coupling. In fact, while the mean span is a useful parameter for tuning hysteron responses in general, it is a particularly powerful complement to systems with same-sign negative coupling. Namely, we have argued in section 5.2.1 that for same-sign negative coupling, all avalanches must be purely antiferromagnetic (i.e., consist of alternating up and down flips). If, in addition to this, the mean span is sufficiently increased, then these purely antiferromagnetic avalanches are truncated to single flips. Thus, systems with both same-sign negative coupling and large span can be employed in order to physically realize hysteron systems which have scram-

bling without avalanches.

For completeness, we finally consider how changes in the mean span affect race conditions. To this end, we inspect the intermediate inequalities associated with an unambiguous up flip from an intermediate state $S^{(\lambda)}$, within an up avalanche $S^{(0)} \uparrow \dots S^{(\lambda)} \uparrow \dots S^{(l)}$. These are:

$$U^+(S^{(0)}) < U_i^+(S^{(\lambda)}) \; \forall i \in I_0(S^{(\lambda)}) \backslash \{k\} \; , \tag{5.48}$$

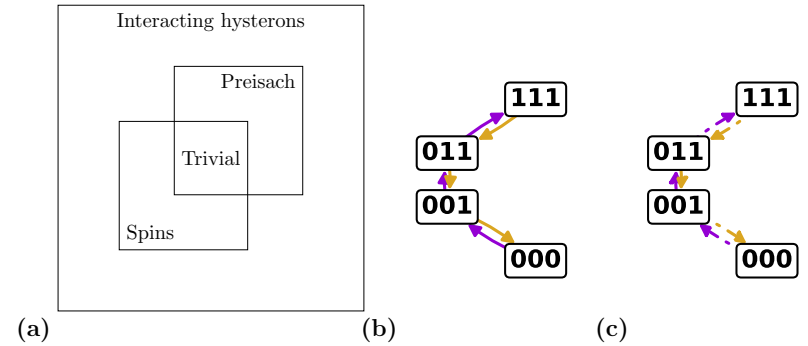
$$U^+(S^{(0)}) > U_i^-(S^{(\lambda)}) \; \forall i \in I_1(S^{(\lambda)}) \; , \tag{5.49}$$

$$U^+(S^{(0)}) > U_k^+(S^{(\lambda)}) \; , \tag{5.50}$$

where k is the critical up hysteron at state $S^{(\lambda)}$, denoted $k^+(S^\lambda)$. We note that Eq. (5.50) must be satisfied in order for the critical hysteron k to be unstable; since this inequality compares two up switching thresholds, according to Theorem 5.3.1, the instability of hysteron k is invariant under changes in the mean span σ. Provided that Eq. (5.50) is satisfied, Eqs. (5.48) and Eqs. (5.49) are then associated with the stability of the noncritical hysterons in phase 0 and 1, respectively. Note that Eqs. (5.48) and (5.49) have a similar form as Eqs. (5.46) and (5.47), except that the latter do not include the critical hysteron k. We therefore refer back to the conclusions we have drawn for the final inequalities: the (in)stability of the noncritical up switching thresholds is invariant under changes to the mean span σ, whereas the noncritical down switching thresholds are always stable when the mean span is sufficiently large. Thus, if an up avalanche encounters race conditions, these can be resolved via a sufficiently large span, but only in part: race conditions where the critical up and down hysteron are both unstable are resolved in favour of the critical up hysteron, but race conditions where multiple up hysterons are unstable are left in place. If these race conditions are explicitly resolved, for example by applying a rule where only the most unstable hysteron flips, then an unambiguous purely ferromagnetic avalanche is retrieved.

5.3.2 The zero-span limit

In the limit of zero span, the interacting hysteron model encompasses models of interacting spins. In turn, interacting spins have emergent hysteretic behaviour, which under specific circumstances can be described by hysterons. Therefore, all hysteron behaviour can also be captured by spins. This raises the question of what behaviours of the model might be described as 'hysteronic' or 'spinlike'.



(a) (b) (c)

Figure 5.5: The spin limit of the hysteron model in the presence and absence of interactions. a) Schematic representation of spins within the parameter space of interacting hysterons: the space of interacting hysterons encompasses that of interacting spins, and the behaviour of independent spins is trivial. b) Non-interacting spins can only exhibit trivial t-graphs, where up and down transitions for each spin are paired. c) Scaffold for independent spins.

In this section we investigate the spin limit of hysteron systems. In these, the upper and lower switching thresholds of hysteron i in state S are identical:

$$U_i^+(S) = U_i^-(S) =: U_i(S) \ . \tag{5.51}$$

Note, we use the phrase 'spin system' here strictly in the context of zero temperature, deterministic models - distinct from, e.g., spin glasses that start from the definition of a Hamiltonian. We show that a fundamental distinction between spin and hysteron behaviours lies in the fact that scaffolds and avalanches are strongly intertwined for spins, and therefore, t-graphs without avalanches are associated with 'hysteronic' behaviour.

Intertwinement of scaffold and avalanches for spins—. The goal of this section is to clarify the distinction between the t-graph topologies of interacting spins and interacting hysterons. We first note that, because binary spins are simply the limit of hysterons where $\sigma_i \to 0$, the space of t-graphs of interacting hysterons encompasses all t-graphs exhibited by interacting spins (Fig. 5.5a). This does not require that a hysteron's span is exactly zero; since the driving response of a hysteron system only depends on the *order* of switching thresholds, the t-graph topologies of hysterons are the same as those of spins, whenever their span is small enough so that it does not affect the ordering of switching thresholds.

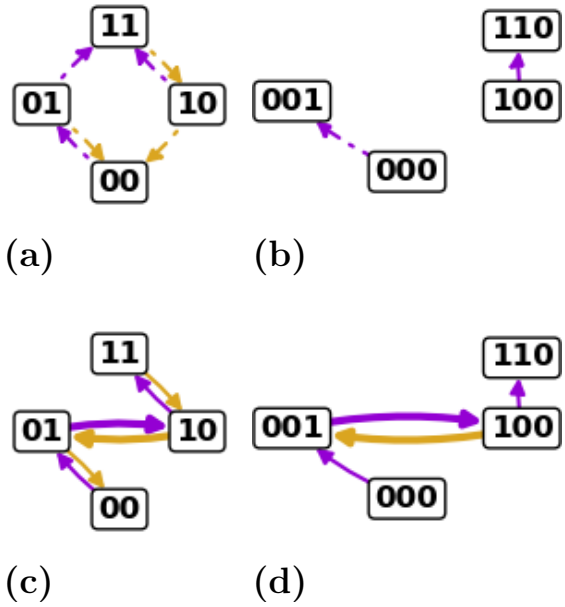


Figure 5.6: Intertwinement of scaffold and avalanches for spins. a) Preisach scaffold for $n = 2$ which is not realizable for independent spins, but can be achieved for interacting spins. b) Scrambling for $n = 3$; this is achievable for interacting spins. c) Avalanches which arise for interacting spins that form the scaffold in (a), where $u_1 = 2, u_2 = 1, c_{21} = -2$. d) Avalanches which arise for interacting spins that form the scaffold in (b), where $u_1 = 2, u_2 = 3, u_3 = 1$ and $c_{31} = -3$.

The crucial point is that there are t-graph topologies that can only be seen for interacting hysterons, so that we can describe a t-graph as being 'hysteronic' or 'spinlike'.

A fundamental difference between hysteronic and spinlike behaviour arises in the relation between scaffolds and avalanches. For hysterons, as outlined in Chapter 3, it is useful to understand t-graphs as being composed of a scaffold which is dressed by avalanches–indeed, it can be beneficial to disregard complexities from avalanches entirely, as we have discussed example for multiperiodic loops in Chapter 4. The scaffold-avalanche structure is also applicable to spins, given that spins are simply a limit of the hysteron model. However, as we illustrate below, scaffolds

and avalanches are strongly intertwined for spins, whereas this is not the case for hysterons.

Before we discuss the difference between interacting spins and interacting hysterons, we first compare the two systems in the absence of interactions (Fig. 5.5). As discussed, in a system of n independent hysterons–i.e., the Preisach model–there are $n!$ possible t-graphs [30, 36]. By contrast, for independent *spins*, the response to driving is trivial: the spins are simply in phase 0 or 1 if their switching threshold is above or below the current value of the driving U, respectively, so only a single 'trivial' t-graph is possible (Fig. 5.5b). Accordingly, there is only a single possible scaffold (Fig. 5.5c). Compared to independent spins, the Preisach model thus increases the number of possible t-graphs – and hence, the number of scaffolds – by $n! - 1$.

In the presence of interactions, interacting spin systems can show complex t-graph responses which, as for hysterons, can be categorized by separately considering the scaffold and avalanches (Chapter 3). To illustrate how the t-graphs of interacting spins differ from the broader space of t-graphs for interacting hysterons, we first outline the effects of spin interactions on the scaffold. For n *independent* spins, as discussed above, the only realizable scaffold is the trivial case where all flips are reversible. In the presence of interactions, however, the remaining $n! - 1$ Preisach scaffolds can also be realized, as we show below. Moreover, just like interacting hysterons, interacting spins can exhibit scrambling (Chapter 2). These are two separate mechanisms, which we illustrate below. We would like to stress that the discussion below focusses on the scaffolds. In particular, we will show that all t-graphs associated with non-trivial scaffolds feature avalanches.

First, interactions in spin systems can be employed to reach Preisach scaffolds that would be impossible for independent spins. As an example of such a construction, suppose that we have a system of two spins, with $u_1 = 2$ and $u_2 = 1$. If the spins are independent, we have $U_1(00) > U_2(00)$ and $U_1(11) > U_2(11)$, so that the critical hysterons for states (00) and (11) are:

$$k^+(00) = 2 \ , \tag{5.52}$$

$$k^-(11) = 1 \ , \tag{5.53}$$

which gives the Preisach scaffold where all flips are reversible. Now suppose, however, that we add a coupling $c_{21} = -2$. The ordering of spins 1 and 2 in state (11) flips so we have $k^-(11) = 2$, and we obtain the other

$n = 2$ Preisach scaffold (Fig. 5.6a).

The mechanism underlying the above example can be used to reach *all* Preisach scaffolds, for any number of spins n. The principle of this mechanism is to use the coupling c_{ik} from a given spin k as a substitute for the span σ_k when comparing two down switching thresholds. In the above example, the coupling $c_{21} = -2$ is used to flip the ordering of spins 1 and 2 in state (11); the same scaffold could be achieved in a Preisach system via a nonzero span $\sigma_1 = 2$. We now prove that, more generally, a Preisach scaffold can be replicated in a spin system by substituting each span σ_k with a coupling $c_{ik} = c_k$ (referred to as global coupling; see also section 5.2.2). We first consider the differences between the up and down switching thresholds of hysterons i, j:

$$U_i^+(S) - U_j^+(S) = (u_i - u_j) - \sum_{k \neq i,j} (c_{ik} - c_{jk}) s_k \ , \tag{5.54}$$

$$U_i^-(S) - U_j^-(S) = (u_i + c_{ji} - u_j - c_{ij}) - \sum_{k \neq i,j} (c_{ik} - c_{jk}) s_k \ , \tag{5.55}$$

The term $\sum_{k \neq i,j} (c_{ik} - c_{jk}) s_k$ in these expressions is responsible for scrambling. If we set $c_{ik} = c_k$, then the scrambling term disappears, and the two expressions simplify to:

$$U_i^+(S) - U_j^+(S) = u_i - u_j \ , \tag{5.56}$$

$$U_i^-(S) - U_j^-(S) = u_i + c_i - u_j - c_j \ . \tag{5.57}$$

By setting $c_k = -\sigma_k$, we can replicate the scaffold of any Preisach system. We emphasize that, while this method is generally applicable, it only applies to the *scaffold*; we discuss the role of avalanches later.

The second mechanism by which interactions affect the scaffold of a spin system is scrambling. We consider a system of three interacting spins, and compare spins 2 and 3 in the states (000) and (100). Suppose that we have $u_1 = 2, u_2 = 3, u_3 = 1$. Without interactions, we would have $U_2(000) > U_1(000)$ and $U_2(100) > U_3(100)$, as the switching thresholds are unaffected by the state of spin 1. However, if we add a coupling $c_{13} = -3$, then $U_2(100) < U_3(100)$, so that $k^+(100) = 2$–the ordering of spins 2 and 3 is scrambled between the states (000) and (100) (Fig. 5.6b).

We note that the mechanisms underlying Preisach scaffolds and scrambling are independent: the Preisach scaffold depends on the average coupling c_k from a spin k, whereas scrambling depends on the differences $c_{ik} - c_{jk}$ between coupling coefficients from the same spin k. Thus, by

combining scrambling with the first mechanism, any scaffold that can be obtained in a hysteron model can also be obtained in a spin model.

These two mechanisms mean that, just from looking at the scaffold, we would not be able to tell the difference between an interacting hysteron system and that of an interacting spin system. There is a crucial difference, however, between the responses of a spin system and of a hysteron system: for spin systems, nontrivial scaffolds *lead to avalanches in the t-graphs*. We illustrate this by constructing the full t-graphs for the examples above. For the first example, where $u_1 = 2, u_2 = 1, c_{21} = -2$, we have that $U_1^+(01) = 2$ but $U_2^-(11) = 3$, so an avalanche $(01) \uparrow (11) \uparrow (10)$ occurs. The same coupling causes an avalanche $(10) \downarrow (00) \downarrow (10)$ when spin 1 flips down from state (10) (Fig. 5.6c). For the second example, where $u_1 = 3, u_2 = 2, u_3 = 1$ and $c_{31} = -3$, we have that $U^-(100) = U_1(100) = 3$ but $U_3(000) = 2$, so a down avalanche $(100) \downarrow (000) \uparrow (001)$ occurs. The same coupling coefficient also causes an avalanche $(001) \uparrow (101) \downarrow (100)$ when spin 1 flips in the other direction (Fig. 5.6d). These two examples illustrate that when interacting spins have nontrivial scaffolds, these naturally lead to avalanches.

In short, while nontrivial scaffolds (both Preisach and scrambled) can occur for both interacting hysterons and interacting spins, t-graphs which have such nontrivial scaffolds *without avalanches* are quintessentially 'hysteronic'. Consequently, the structure we have presented for hysterons, where we see t-graphs as scaffolds independently dressed by avalanches (Chapter 3) is not a natural approach for spin systems.

5.3.3 Spin pair constructions for a single hysteron.

We have illustrated that t-graphs of spin systems cannot have nontrivial scaffolds without exhibiting avalanches. We now show that, using avalanches, we can replicate the behaviour of a hysteron in a pair of spins. We lay out two distinct constructions: the first uses symmetric coupling, and the second uses asymmetric coupling [2].

The first method for reproducing hysteron behaviour uses pairs of spins, A and B, with symmetric coupling $c_{AB} = c_{BA} = C > 0$. Further, we assumes that $u_B - u_A := \Delta > 0$. Using this construction, spins A and B collectively behave as a hysteron which switches up at u_A and switches down at $u_B - C$ (Fig. 5.7a). To mimic a target hysteron with switching thresholds $u^\pm$ with a pair of spins, we set $u_A = u^+$, $u_B = u^+ + \Delta$, and

[2] A version of this work was previously published as supplementary information [60].

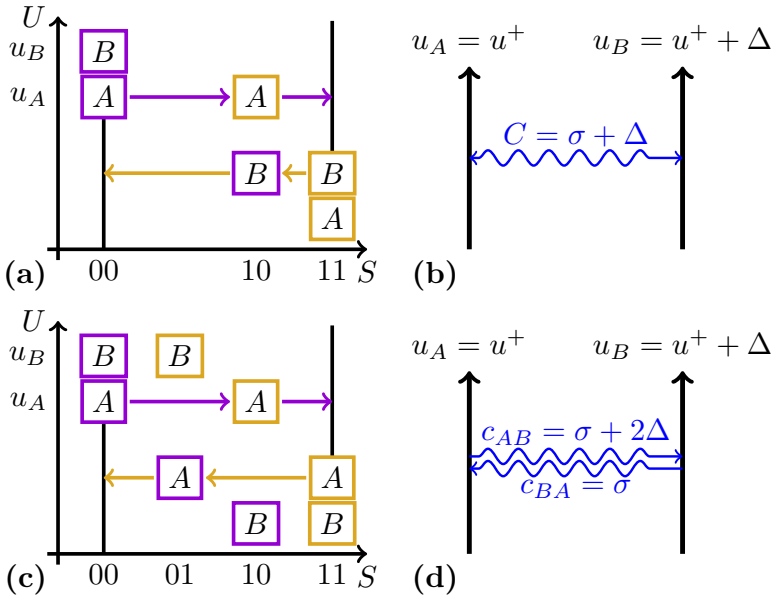


Figure 5.7: Two constructions to replicate hysteron behaviour using ferromagnetically interacting spins. a) Hysteretic response for two spins in the symmetrically coupled construction ($c_{AB} = c_{BA}$). Indicated are the switching thresholds (boxes; the labels A and B indicate the spin) and transitions (arrows). The collective state of the spins is labelled as $S = (s_A, s_B)$. b) Schematic of a coupled pair of spins; parameters are indicated for mimicking a given hysteron using the symmetric construction. c) Hysteretic response from two spins with asymmetric coupling $c_{AB} > c_{BA}$. Note that spin A is the first spin to flip in both the up and down direction. d) Parameters for mimicking a given hysteron with switching thresholds $u^{\pm}$ and resulting span σ in the asymmetric construction.

$C = \sigma + \Delta$ (Fig. 5.7b): note that the up transition is initiated by spin A switching up, yet the down transition is initiated by spin B switching down. The parameter Δ can be chosen arbitrarily for a single hysteron, but for multiple interacting hysterons there are subtleties that we discuss below.

The second method uses a spin pair with asymmetric coupling where we again impose $u_B - u_A = \Delta > 0$. We let the coupling from spin A to spin B be large enough to trigger an avalanche ($c_{BA} > u_B - u_A$). Finally, we let spin B couple back to spin A with a coupling $c_{AB} > 0$, which is weak enough that $u_A - c_{AB} > u_B - c_{BA}$. In this way we obtain a hysteretic response where there is an up transition at u_A and a down transition at $u_A - c_{AB}$(Fig. 5.7c). We can mimic a target hysteron with switching thresholds $u^{\pm}$ and resulting span $\sigma = u^+ - u^-$ by setting $u_A = u^+$ and $c_{BA} = \sigma$: note that, in contrast with the symmetrically coupled construction, the up and down avalanches are both initiated by spin A switching up and down respectively. In addition, u_B then follows from the requirement that $u_B - u_A = \Delta > 0$. Finally, for the coupling c_{AB}, we must then have that $c_{AB} > \sigma + \Delta$ (Fig. 5.7c); for the sake of symmetry, we set $c_{AB} = \sigma + 2\Delta$ (Fig. 5.7d). Again, the parameter Δ can be freely chosen.

The two constructions given here are not exhaustive with respect to the hysteretic behaviour that can emerge from interacting spins. Still, these two simple constructs powerfully illustrate the different ways that hysterons can emerge in a system of interacting spins.

Reproducing t-graphs using spin pairs We have outlined two methods to mimic hysteron behaviour using ferromagnetically interacting pairs of spins. We can use these constructions to replicate the behaviour of a collection of n interacting hysterons using $2n$ interacting spins. As an illustration, suppose that we have a pair of hysterons (Fig. 5.8a) with bare switching thresholds:

$$(u_1^+, u_2^+, u_1^-, u_2^-) = (2, 1, -2, -1) \tag{5.58}$$

and antiferromagnetic coupling $c_{21} = -4$, so that the coupling matrix is:

$$c_{ij} = \begin{pmatrix} 0 & 0 \\ -4 & 0 \end{pmatrix}$$

This set of parameters produces the t-graph shown in Fig. 5.8b. By replacing each hysteron with a spin pair, using one of the two constructions

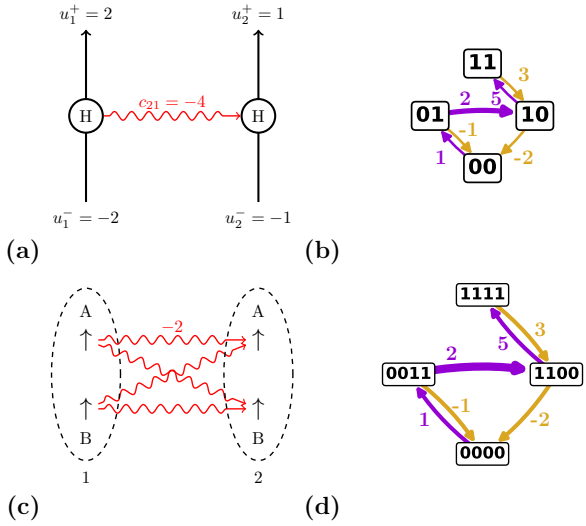


Figure 5.8: Replicating a system of interacting hysterons using spin pairs. a) Schematic of an example system of two interacting hysterons. b) T-graph for example hysteron parameters in panel (a); for each transition, the critical switching threshold is indicated. c) System of two coupled pairs of spins which mimicks the system in panel (a-b). The hysteron coupling coefficient $c_{21} = -4$ is distributed over the four spins $1A, 1B, 2A, 2B$. Note that we do not indicate the internal coupling between A and B for the two spin pairs; either the symmetric or the asymmetric construction can be substituted here. d) T-graph for $n = 4$ spins which mimicks the $n = 2$ t-graph in panel (b).

outlined above, we can convert this $n = 2$ hysteron system to a system of four spins, which we label $1A, 1B, 2A, 2B$ (Fig. 5.8c-d). We now detail the required parameters such that the desired t-graph topology is realized. We first outline the coupling between the spin pairs that is required to replicate the coupling c_{ij} between the hysterons. We then give the full parameters when using the symmetric or asymmetric construction, where we discuss subtleties arising from race conditions.

To start with, we must convert the original coupling c_{21} to a coupling between the spins $1A, 1B, 2A, 2B$. We remark that, since spins $2A, 2B$ collectively form hysteron 2, both spins must be shifted by c_{21}. Furthermore, the contribution from hysteron 1 is now divided over two spins $1A$, $1B$. By letting spins $1A$, $1B$ contribute equally to the coupling c_{21}, we

obtain:

$$c_{2A1A} = c_{2A1B} = c_{2B1A} = c_{2B1B} = c_{21}/2 \ . \tag{5.59}$$

Using that $c_{21} = -4$, we find $c_{1A2A} = c_{2A1B} = c_{2B1A} = c_{2B1B} = -2$, as shown in Fig. 5.8c.

We now consider the internal coupling between $1A, 1B$ and $2A, 2B$ that is required when either the symmetric or asymmetric construction is employed. Starting with the symmetric construction, by referring back to Fig. 5.7d, we find for the switching thresholds:

$$(u_{1A}, u_{1B}, u_{2A}, u_{2B}) = (2, 2+\Delta, 1, 1+\Delta) \tag{5.60}$$

and for the coupling:

$$c_{1A1B} = c_{1B1A} = 4 + \Delta \ , \tag{5.61}$$
$$c_{2A2B} = c_{2B2A} = 2 + \Delta \ . \tag{5.62}$$

The coupling matrix for our example system then becomes:

$$c_{ij} = \begin{pmatrix} 0 & 4+\Delta & 0 & 0 \\ 4+\Delta & 0 & 0 & 0 \\ -2 & -2 & 0 & 2+\Delta \\ -2 & -2 & 2+\Delta & 0 \end{pmatrix} \ .$$

When a t-graph has no avalanches, then the above construction is sufficient to mimic the t-graph response using pairs of spins. However, if the original t-graph has avalanches such as the transition $(01) \uparrow (11) \downarrow (10)$ Fig. 5.8b, then issues might arise due to race conditions, and the parameter Δ becomes relevant.

There are two types of race conditions that can occur. The first of these are race conditions where both spins A, B within the same 'hysteron' are unstable at the same time. These race conditions can be accounted for by making the parameter Δ sufficiently large. The second type of race conditions occurs when spins from different 'hysterons' are unstable at the same time, and this type of race conditions cannot be easily resolved. We illustrate these two types of race conditions below.

The first type of race condition occurs if Δ is very small. As an illustration, we consider how the avalanche $(01) \uparrow (11) \downarrow (10)$ in Fig. 5.8b translates to the avalanche $(0011) \uparrow (1011) \uparrow (11111) \downarrow (1110) \downarrow (1100)$ in Fig. 5.8c. For the above set of parameters, the part of the transition from (0011) to (1011) occurs as intended: spin $1A$ flips first, followed by spin

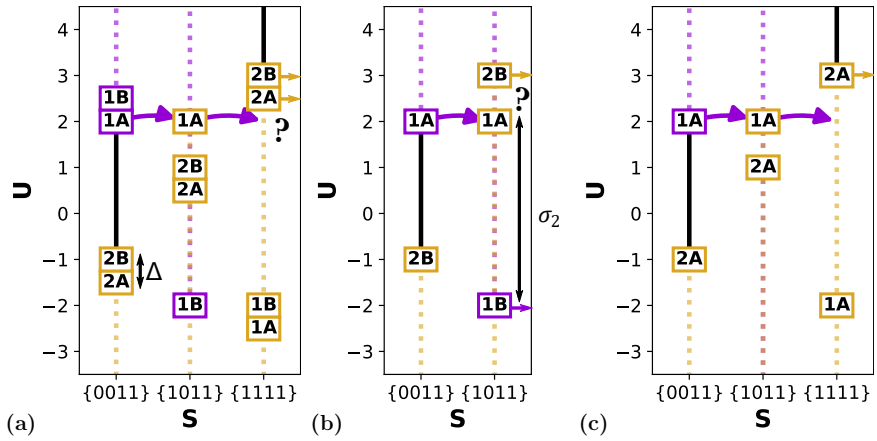


Figure 5.9: Race conditions when replicating hysteron behaviour using spin pairs. a) Race conditions for spins $2A$ and $2B$ in the symmetrically coupled construction; small arrows indicate unstable hysterons. b) Race conditions for spins $1B$ and $2B$ in the symmetrically coupled construction; Δ is assumed to be large. c) Resolved race conditions for spins $1B$ and $2B$ in the asymmetrically coupled construction; Δ is assumed to be large.

$1B$. At state (1111), spin $2B$ must flip, and indeed becomes unstable as intended. Yet if Δ is small, say $\Delta = 0.1$, then spin $2A$ is unstable as well, leading to a race condition (Fig. 5.9a). Such race conditions can be trivially resolved by making Δ sufficiently large. Furthermore, if the rule is employed where only the most unstable spin flips (see Chapter 2.4), then this type of race conditions poses no issue to begin with. Provided that these race conditions are properly resolved, for the above set of parameters, the t-graph in Fig. 5.8c is realized successfully.

The occurence of the second type of race conditions depends on the parameters of the original hysteron system, and it is not always possible to resolve these. To illustrate these race conditions, we consider a variant on the system shown in Fig. 5.8a, where we double the strength of the nonzero coupling coefficient such that $c_{21} = -8$. For such a system, the t-graph topology is the same as in Fig. 5.8b. Yet, if we try to replicate this system as in Fig. 5.8c-d, we encounter race conditions. Namely, while spin $2B$ should only become unstable in state (1111) when spins $1A$ and $1B$ have both flipped, the coupling c_{21} is strong enough that spin $2B$ already becomes unstable in state (1011) (Fig. 5.9b). The occurence

of this type of race conditions does not depend on the choice for Δ. Furthermore, these race conditions cannot always be resolved by using the most-unstable rule: if we increase the coupling even further to, say, $c_{21} = -16$, then spin $2B$ is the most unstable rather than spin $1B$. In summary, the symmetrically coupled construction can fail in replicating a system of interacting hysterons in the part of parameter space where interactions are strong.

We now apply the same methodology for the asymmetric construction, where we show that unlike the symmetric construction, the asymmetric construction is always applicable. As before, we start by converting the individual hysterons to spin pairs. The switching thresholds for the asymmetric construction are the same as for the symmetric construction, and for the coupling we have:

$$c_{1A1B} = 4 + 2\Delta \tag{5.63}$$
$$c_{1B1A} = 4 \tag{5.64}$$
$$c_{2A2B} = 2 + 2\Delta \tag{5.65}$$
$$c_{2B2A} = 2 \tag{5.66}$$

so that the coupling matrix is:

$$c_{ij} = \begin{pmatrix} 0 & 4 & 0 & 0 \\ 4+2\Delta & 0 & 0 & 0 \\ -1 & -1 & 0 & 2 \\ -1 & -1 & 2+2\Delta & 0 \end{pmatrix}$$

The same race conditions that occur for the symmetrically coupled construction also occur for the asymmetrically coupled construction. Like for the symmetrically coupled construction, we can prevent the first type of race conditions by setting Δ sufficiently high and/or using the most-unstable rule. The second type of race conditions also occurs for the asymmetric construction, for the same parameters of the original system. However, a crucial difference between the asymmetric and symmetric constructions is that these race conditions can always be resolved for the asymmetric construction, given that Δ is large enough. Namely, whereas the difference between the switching thresholds of spins $1A$ and $1B$ for the symmetric construction is σ_1, for the symmetric construction this difference is $\sigma_1 + \Delta$. Thus, by setting Δ large enough, we can always enforce that it is more energetically favourable for spin B to flip first (Fig. 5.9c)– note, however, that this still requires the most-unstable rule to be used,

as the race conditions are not prevented entirely. The takeaway from this argument is that, in the limit of large Δ, the asymmetric construction yields spin pairs that robustly functions like a hysteron, whereas the hysteron mimicked by two symmetrically coupled spins can be 'broken apart' by strong interactions.

In summary, we have outlined two constructions by which a system of n hysterons can be replicated by, at most, $2n$ spins. Due to race conditions, the symmetric construction can fail for some parameters of the original hysteron system – in particular, when interactions are strong – whereas race conditions in the asymmetric construction can be resolved. This discussion of race conditions is relevant when we consider the physical reality of hysterons. We can view the hysteron in the symmetric construction as a small domain of two spins. These may collectively function as hysterons when there are no avalanches, or when interactions between domains are weak. However, if interactions between domains are too strong, then the domains are broken up and the hysteron description falls apart. By contrast, the asymmetric construction functions like a 'true' hysteron, which remains identifiable as a hysteron even when interactions are strong. A notable takeaway from these two simple constructions is that, while strong interactions may only be meaningful for 'true' hysterons, weak interactions–and in particular, scrambling without avalanches–are more broadly applicable.

5.4 Outlook and Conclusions

	$c_{ij} \leq 0$	c_{ij} **mixed**	$c_{ij} \geq 0$
Large span	No avalanches	Purely ferro	Purely ferro
Small span	Purely antiferro	Complex	

Table 5.1: Overview of different parameter regimes distinguished by the sign of interactions and the magnitude of the mean span σ. Here 'large' mean spans are much larger than $|u_i^+ - u_j^+|$, $|u_i^- - u_j^-|$ and $|c_{ij}|$ for all i, j; when this requirement is not satisfied, we refer to the span as small.

In this chapter, we have described multiple parameter regimes of the pairwise additive model of interacting hysterons, for which the space of potential t-graphs is simpler than in the general model. First, we have discussed restrictions on the coupling coefficients c_{ij}. For same-sign coupling, we have seen that the only allowed avalanches are purely ferromag-

netic and purely antiferromagnetic, when coupling is positive and negative, respectively. For global coupling, scrambling is not possible, and avalanches are grouped based on the hysterons flipped in the avalanche. Furthermore, for serial coupling – global coupling where all coupling coefficients are negative or zero – all avalanches are restricted to length-two, and it is straightforward to construct a hierarchy of possible t-graphs.

Next, we have discussed regimes of the hysteron span. We have shown that, when the mean hysteron span $\sigma = \langle u_i^+ - u_i^- \rangle$ is sufficiently large, antiferromagnetic avalanches and persistently unstable states are forbidden. By contrast, for spins (hysterons with zero span), scaffolds and avalanches are intertwined, as it is not possible to have irreversible flips without avalanches. To close off this discussion concerning spins, we have shown that hysterons can emerge from spin pairs, such that all behavior which is possible for n hysterons can be mimicked by at most $2n$ spins.

We have treated several isolated parameter regimes in this chapter. These regimes can also guide our navigation of the full design space of the pairwise additive model. We can see this in particular from our descriptions of same-sign coupling (section 5.2.1) and large span (section 5.3.1): since t-graphs for same-sign coupling must be either purely ferromagnetic or purely antiferromagnetic, and a sufficiently large span restricts avalanches to purely ferromagnetic avalanches, we can distinguish six regimes based on the mean span and the sign of the coupling coefficients (Table 5.1). We see from Table 5.1 that a system with same-sign negative coupling and sufficiently large mean span has no avalanches, and that complex t-graph responses are contained in the region where the mean span σ is small and the coupling coefficients c_{ij} have mixed signs.

We close this chapter by discussing extended models. This work focussed on abstract hysterons with phenomenologically introduced interactions. More realistic models can give insight into the physical reality of hysterons, as well as the shortcomings of hysteron models. In addition, they may help to establish a physical picture for the interactions, and may allow access to additional physical effects.

To start with, for bistable elements where each phase is associated with a different relation between two conjugated variables - such as force and deformation - one can explicitly work out the interactions that are mediated in such networks, and map these to interacting hysterons [3,6]. Such enhanced models are one step in a hierarchy of increasingly realistic models, that may give insight into the mechanisms that govern hysteron interactions, as well as provide design strategies to realize metamaterials

that leverage such interactions. An interesting question is if we can define enhanced hysteron models that avoid race conditions and self-loops, and conversely, under which conditions complex energy landscapes can still be meaningfully described by interacting hysterons. In this regard, progress has been made regarding symmetric coupling ($c_{ij} = c_{ji}$) and its relation to self-loops [37]. Namely, it has been shown that for symmetrically coupled hysteron systems, self-loops are consistently avoided. Moreover, an explicit mapping has been made from a network of physically active elements to interacting hysterons – thus showing that interacting hysteron models encompass not just passive systems, but also active systems, for which self-loops may be physically realized. These findings provide insights into the underlying mechanisms of self-loops in the interacting hysteron model.

Beyond the question of mapping physical systems to interacting hysteron models and vice versa, several further directions remain for future research. First, while (thermal) noise may lead to enhanced or suppressed memories [61], its role for interacting hysteron models is an important topic for future study. Second, many complex systems exhibit slow relaxations; determining which aspects stem from the complex transients exhibited by interacting hysterons, and which are due to slow relaxations of non-hysteron degrees of freedom, remains an open question. Finally, this work focussed on the case of a few hysterons. While the continuum limit of the Preisach model has been studied in detail [62, 63, 64], we have no continuum model for describing the statistics of large numbers of interacting hysterons.

Bibliography

[1] D. J. Griffiths, *Introduction to electrodynamics*. Cambridge University Press, 2023.

[2] T. Poston and I. Stewart, *Catastrophe theory and its applications*. Courier Corporation, 2014.

[3] D. Shohat, D. Hexner, and Y. Lahini, "Memory from coupled instabilities in unfolded crumpled sheets," *Proceedings of the National Academy of Sciences*, vol. 119, no. 28, p. e2200028119, 2022.

[4] M. Mungan, S. Sastry, K. Dahmen, and I. Regev, "Networks and hierarchies: How amorphous materials learn to remember," *Phys. Rev. Lett.*, vol. 123, 2019.

[5] N. C. Keim, J. D. Paulsen, Z. Zeravcic, S. Sastry, and S. R. Nagel, "Memory formation in matter," *Rev. Mod. Phys.*, vol. 91, no. 3, p. 035002, 2019.

[6] J. Liu, M. Teunisse, G. Korovin, I. R. Vermaire, L. Jin, H. Bense, and M. van Hecke, "Controlled pathways and sequential information processing in serially coupled mechanical hysterons," *Proceedings of the National Academy of Sciences*, vol. 121, no. 22, p. e2308414121, 2024.

[7] D. Marković, A. Mizrahi, D. Querlioz, and J. Grollier, "Physics for neuromorphic computing," *Nature Reviews Physics*, vol. 2, no. 9, pp. 499–510, 2020.

[8] J. D. Paulsen and N. C. Keim, "Minimal descriptions of cyclic memories," *Proc. Roy. Soc. A*, vol. 475, 2019.

[9] M. Mungan and M. M. Terzi, "The structure of state transition graphs in systems with return point memory: I. general theory," *Annales Henri Poincaré*, vol. 20, pp. 2819–2872, 2019.

[10] M. van Hecke, "Profusion of transition pathways for interacting hysterons," *Phys. Rev. E*, vol. 104, 2021.

[11] J. D. Paulsen, "Mechanical hysterons with tunable interactions of general sign," *Nature Communications*, vol. 17, no. 1, p. 2799, 2026.

[12] C. W. Lindeman, T. R. Jalowiec, and N. C. Keim, "Generalizing multiple memories from a single drive: The hysteron latch," *Science Advances*, vol. 11, no. 5, p. eadr5933, 2025.

[13] C. W. Lindeman and S. R. Nagel, "Multiple memory formation in glassy landscapes," *Science Advances*, vol. 7, 2021.

[14] J. D. Paulsen and N. C. Keim, "Multiperiodic orbits from interacting soft spots in cyclically sheared amorphous solids," *Science Advances*, vol. 7, no. 33, 2021.

[15] A. Szulc, M. Mungan, and I. Regev, "Cooperative effects driving the multi-periodic dynamics of cyclically sheared amorphous solids," *The Journal of Chemical Physics*, vol. 156, no. 16, 2022.

[16] S. G. Das, J. Krug, and M. Mungan, "Driven disordered systems approach to biological evolution in changing environments," *Phys. Rev. X*, vol. 12, no. 031040, 2022.

[17] D. Shohat, Y. Lahini, and D. Hexner, "Are crumpled sheets marginally stable?," *arXiv preprint arXiv:2408.08030*, 2024.

[18] D. Shohat, P. Baconnier, I. Procaccia, M. van Hecke, and Y. Lahini, "Aging of amorphous materials under cyclic strain," *Proceedings of the National Academy of Sciences*, vol. 123, no. 8, p. e2515075123, 2026.

[19] H. Bense and M. van Hecke, "Complex pathways and memory in compressed corrugated sheets," *Proc. Natl. Acad. Sci.*, vol. 118, no. 50, 2021.

[20] T. Jules, A. Reid, K. E. Daniels, M. Mungan, and F. Lechenault, "The delicate memory structure of origami switches," *Phys. Rev. Research*, vol. 4, 2022.

[21] C. Merrigan, D. Shohat, C. Sirote, Y. Lahini, C. Nisoli, and Y. Shokef, "Disorder, multistability, and mechanical memory in an ordered metamaterial," 2022.

[22] A. El Elmi and D. Pasini, "Tunable sequential pathways through spatial partitioning and frustration tuning in soft metamaterials," *Soft Matter*, vol. 20, no. 6, pp. 1186–1198, 2024.

[23] G. Muhaxheri and C. D. Santangelo, "Bifurcations of inflating balloons and interacting hysterons," *Physical Review E*, vol. 110, no. 2, p. 024209, 2024.

[24] D. Melancon, A. E. Forte, L. M. Kamp, B. Gorissen, and K. Bertoldi, "Inflatable origami: multimodal deformation via multistability," *Advanced Functional Materials*, vol. 32, no. 35, p. 2201891, 2022.

[25] P. Ducarme, B. Weber, M. van Hecke, and J. T. Overvelde, "Exotic mechanical properties enabled by countersnapping instabilities," *Proceedings of the National Academy of Sciences*, vol. 122, no. 16, p. e2423301122, 2025.

[26] D. Shohat and M. van Hecke, "Geometric control and memory in networks of hysteretic elements," *Physical Review Letters*, vol. 134, no. 18, p. 188201, 2025.

[27] G. Muhaxheri, V. Antonetti, and C. D. Santangelo, "A catastrophic approach to designing interacting hysterons," *New Journal of Physics*, vol. 27, no. 12, p. 125004, 2025.

[28] I. Regev, I. Attia, K. Dahmen, S. Sastry, and M. Mungan, "Topology of the energy landscape of sheared amorphous solids and the irreversibility transition," *Phys. Rev. E*, vol. 103, no. 6, p. 062614, 2021.

[29] C. W. Lindeman, V. F. Hagh, C. I. Ip, and S. R. Nagel, "Competition between energy and dynamics in memory formation," *Phys. Rev. Lett.*, vol. 130, no. 19, p. 197201, 2023.

[30] M. M. Terzi and M. Mungan, "State transition graph of the preisach model and the role of return-point memory," *Phys. Rev. E*, vol. 102, no. 012122, 2020.

[31] C. W. Lindeman, T. R. Jalowiec, and N. C. Keim, "Isolating the enhanced memory of a glassy system," 2023.

[32] A. Szulc, M. Mungan, and I. Regev, "Cooperative effects driving the multi-periodic dynamics of cyclically sheared amorphous solids," *The Journal of Chemical Physics*, vol. 156, no. 16, 2022.

[33] F. Preisach, "Über die magnetische nachwirkung," *Zeitschrift für Physik*, vol. 94, pp. 277–302, 1935.

[34] J. Ding and M. van Hecke, "Sequential snapping and pathways in a mechanical metamaterial," *The Journal of Chemical Physics*, vol. 156, no. 20, 2022.

[35] L. P. Hyatt and R. L. Harne, "Programming metastable transition sequences in digital mechanical materials," *Extreme Mechanics Letters*, vol. 59, p. 101975, 2023.

[36] P. L. Ferrari, M. Mungan, and M. M. Terzi, "The preisach graph and longest increasing subsequences," *Annales de l'Institut Henri Poincaré D*, 2022.

[37] P. Baconnier, M. H. Teunisse, and M. van Hecke, "Dynamic self-loops in networks of passive and active binary elements," *Physical Review Letters*, vol. 135, no. 20, p. 207402, 2025.

[38] D. A. Huffman, "The synthesis of sequential switching circuits," *Journal of the Franklin Institute*, vol. 257, pp. 161–190, 1954.

[39] W. D. Wallis, *A beginner's guide to discrete mathematics*. Springer Science & Business Media, 2011.

[40] A. Grami, *Discrete Mathematics: Essentials and Applications*. Academic Press, 2022.

[41] S. Warshall, "A theorem on boolean matrices," *Journal of the ACM (JACM)*, vol. 9, no. 1, pp. 11–12, 1962.

[42] G. B. Dantzig and B. C. Eaves, "Fourier-motzkin elimination and its dual with application to integer programming," in *Combinatorial Programming: Methods and Applications*, pp. 93–102, Springer, 1975.

[43] G. B. Dantzig and M. N. Thapa, *The simplex method*. Springer, 1997.

[44] A. B. Kahn, "Topological sorting of large networks," *Communications of the ACM*, vol. 5, no. 11, pp. 558–562, 1962.

[45] D. E. Knuth, *The Art of Computer Programming: Fundamental Algorithms, volume 1*. Addison-Wesley Professional, 1997.

[46] L. Jin and M. Van Hecke, "Dynamic avalanches: Rate-controlled switching and race conditions," *Physical Review Letters*, vol. 135, no. 21, p. 218201, 2025.

[47] L. J. Kwakernaak and M. van Hecke, "Counting and sequential information processing in mechanical metamaterials," *Phys. Rev. Lett.*, vol. 130, no. 26, p. 268204, 2023.

[48] P. Holmes, R. J. Full, D. Koditschek, and J. Guckenheimer, "The dynamics of legged locomotion: Models, analyses, and challenges," *SIAM review*, vol. 48, no. 2, pp. 207–304, 2006.

[49] J. T. Overvelde, T. Kloek, J. J. D'haen, and K. Bertoldi, "Amplifying the response of soft actuators by harnessing snap-through instabilities," *Proceedings of the National Academy of Sciences*, vol. 112, no. 35, pp. 10863–10868, 2015.

[50] J. Byun, A. Pal, J. Ko, and M. Sitti, "Integrated mechanical computing for autonomous soft machines," *Nature Communications*, vol. 15, no. 1, p. 2933, 2024.

[51] E. Szpilrajn, "Sur l'extension de l'ordre partiel," *Fundamenta mathematicae*, vol. 1, no. 16, pp. 386–389, 1930.

[52] G. Pruesse and F. Ruskey, "Generating linear extensions fast," *SIAM Journal on Computing*, vol. 23, pp. 373–386, 1994.

[53] D. E. Knuth and J. L. Szwarcfiter, "A structured program to generate all topological sorting arrangements," *Information Processing Letters*, vol. 2, no. 6, pp. 153–157, 1974.

[54] Y. L. Varol and D. Rotem, "An algorithm to generate all topological sorting arrangements," *The Computer Journal*, vol. 24, no. 1, pp. 83–84, 1981.

[55] A. D. Kalvin and Y. L. Varol, "On the generation of all topological sortings," *Journal of Algorithms*, vol. 4, no. 2, pp. 150–162, 1983.

[56] G. Brightwell and P. Winkler, "Counting linear extensions," *Order*, vol. 8, pp. 225–242, 1991.

[57] M. Peczarski, "New results in minimum-comparison sorting," *Algorithmica*, vol. 40, pp. 133–145, 2004.

[58] B. Grünbaum, *Convex Polytopes*. Springer, second ed., 2003.

[59] J. M. Deutsch and O. Narayan, "Subharmonics and aperiodicity in hysteresis loops," *Phys. Rev. Lett.*, vol. 91, no. 20, p. 200601, 2003.

[60] C. M. Meulblok and M. Van Hecke, "Transients and multiperiodic responses: a hierarchy of material bits," *New Journal of Physics*, vol. 28, no. 2, p. 025002, 2026.

[61] N. C. Keim and S. R. Nagel, "Generic transient memory formation in disordered systems with noise," *Phys. Rev. Lett.*, vol. 107, no. 1, p. 010603, 2011.

[62] M. Brokate and J. Sprekels, *Hysteresis and phase transitions*, vol. 121. Springer Science & Business Media, 2012.

[63] I. Mayergoyz, "Hysteresis models from the mathematical and control theory points of view," *Journal of Applied Physics*, vol. 57, no. 8, pp. 3803–3805, 1985.

[64] J. Ortin, "Preisach modeling of hysteresis for a pseudoelastic cu-zn-al single crystal," *Journal of applied physics*, vol. 71, no. 3, pp. 1454–1461, 1992.

Summary

This dissertation discusses a new framework for multistable materials. A multistable material is a material which can hold many different states. A wad of paper, for example, can take many different shapes, depending on the way in which it was crumpled. Other examples of multistable materials are rubber structures, and amorphous matter such as plastic or glass.
In this new framework, multistable materials are modelled via local, bistable memory elements: for example, the individual mountain and valley folds in a wad of paper. These memory elements are called hysterons, as they display hysteresis, a form of memory which is common in physics.
Hysterons are not new: as far back as the start of the twentieth century, they were already used by Ferenc Preisach to model magnetic domains. However, only in the last decade did it become clear that hysterons could also be used to model varying forms of multistable matter. The novelty of these hysteron models, in comparison to the original Preisach model, is that hysterons interact.
At heart, this project is about expanding our understanding of memory. When a wad of paper can hold eight different states, we can say that it has three 'bits' of memory. In the hysteron model this memory is ascribed to physical bits. We can compare this to the memory of a hard drive, which is stored in magnetic 'bits'.
What is surprising about multistable materials, however, is that they can not only *store*, but also *process* information. Experiments have shown, for example, that some multistable materials can count, or display multi-periodic responses. This goes beyond storage, as we would see in a hard drive or SD card; in some way, there is a logical 'circuit' embedded in

these materials! Interactions between hysterons provide an explanation for such logical circuits.
While the interacting hysteron model is simple and abstract, it is staggeringly effective at describing the behaviour of multistable materials. We thus see that memory storage and processing are not just relevant to computers, or to our own brains, but that simple forms of memory occur far more broadly.

Chapter 1 is the introduction to this thesis. Starting from a general explanation of hysteresis, it discusses how hysteresis occurs in multistable materials such as crumpled sheets. This chapter subsequently delves into hysterons, which are the focus of this research. It shows that multistable materials can be understood via hysterons, and that interacting hysterons in particular provide a good description for the unusual behaviour which is observed in these systems. This behaviour encompasses simple behaviours such as counting, but also more complex forms of information processing.

Chapter 2 establishes a basis for the interacting hysteron model. This general model forms the core on which the remainder of this dissertation builds. When hysterons are exposed to a driving field, for example a compressive force or magnetic field, they undergo transitions. When hysterons interact, transitions can take the form of multi-step 'avalanches', in which a single hysteron flip causes other hysterons to flip as well. In some multistable systems, for example in a Mylar rescue blanket, avalanches even lead to an audible crackling noise.
Besides causing avalanches, interactions also affect the order in which hysterons flip. This 'scrambling' effect was previously observed, but we now provide a formal definition.
A single hysteron system can display many different transitions, based on its starting state and the driving protocol. We can combine all these transitions and starting states of a in a so-called transition graph. Transition graphs powerfully represent the behaviour of a hysteron system, because they capture all possible responses of a hysteron system to driving. They are therefore the focus of this thesis.
The transition graph of a given hysteron system is easily determined. The inverse question, however, is more challenging: which conditions must be met in order for a hysteron system to realize a given transition graph? While it is possible to work out these conditions, or by hand, the list of

conditions quickly gets out of hand. We therefore compose a systematic algorithm to determine these so-called 'design inequalities'.

Chapter 3 describes an algorithm to generate all possible transition graphs. Because the conditions of a transition graphs vary wildly, it's practically impossible to draw all realizable graphs in one go. The strategy, therefore, is to first draw a list of 'candidate graphs', and then eliminate all candidates which are not realizable. This is a combinatorical problem, and we show that the number of candidate graphs increases very rapidly with the number of hysterons. For two hysterons, we can exactly determine that there are thirteen possible transition graphs, which is in agreement with previous numeric results. For three hysterons, however, we would have to evaluate over four billion candidate graphs. At the same time, we know that, thus far, only a little over fifteen thousand graphs were found numerically for three hysterons.
The findings of this chapter expose a core issue in the systematic construction of transition graphs: while the number of candidate graphs increases rapidly with the number of hysterons, the probability that a given candidate can be realized decreases. This shows that the interacting hysteron model encompasses diverse types of systems, and that it is therefore not very useful to attempt to categorize all transition graphs at once. Instead, it is more useful to consider more restricted systems.

Chapter 4 zooms in on two specific, related features which we encounter in interacting hysterons: self-loops and multiperiodic responses. A self-loop is an avalanche which returns to previously visited states, such that in theory it would keep looping forever. These 'endless loops' have been encountered in simulations, but have typically been considered unphysical. When interactions are symmetric, for instance, self-loops cannot occur. It is difficult to exclude self-loops from the outset, however, due to the many different paths that an avalanche can take.
Multiperiodic behaviour entails that a system returns to an initial state after multiple driving cycles. The principle of this multiperiodic response is comparable to a retractable pen, which toggles between its two states after each 'click'. A retractable pen requires two clicks in order to return to its initial state, and we therefore say that it has a 'period-two' response. Similarly, hysteron systems can exhibit 'period-T' responses, where they return to their initial state after T driving cycles. To obtain periods of

two or larger in a hysteron system, interactions are required. We establish formal conditions in order to realize such multiperiodic responses.

Chapter 5 considers a number of restricted variants of the interacting hysterons. In all cases, we assume that hysterons interact via a pairwise coupling.
First, we consider the sign of the coupling. When all coupling coefficients are positive, all avalanches must be monotone, which entails that all hysterons flip in the same direction, similarly to a domino effect. Conversely, when all coupling coefficients are negative, avalanches are alternating: an up flip is followed by a down flip, and vice versa. These alternating avalanches can take the form of self-loops.
We also consider hysterons which are coupled 'in series'. This model is directly based on experiments, and has the remarkable property that avalanches are limited to alternating avalanches of length 2 (up then down, or down then up). For this model, we have worked out exactly that there are 45 candidate graphs for three hysterons, out of which 44 are realizable.
Finally, we consider how the behaviour of a hysteron system is influenced by the difference between the two switching thresholds of a hysteron, called the 'span'. The span measures the degree of hysteresis in a single hysteron. In the limit where the average span is much larger than all other relevant parameters, all avalanches are monotone. When, in addition, the coupling has a negative sign, avalanches are forbidden entirely. In contrast, we also consider the 'spin' limit. Spins are hysterons which have a span of zero. Because spins have no memory in and of themselves, memory in spin systems can only emerge as a result of interactions. We show that a single hysteron can be constructed out of two interacting spins. At the same time we show that this construction is highly improbable, and therefore, that interacting hysterons are substantially different from interacting spins.

Samenvatting

Deze dissertatie gaat over een nieuw framework voor multistabiele materialen. Een multistabiel materiaal is een materiaal dat veel verschillende toestanden kan vasthouden. Een prop papier, bijvoorbeeld, kan veel verschillende vormen aannemen, afhankelijk van de manier waarop we het hebben opgefrommeld. Ander multistabiele materialen zijn onder andere rubberen structuren, en amorfe materie, zoals plastic of glas.
In dit nieuwe framework worden multistabiele materialen gemodelleerd door middel van lokale, bistabiele geheugenelementjes: de individuele vouwen in een prop papier, bijvoorbeeld. Deze geheugenelementjes heten hysterons omdat ze hysterese vertonen, een vorm van geheugen die in de natuurkunde veel voorkomt.
Hysterons zijn op zich niet nieuw: in het begin van de twintigste eeuw werden hysterons al gebruikt door Ferenc Preisach om magnetische domeinen te beschrijven. Pas in de laatste tien jaar is echter gebleken dat hysterons ook een goed model vormen voor verschillende soorten multistabiele materialen. Het nieuwe aan deze hysteronmodellen, ten opzichte van het oorspronkelijke model van Preisach, is dat de hysterons wisselwerken.
In de kern gaat dit project over het verbreden van ons begrip van geheugen. Als een prop papier acht verschillende toestanden kan aannemen, heeft deze drie 'bits' aan geheugen. In het hysteronmodel schrijven we dit geheugen toe aan fysieke 'bits'. We kunnen dit vergelijken met het geheugen van een harde schijf, dat is opgeslagen in magnetische 'bits'.
Wat echter verrassend is aan multistabiele materialen, is dat ze informatie niet alleen kunnen *opslaan*, maar ook kunnen *verwerken*. Uit experimenten blijkt bijvoorbeeld dat sommige multistabiele materialen kunnen tellen, of multiperiodiek gedrag vertonen. Dit gaat verder dan alleen opslag, zoals we zouden vinden in een harde schijf of SD-kaart; er zit een

logisch 'circuitje' in deze materialen ingebakken! We kunnen deze circuitjes verklaren door hysterons te laten wisselwerken.
Hoewel het wisselwerkende hysteronmodel simpel en abstract is, is het verbluffend effectief in het beschrijven van multistabiele materialen. Zo zien we dat geheugen en informatieverwerking niet alleen van belang zijn voor computers, of voor het menselijk brein, maar dat simpele vormen van geheugen veel breder voorkomen.

Hoofdstuk 1 is de introductie van dit proefschrift. Het begint met een algemene uitleg van hysterese, en illustreert hoe we hysterese kunnen terugvinden in multistabiele materialen, zoals verfrommeld papier. Vervolgens gaat dit hoofdstuk dieper in op hysterons, die de focus vormen van dit onderzoek. Het laat zien dat multistabiele materialen begrepen kunnen worden via hysterons, en dat juist wisselwerkende hysterons een goede beschrijving zijn van het ongebruikelijke gedrag dat in deze materialen wordt geobserveerd. Daarbij gaat het bijvoorbeeld om tellen, maar ook complexere vormen van informatieverwerking kunnen zich voordoen.

Hoofdstuk 2 legt de basis voor een model van wisselwerkende hysterons. Dit algemene model vormt de kern waarop de rest van deze dissertatie voortbouwt.
Als hysterons worden blootgesteld aan een aandrijving, bijvoorbeeld een compressieve kracht of een magneetveld, ondergaan deze transities. Wanneer hysterons wisselwerken kunnen transities de vorm aannemen van 'lawines', waarbij het omklappen van één element ook andere elementjes laat omklappen. In sommige multistabiele systemen, bijvoorbeeld in een reddingsdeken, zijn lawines zelfs hoorbaar als een krakend geluid.
Naast het veroorzaken van lawines, heeft wisselwerking ook een subtieler effect, waarbij de volgorde waarin hysterons omklappen 'gehusseld' wordt. Dit hussel-effect was al eerder geobserveerd, maar we geven er nu een formele definitie voor.
Een enkel hysteronsysteem kan veel verschillende transities vertonen, afhankelijk van de begintoestand en de manier waarop we het aandrijven. We kunnen al die begintoestanden en transities samenvoegen in een zogeheten transitiegraaf. Transitiegrafen zijn een krachtige representatie, omdat ze alle mogelijke responses van een hysteronsysteem in zich dragen. Ze vormen daarom de focus van dit proefschrift.
Voor een gegeven hysteronsysteem is de transitiegraaf makkelijk te bepalen.

De omgekeerde vraag is lastiger: stel dat we een bepaalde transitiegraaf willen realizeren, aan welke voorwaarden moeten de hysterons en hun interacties dan voldoen? Het is mogelijk om dit probleem met de hand uit te werken, maar de lijst van voorwaarden wordt dan al snel moeilijk te overzien. We stellen daarom een systematisch algoritme op om de voorwaarden te bepalen. Dit algoritme is een heel nuttig gereedschap: voor elke transitiegraaf die we uittekenen, kunnen we nu efficient bepalen of deze realiseerbaar is of niet.

Hoofdstuk 3 stelt een algoritme op om alle mogelijke transitiegrafen te genereren. Omdat de voorwaarden voor een transitiegraaf zeer uiteenlopen, is het haast onmogelijk om in één keer alle realiseerbare grafen te tekenen. De strategie is daarom om eerst een aantal 'kandidaatgrafen' te genereren, en vervolgens alle kandidaten te elimineren die niet realiseerbaar zijn. Dit is een combinatorisch probleem, en we laten zien dat het aantal kandidaatgrafen razendsnel toeneemt als functie van het aantal hysterons. Voor twee hysterons kunnen we exact bepalen dat er dertien mogelijke transitiegrafen zijn, wat overeenkomt met eerdere numerieke resultaten. Voor drie hysterons zouden we echter meer dan vier biljoen kandidaatgrafen moeten evalueren, terwijl numeriek tot dusver slechts een ruime vijftienduizend grafen realiseerbare grafen zijn gevonden.
De bevindingen van dit hoofdstuk leggen een kernprobleem bloot in het construeren van transitiegrafen: terwijl het aantal kandidaatgrafen snel toeneemt met het aantal hysterons, neemt de waarschijnlijkheid juist af dat een specifieke kandidaat gerealiseerd kan worden. Dit laat zien dat het wisselwerkende hysteronmodel uiteenlopende systemen beschrijft, en dat het daarom niet zo zinvol is om te proberen alle transitiegrafen in één keer te categoriseren. In plaats daarvan is het nuttiger om te kijken naar meer beperkte systemen.

Hoofdstuk 4 zoomt in op twee specifieke, gerelateerde gedragingen die we vinden in wisselwerkende hysterons: zelflussen en multiperiodiek gedrag. Een zelflus is een lawine die terugkeert naar een eerder bezochte toestand, zodat deze in theorie eeuwig zou voortduren. Deze 'oneindige loops' zijn geobserveerd in simulaties, maar zijn daarbij vaak beschouwd als onfysisch. Als wisselwerking bijvoorbeeld symmetrisch is, komen zelflussen niet voor. Het is echter lastig om zelflussen op voorhand uit te sluiten, omdat lawines zo veel verschillende paden kunnen afleggen.
Multiperiodiek gedrag doet zich voor wanneer een systeem na meerdere

aandrijfcycli terugkeert naar de oorspronkelijke toestand. Het principe hiervan is vergelijkbaar met dat van een klikpen, die bij elke klik van toestand alterneert. Een klikpen heeft twee kliks nodig om naar de oorspronkelijke toestand terug te keren: we noemen dit een 'periode-2 respons'. Op dezelfde manier kunnen hysteronsystemen een 'periode-T' respons vertonen, waarbij T aandrijfcycli nodig zijn om naar de oorspronkelijke toestand terug te keren. Om periodes van 2 of hoger te krijgen in een hysteronsysteem, is wisselwerking nodig. We stellen formele voorwaarden op om zulke multiperodieke responses te krijgen.

Hoofdstuk 5 beschouwt een aantal beperktere varianten van het wisselwerkende hysteronmodel. In alle gevallen wordt er vanuit gegaan dat de hysterons paargewijs wisselwerken.
Ten eerste wordt gekeken naar het teken van de koppeling. Als alle koppelingen een positief teken hebben, moeten alle lawines monotoon zijn: dit wil zeggen dat alle hysterons dezelfde kant op klappen, als bij een domino-effect. Als alle koppelingen daarentegen negatief zijn, zijn de lawines alternerend: klapt er één hysteron omhoog, dan klapt de volgende omlaag en vice versa. Deze alternerende lawines kunnen ook de vorm aannemen van zelflussen.
We kijken ook naar hysterons die 'in serie' gekoppeld zijn. Dit model is direct gebaseerd op experimenten, en heeft onder andere de bijzondere eigenschap dat lawines zijn gelimiteerd tot alternerende lawines van lengte 2. Voor dit model hebben we precies kunnen uitwerken dat er 45 kandidaatgrafen zijn voor drie hysterons, waarvan er 44 realiseerbaar zijn.
Tot slot beschouwen we hoe het gedrag beinvloed wordt door de afstand tussen de twee drempelwaardes van een hysteron, aangeduid als de 'span'. De span geeft de mate van hysterese aan in een individueel hysteron. In de limiet waarin de gemiddelde span groter is dan alle andere relevante variabelen, zijn alle lawines monotoon. Als de koppeling bovendien negatief is, worden lawines in het geheel verboden. Daartegenover staat de 'spin'-limiet. Spins zijn hysterons die een span hebben van nul. Omdat spins van zichzelf geen geheugen hebben, komt het geheugen in spinsystemen puur voort uit interacties. We laten in dit hoofdstuk zien dat een enkel hysteron geconstrueerd kan worden uit twee wisselwerkende spins. Tegelijkertijd laten we zien dat deze constructie hoogst onwaarschijnlijk is, en dat er dus een wezenlijk verschil is tussen wisselwerkende hysterons en wisselwerkende spins.

List of publications

- **M.H. Teunisse** and M. van Hecke, "Interacting hysterons with asymptotically small or large spans", *New Journal of Physics* 28, p. 043505, 2026.
  DOI:10.1098/rsos.250753

- **M. Teunisse** and M. van Hecke, "Transition graphs of interacting hysterons: Structure, design, organization and statistics" *Royal Society Open Science*, vol. 12, no. 9, 2025.
  DOI:10.1098/rsos.250753

- P. Baconnier, **M. H. Teunisse**, and M. van Hecke, "Dynamic self-loops in networks of passive and active binary elements," *Physical Review Letters*, vol. 135, no. 20, p. 207402, 2025
  DOI:10.1103/x1b1-rynn.

- J. Liu, **M. Teunisse**, G. Korovin, I. R. Vermaire, L. Jin, H. Bense, and M. van Hecke, "Controlled pathways and sequential information pro- cessing in serially coupled mechanical hysterons," *Proc. Natl. Acad. Sci.*, vol. 121, no. 22, p. e2308414121, 2024.
  DOI:10.1073/pnas.2308414121

About the author

I was born on October 8th, 1998 in Bodegraven, and went to pre-university education (Atheneum incl. philosophy, IT) at the GSG Leo Vroman in Gouda. After graduating in 2016, I started my double bachelor in Physics and Astronomy at Leiden University. I closed off my bachelor studies with an experimental research project in the lab of Daniela Kraft, which studied 3D-printed, colloidal 'swimmers' in the shape of partially grooved cilinders.

After earning my bachelor's degree in 2019, I continued my studies at Leiden University with a master in the Biological and Soft Matter Physics track. In 2020-2021 I closed off my master with two research projects. For my first research project, I implemented a Python model for the movement of a colloidal particle near a substrate, under the supervision of Luca Giomi. I carried out my second, larger project in the lab of Martin van Hecke, where I analyzed non-commutative responses in buckling beams, based on simulation and experiment. I worked out how these responses could be explicitly represented in the language of computer science, by converting these to a truth table and then to a logic circuit.

In the fall of 2021, I returned to Martin's lab to carry out my PhD research, of which this dissertation is the result. Outside of the research itself, I functioned as a teaching assistant, first for a week-long 'Computational Physics' pilot, and subsequently for two semesters of the 'Mechanical Metamaterials' course. During the last year of my PhD, I shifted my focus more explicitly towards software engineering, as I attended a retreat organized by the TDCC-NES, and followed two courses by the Netherlands eScience Center. For my next steps after my PhD, I am continuing to delve into software engineering, with a particular focus on domain-driven design.

Acknowledgements

These past four years have been a very special time to me. In part that's because of the nature of the work itself, where I got to delve into a single theoretical framework and explore all the little nooks and crannies that it had to offer. At least as important, though, were the people that I was fortunate enough to meet.

First, I am deeply grateful to Martin for giving me the opportunity to do this project, and for his supervision throughout. Over the course of these four years, I never had to think twice about saying what was on my mind, yet I never felt that the project was going off the rails either, and I think that really speaks to Martin's skill as a supervisor.

I also want to express special thanks to Muhittin Mungan. It was his expert analysis of state transition graphs for athermal, quasistatic systems which formed a basis for my PhD research, and I enjoyed the interesting mathematical discussions which we had the few times we met in person.

Over the course of my PhD, I have been greatly influenced by my colleagues in the Van Hecke group. Out of these, there are a few people that deserve special mention for their contributions to the contents of this thesis. First, I want to thank Paul for our enthusiastic discussions regarding self-loops and asymmetric coupling, which are represented in chapter 4.2, and in a paper that I'm quite proud to have my name on. Next, I want to thank Colin for his continued persistence and curiosity regarding the topics of multiperiodicity and spins. These brief, yet frequent discussions eventually found their way into chapters 4.3 and 5.3. I further want to thank Sourav, whose observations concerning large span and global coupling inspired parts of 5.2 and, again, 5.3. I very much enjoyed the discussions I had with all three of you, and I hope this is

reflected in the corresponding chapters. Beyond the scientific content, I also want to thank Lennard for teaching me the basics of Git in my first year, and for sharing in my enthusiasm to improve the structural soundness of my code. It should not be understated how much that helped me over the course of this project.

More broadly, I want to extend my personal thanks to Martin's group as a whole. Frankly, it means more to me than I can express here that I was able to work with all of you. I hope I've done enough to make that clear, in person, to each of you. My extended thanks go to the other Soft Matter groups in Leiden, who have always made the 10th floor feel like a very welcoming place to me.

Finally, I want to thank my parents and my brother Joris for, quite simply, always supporting me and hearing me out. It's thanks to all of you that this has been a very pleasant and rewarding time for me, and one that I expect I will look back on often and fondly in the years to come.